International
Progress Report

IPR-02-43

Äspö Hard Rock Laboratory

Impact of the tunnel construction on the groundwater at Äspö

Task 5. Numerical modelling of the transient groundwater flow and conservative solute transport during the construction (1990/10/01-1997/01/01)

J. Molinero
J. Samper
R. Juanes

ENRESA and University of La Coruña, Spain

May 2001

Svensk Kärnbränslehantering AB
Swedish Nuclear Fuel
and Waste Management Co
Box 5864
SE-102 40 Stockholm Sweden
Tel +46 8 459 84 00
Fax +46 8 661 57 19

Äspö Hard Rock
Laboratory

Report no.	No.
IPR-02-43	F65K
Author	Date
Molinero, Samper, Juanes	01-05-01
Checked by	Date
Samper	01-05-31
Approved	Date
Christer Svemar	02-11-19

Äspö Hard Rock Laboratory

Impact of the tunnel construction on the groundwater at Äspö

Task 5. Numerical modelling of the transient groundwater flow and conservative solute transport during the construction (1990/10/01-1997/01/01)

J. Molinero

J. Samper

R. Juanes

ENRESA and University of La Coruña, Spain

May 2001

Keywords: Groundwater flow, solute transport, coupled hydrogeochemistry, Äspö, Task 5

Summary

The numerical modelling of the groundwater flow and solute transport of the €spš site has been successfully performed.

The tunnel construction process has been simulated by means of 29 stages for the transient groundwater flow model. Flow rates into the tunnel are computed by the model and not prescribed as a boundary condition.

Computed flow rates show an excellent agreement with measured data in most of the tunnel sections. The comparison of the computed pressure heads and the measured values indicates that in general the numerical model is able to reproduce the measured drawdowns. Calibrated transmissivities are within the range of field measured values except for two of the 19 considered hydraulic domains, were a little lower transmmissivity value was calibrated. Finally, the groundwater flow numerical model has been succesfully validated against field data not used in the calibration stage.

Numerical results in terms of concentrations show an excellent agreement with measured data of chlorides and 18-oxygen. It is important to remark that solute transport results were achieved without calibration. With a strongly consistent (and calibrated) flow model, the numerical model reproduces conservative chemical concentrations using available transport parameters.

In order to assess uncertainty in initial and boundary conditions and parameters, a sensitivity analyses of the numerical model was done for groundwater flow and solute transport. Groundwater flow model is strongly sensitive to the initial conditions and transsmissivities of the Hydraulic Domains. On the contrary, the model is not sensitive to the parameters of the intersections among domains and with respect to the boundary conditions. Solute transport model is strongly dependent on initial conditions of concentrations. Initial concentration field was found as the most important source of uncertainty.

A good agreement was found between M3 model results and hydrodynamic numerical model of groundwater flow and solute transport. In general, it can be stated that a there is a consistency between both types of models. This consistency supports the hypothesis of the mixing of 4 extreme reference waters at the €spš groundwater system, as proposed by M3 model. M3 results has been useful to shape some aspects of the €spš site hydrogeology. However, the comparison of hydrodynamic and mixing models results must be taken carefuly, due to the combination of uncertainties on the mixing model (+/- 10%) together with the detected uncertainties in the interpolation of the mixing fractions further on the sampling points (+/- 10%).

Predictions at 3 of the 4 proposed prediction points have been made. They include a base run (best prediction) and a second run using an alternative initial concentrations field. The results of both runs provided a reliable prediction range which was in agreement with field measurements.

The role of the chemical reaction have been evaluated by means of comparison of computed results and measured concentrations of the typically non-conservative species. Sources of bicarbonate, calcium and sulphate have been clearly detected, which are assumed to be caused by chemical processes. A different behaviour of calcium and bicarbonates have been found depending on the location of the fracture zones. As a cualitative hypothesis, the carbonate system could be affected by the higher availability of Fe(III) expected under the islands. As proposed by Banwart (1999) for the Redox Zone, carbon oxidation through Fe(III) reduction could constitute a source of bicarbonates. This hypothesis (and other chemical behaviours which remains still unclear) can be quantitatively validated or rejected by means of coupled groundwater flow and reactive transport modelling.

SAMMANFATTNING

Numerisk modellering av grundvattenflöde och transport av lösningar på Äspö har genomförts med lyckat resultat.

Tunneldrivningen har simulerats i 29 steg för beskrivning av det transienta grundvattenflödet. Flödesmängderna in i tunneln datorberäknas av modellen och ansätts inte som randvillkor.

Datorberäknade flöden visar utmärkt överensstämmelse med uppmätta data i de flesta tunnelsektioner. Jämförelsen av datorberäknade vattentryck och uppmätta värden indikerar att den numeriska modellen generellt sett kan återskapa de uppmätta avsänkningarna. Kalibrerade transmissiviteter ligger inom gränsen för uppmätta fältdata med undantag för två av de 19 studerade hydrauliska domänerna, för vilka en något mindre transmissivitet kalibrerades. Slutligen har den numeriska modellen för grundvattenflöde validerats med hjälp av fältdata, som inte använts i tidigare kalibreringsfaser, med lyckat resultat.

Numeriska resultat i form av koncentrationer visar utmärkt överensstämmelse med uppmätta värden för klorider och syre-18. Det är viktigt att påpeka att resultatet rörande lösningstransport erhölls utan föregående kalibrering. Med en starkt enhetlig (och kalibrerad) flödesmodell simulerar den numeriska modellen icke-sorberande kemiska koncentrationer vid användande av tillgängliga transportparametrar.

För att utvärdera osäkerheter i ursprungliga förhållanden, randvillkor och parametrar gjordes en känslighetsanalys av den numeriska modellen för grundvattenflöde och lösningstransport. Modellen för grundvattenflöde är mycket känslig för de ursprungliga förhållandena och transmissiviteterna hos de hydrauliska domänerna. Däremot är modellen inte känslig för parametrar för korsningar mellan domänerna, då dessa tar hänsyn till randvillkoren. Modellen för lösningstransport är kraftigt beroende av ursprungliga koncentrationsförhållanden. Ursprungligt koncentrationsfält befanns stå för den mest betydelsefulla osäkerheten.

Bra överensstämmelse fanns mellan M3-modellens resultat och den hydrodynamiska modellen för grundvattenflöde och transport av lösning. Generellt kan påstås att det finns en överensstämmelse mellan båda modelltyperna. Denna överensstämmelse stöttar hypotesen om att Äspös grundvattensystem består av en blandning av fyra olika grundvattentyper, på det sätt som M3-modellen visar. M3-resultaten har varit värdefulla för att mejsla ut vissa aspekter på Äspös hydrogeologi. Jämförelsen av resultat från hydrodynamiska modellen med resultat från blandningsmodellen måste emellertid tas på största allvar till följd av kombinationen av osäkerheter hos blandningsmodellen (±10%) i kombination med upptäckta osäkerheter vid interpolationen av blandningsfraktionerna på provtagningsplatserna (±10%).

Prediktion på 3 av de 4 föreslagna prediktionsplatserna har utförts. De inkluderar en grundberäkning (bästa prediktion) och en andra beräkning under användande av alternativa ursprungliga koncentrationsfält. Resultaten i båda beräkningarna redovisar pålitliga prediktionsspann, vilket var i överensstämmelse med fältmätningar.

Den kemiska reaktionens roll har utvärderats med hjälp av jämförelse av datorberäknade resultat med uppmätta koncentrationer för de typiska icke-sorberande ämnena. Källor för bikarbonat, kalcium och sulfat har tydligt detekterats, och antas bestå av kemiska processer. Ett annorlunda uppträdande av kalcium och bikarbonater har påvisats beroende på placeringen av sprickzoner. En hypotes är att karbonatsystemet kan påverkas av den högre tillgängligheten av Fe(III) som antas finnas under Äspö ö. Såsom Banwart (1999) föreslår för redoxzonen kan koloxidering via reduktion av Fe(III) utgöra en källa för bikarbonater. Denna hypotes (och andra kemiska uppträdanden som fortfarande är oklara) kan valideras eller förkastas kvantitativt med hjälp av kopplat grundvattenflöde och reaktiv transportmodellering.

INDEX

ACKNOWLEDGMENTS

Work contained in this report has been carried within the framework of a Research Project funded by ENRESA dealing with Testing and Validation of Coupled Water Flow and Reactive Solute Transport. We want to thank ENRESA and SKB for their support, and also to the people involved in the Task 5, specially to P. Wikberg and I. Manson. Thanks also go to I. Rhén and U. Svensson for his kindness and fruitful discussions and comments during the Task Force meetings. We also thank the comments and suggestions of M. Laaksoharju, I. Gurban and J. Smellie regarding the hydrochemistry of the Äspö site. The permission to pursue a stay at the Äspö Hard Rock Laboratory is aknowledged to Ö. Olsson. The first author gratefully appreciate the kindly assistance provided by all the Äspö staff, and specially by M. Morosini, during the performed stay at the Äspö HRL.

This version of the Final Report has been updated taking into account the comments and suggestions of the Äspö Task Force Reviewers. We think these comments were well taken and relevant and we wish to record here our gratefulnes to them.

1 INTRODUCTION

1.1 BACKGROUND

The Äspö HRL is an underground laboratory for the development and testing of methods for detailed characterisation of fractured rock volumes. In addition to be a full scale laboratory, the Äspö HRL provides a multitude of data to improve the knowledge of the crystalline bedrock and for testing models of groundwater flow, groundwater composition and solute migration.

After the regional geological investigations, the construction of the Äspö HRL underground facilities was started in October 1990 and completed during the summer of 1995.

The Äspö Task Force on Modelling of Groundwater Flow and Transport of Solutes was initiated in 1992. The Task Force is a forum where the different organizations involved into the Äspö HRL interact in the area of conceptual, mathematical and numerical modelling of groundwater flow and solute transport in fractured rock. Within these activities, Task Force #5 was initiated in February 1997 with the aim to compare and integrate hydrochemistry and hydrogeology.

The nature of the flow at repository level and the chemical composition of the groundwater are essential for the calculations of nuclide migration. The composition and evolution of the groundwater chemistry depends on: (1) Groundwater flow, (2) Solute transport through fractures and matrix blocks, (3) Heat transport and (4) Homogeneous (solute-solute) and heterogeneous (solute-mineral) chemical reactions.

Therefore, it is of interest to combine groundwater flow and chemistry. However, this is difficult for several reasons. First of all, a wide range of physical, chemical, thermal and hydrodynamic processes are involved. A second reason has to do with numerical aspects. The problem involves many partial differential equations together with nonlinear algebraic equations. The simultaneous solution of water flow, reactive solute transport and heat transfer equations requires a numerical effort which is orders of magnitude greater than that required for modelling conservative solute transport or speciation of a static water solution.

In addition of the numerical aspects, carrying out a reactive transport model requires a solid hydrogeological model and a good knowledge of the hydrochemical patterns.

1.2 OBJECTIVES

The aim of Task #5 is to compare and ultimately integrate hydrochemistry and hydrogeology. The Task will also be useful for a future assessment of the stability of the hydrodynamic and hydrochemical conditions at Äspö. This modelling approach could then be used for any future repository site investigations and evolution, especially in crystalline bedrock environment.

The specific objectives of the Task #5 are:

- To assess the consistency of groundwater flow models and hydrochemical mixing-reactions models through integration and comparison of hydraulic and chemical data obtained before and during tunnel construction.
- To develop a procedure for integration of hydrological and hydrochemical information which could be used for disposal site assessments.

On the other hand, the main objective of the University of La Coruña (ULC) – ENRESA team is to validate (to the extent that is possible) current Thermo-Hydro-Geochemical (THG) codes for coupled water flow, heat transfer and multicomponent reactive transport. In other words, the objective is to test the ability of these codes to cope with the complex hydrogeological and hydrochemical settings which are expected to be found in a real HLW repository. The calibration-validation-prediction scheme that has been follow in this work is illustrated in Figure 1.1. This figure is a sketch of the general modeling methodology.

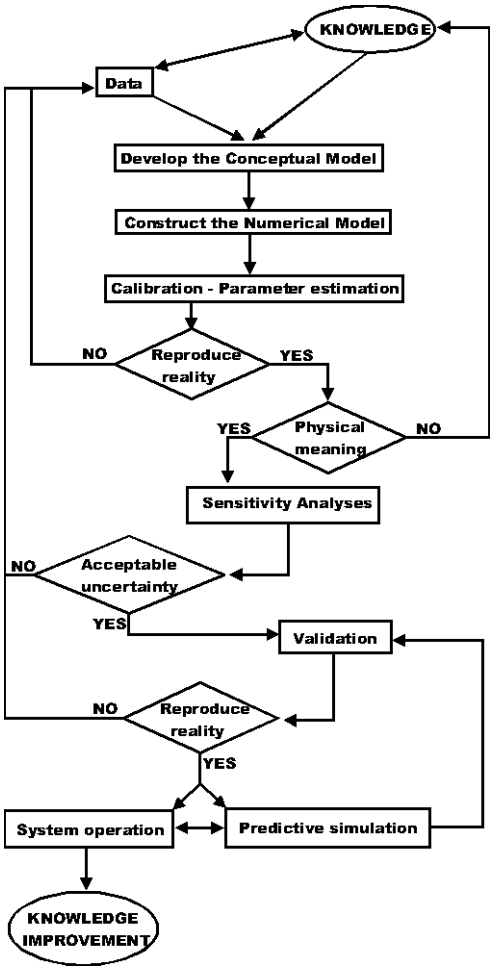

Figure 1.1 Sketch of the general modeling methodology

As it was said before, setting up a fully coupled groundwater flow and reactive transport model requires solid hydrogeological and hydrochemical models and, in addi-

tion, implies to make a big effort of integration. For this reason, the Task #5 provides to the ULC-ENRESA team a unique opportunity to finally reach the proposed main goal.

1.3 SITE DESCRIPTION

The Äspö island is situated in the southeast part of Sweden, 400 km south of Stockholm, and geographically is a granitic coastal island in the Baltic Sea, separated from the mainland and several other islands by shallow sea branches (see Figure 1.2).

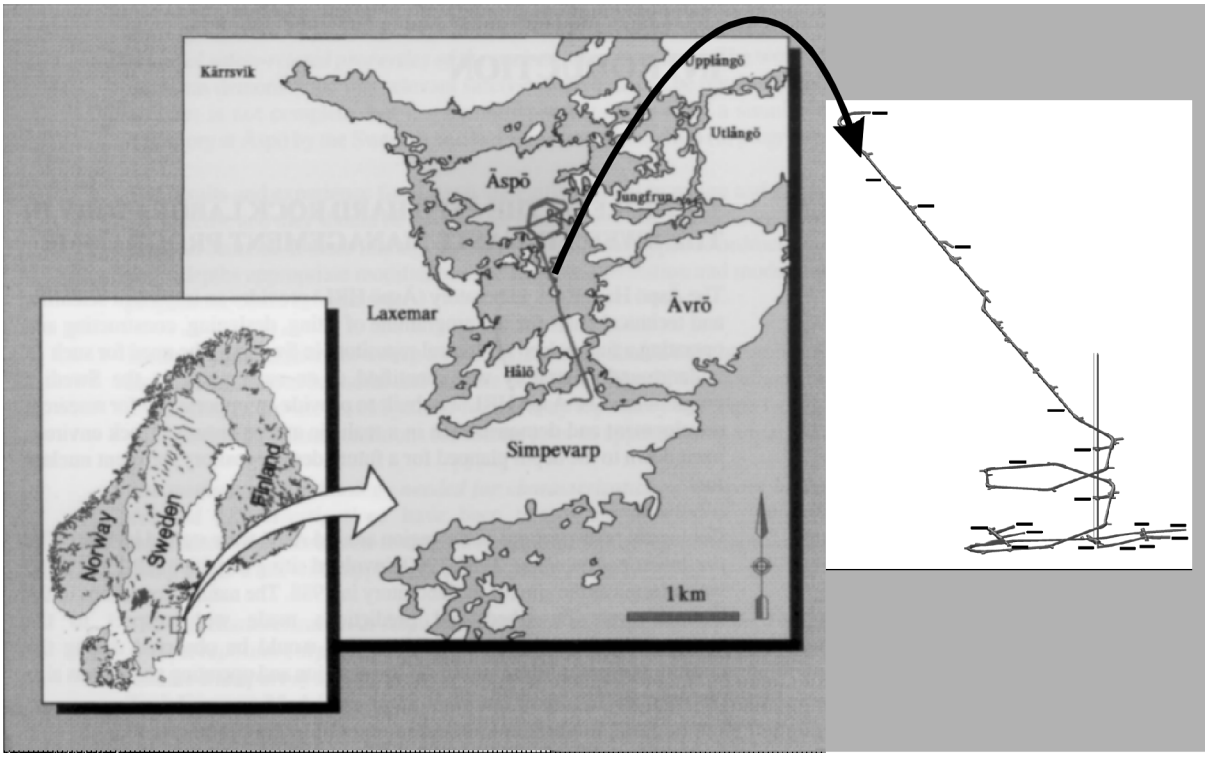

Figure 1.2. Location of the Äspö Hard Rock Laboratory and 3D view of the underground facilities (tunnel & elevator). Modified after Rhén et al. (1997 a).

The rocks of the area are predominantly granitoids, belonging to the TransScandinavian Igneous Belt. This rocks together with some volcanics others were emplaced and extruded during several pulses of Precambrian magmatism (Larson & Berglund, 1992). This granitoids have a range of mineralogical composition between true granites, which occur on Ävrö island and the Southern part of Äspö, to granodioritic to dioritic composition, which is most common on the northern part of Äspö (Kornfalt & Wikman, 1988).

The Äspö HRL facilities consist on a 3600 m lenght tunnel with a long tunnel ramp coming from the Simpevarp peninsula, and an spiral part under the Äspö island. The tunnel goes down more than 450 m depth (Figure 1.2). On the Äspö island surface, the Research Village of the laboratory is connected with the underground facility by means of an elevator (Figure 1.2).

2 CONCEPTUAL MODEL

The huge amount of research efforts done during the pre-investigation and construction phases (years 1986-1995) at Äspö site has provided strong conceptual models about the geology (litology and structure), hydrogeology and hydrochemistry. An excellent compilation of these topics can be found in Rhén et al. (1997a) and Rhén et al. (1997b). In order to introduce some concepts and ideas used in the numerical model, a brief summary of the conceptual models is presented in this chapter. Most data and concepts have been found in Rhén et al. (1997 a,b).

2.1 SURFACE HYDROLOGY

The land surface of Äspö is slightly undulating, with a maximum height of 14 m. There are no perennial streams on the island, and the surface water is drained to the sea by the peatlands, sediments or directly to the sea.

The mean precipitation in the area is about 675 mm/year and about 18% falls as snow. The calculated actual evapo-transpiration (ET) is 490 mm/year and the potential ET is 616 mm/year. Run off for the area around Äspö is estimated to be between 150 and 200 mm/year. The annual mean temperature (presently) is around 6.5 ºC.

Svensson (1997) studied the groundwater recharge by means of numerical modelling. The author concluded that the value of the infiltration depends on the local level of the water table ranging between 0.4 mm/year in natural conditions and 134 mm/year with the tunnel construction completed.

Knutson & Morfeldt (1993) suggest a value of 10% of the total precipitation for groundwater recharge to outcrop-moraine areas (which correspond to 55-68 mm/year). Previous ,modelling of the groundwater flow at Äspö suggest that 10% to 20% of the total amount available for run-off and recharge actually infiltrates to the deeper rock (which correspond to 5-35 mm/year) (Banwart et al., 1999).

2.2 WATER TABLE

The groundwater level under natural conditions ranges between 0-4 m above mean sea level and approximately follows the topography. Due to the drawdown caused by the inflow to the tunnel, the elevation of the water table decreased during its construction. The minimum water table elevation in 1995 was about 100 m below sea level and the piezometric heads measured are more or less stable since the excavation was ended in February 1995 (Stanfors et al., 1999).

2.3 TEMPERATURE AND SALINITY

The salinity of the Baltic Sea around Äspö is approximately 6 g/l, but varies with location and time of sampling. There is a clear depth dependence of the salinity in the groundwater of Äspö site. The fresh water lens below Äspö has a thickness of 100-200 m under natural conditions and below this level, the salinity increases to reach a

value about 20 g/l at a depth of 800 m. The temperature gradient is more or less 15 ºC/km (Ahlbom et al, 1995).

2.4 GROUNDWATER FLOW

The Äspö site scale model covers a block of 2x2 km and 1 km depth, with the Äspö island located approximately in the middle of the top surface. Geometrically the model comprises two fundamental concepts:

a) *Hydraulic conductors domains*, which are large two-dimensional features with hydraulic properties different from the surrounding rock. They are generally defined geologically as major discontinuities but in some cases they may mainly be defined by interpretation of results from hydraulic interference testing.
b) *Hydraulic rock mass domains* are geometrically defined volumes in space with properties different from surrounding domains (rock mass or conductors). They may either be defined by lithological domains or purely by interpretation of results from hydraulic test.

Figure 2.1 shows the schematic description of these two main geohydrological concepts.

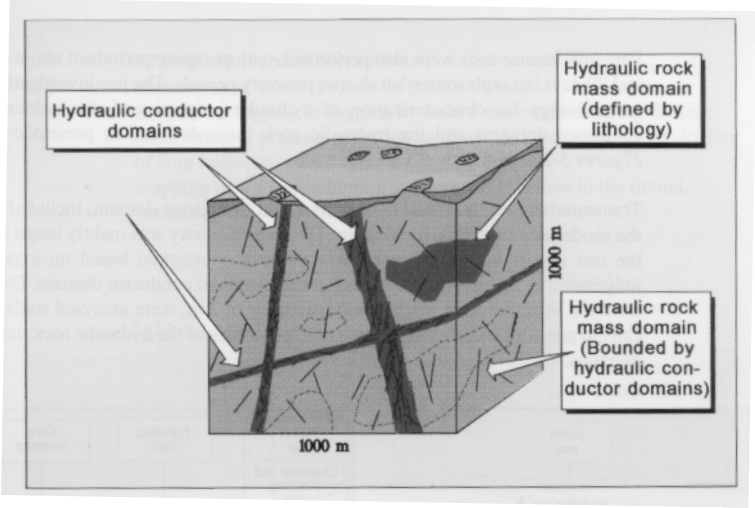

Figure 2.1 Schematic description of two main hydrogeological concepts: hydraulic conductors domains and hydraulic rock mass domains. Rhén et al. (1997 a)

Figure 2.2 shows a map of the hydraulic conductor and rock mass domains of the Äspö site scale conceptual model.

The exact location and the hydrogeological parameters of each domain can be found in Rhén et al. (1997 b). For hydraulic conductor domains the transmisivity and the storage coefficient is provided deterministically, meanwhile for rock mass domains the properties are assigned stochastically.

The evaluated transmissivities for the hydraulic conductors domains are generally within the range 10^{-6} – 10^{-4} m^2/s with a median about 10^{-5} m^2/s. The maximum transmissivity is $3x10^{-4}$ m^2/s for hydraulic conductor domain NE-1. For the rock

mass domains the hydraulic conductivity takes values around 3 x 10^{-10} m/s.

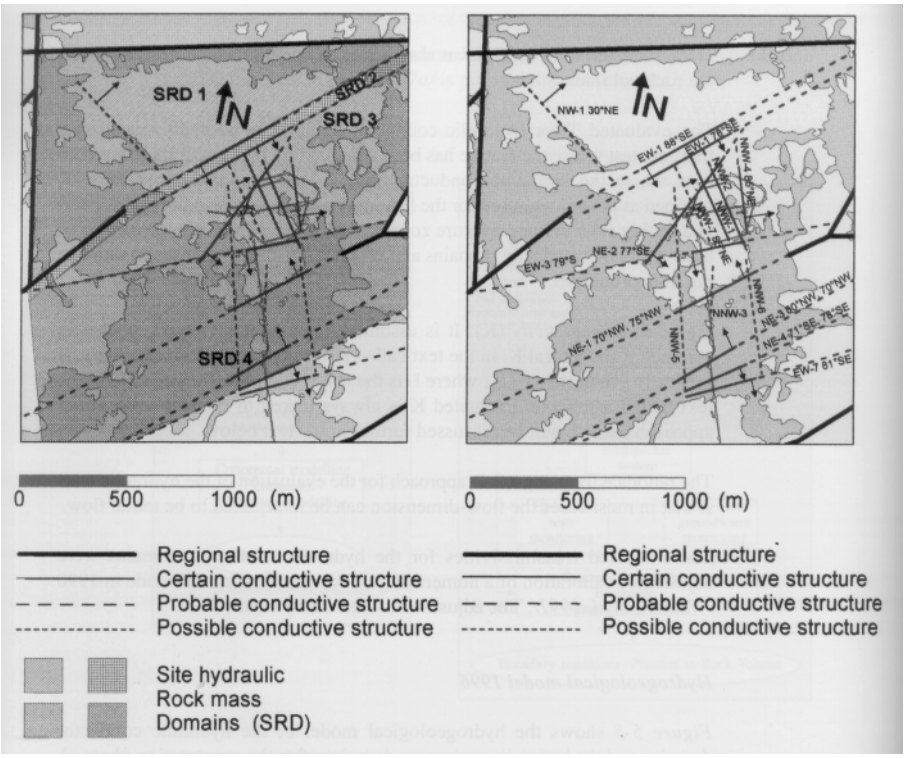

Figure 2.2 Hydraulic rock mass and conductor domains of the conceptual model. Rhén et al. (1997 b).

There are a few interference tests at Äspö HRL that are judged to be useful for evaluation of the storage coefficient because it is difficult to assume the radial flow condition in a fractured media. However it was possible to assume the radial flow condition in some test, mainly within a subplanar feature highly conductive, and using these data, Rhén et al (1997 b) obtain the following relationship:

$$S = aT^b \tag{2.1}$$

where T is the transmissivity (m^2/s), S is the storage coefficient, a = 0.00922 and b=0.785. The relationship was adjusted using 5 values obtained with a test scale of 100 m. The correlation coefficient was $\rho = 0.71$.

In general, the major fractures and fracture zones control recharge, discharge and groundwater flow through the island (Smellie & Laaksoharju, 1992).

2.5 TRANSPORT OF SOLUTES

In order to estimate the transport properties of the rocks in the Äspö area, a few tests have been performed. Most of the data concerning transport of contaminants were evaluated from the LPT2 test, the NE-1 test and the TRUE project.

Rhén et al. (1997b) obtained a relationship between the kinematic porosity (n_e) and the hydraulic conductivity (K in m/s). The equation 2.2 shows this relationship:

$$n_e = 34.87K^{0.753} \quad (2.2)$$

Values for matrix porosity have been measured in samples of different rocks. This values ranges from the minimum of the fine-grained granites (0.23%-0.27%) to the maximum of the Äspö diorite (0.40%-0.45%).

An important parameter concerning the transport of solutes is the dispersivity. This parameter takes into account the heterogeneity of the velocity field. Actual flow paths in porous and fractured media are highly irregular and some water particles move faster than the average velocity while others displace more slowly. Rhén et al. (1997 b) plotted the available values of the dispersivity coefficients (α) as a function of the spatial scale (s in m), fitting a linear approximation between Log10 (s) and Log10 (α). The obtained relationship was:

$$\alpha = 0.053s^{1.21} \quad (2.3)$$

Recently, Holmquist & Anderssson (1999) carried out a compilation of transport parameters derived from 3 in-situ tracer transport experiments performed at the Äspö island and within the Äspö HRL. This work was the main available database for transport parameters.

3 MATHEMATICAL MODEL

3.1 GROUNDWATER FLOW

Water flow through porous media is governed by Darcy's Law which in its most general form relates water flux $\underline{q}$ to the gradient of water pressure p and elevation z through:

$$\underline{q} = -\frac{\underline{\underline{k}}}{\mu}(\nabla p + \rho \underline{g}) \tag{3.1}$$

where ρ and μ are water density (mass per unit volume) and dynamic viscosity, $\underline{\underline{k}}$ is intrinsic permeability and $\underline{g}$ is a vertical vector pointing downwards of modulus equal to gravity acceleration. When density changes are negligible, Darcy's Law can be written in terms of hydraulic head h as:

$$\underline{q} = -\underset{\sim}{K}\nabla h \tag{3.2}$$

where

$$\underset{\sim}{K} = \frac{\rho \underline{\underline{g}}}{\mu}\underline{\underline{k}} \tag{3.3}$$

and

$$h = \frac{p}{\rho g} + z \tag{3.4}$$

Here $\underset{\sim}{K}$ is the hydraulic conductivity tensor. By combining Darcy's Law and the mass balance equation one has:

$$\nabla \cdot (\underset{\sim}{K}\nabla h) + w = S_s \frac{\partial h}{\partial t} \tag{3.5}$$

where w represents fluid sink/sources per unit volume of medium and S_s is the specific storage coefficient, defined as the volume of water delivered per unit time and unit volume of medium in response to a unit change of hydraulic head.

At the boundary Γ of the domain R either the head or its gradient (water flux) are known. Possible conditions include:

(1) Dirichlet condition:

$$h(x, y, z, t)\big|_{\Gamma_1} = H \tag{3.6}$$

(2) Neumann condition:

$$\underset{\sim}{T}\nabla h \cdot n\Big|_{\Gamma_2} = Q \tag{3.7}$$

(3) Mixed condition:

$$\underset{\sim}{T}\nabla h \cdot n\Big|_{\Gamma_3} = \alpha(H-h) \tag{3.8}$$

where H and Q are specified heads and fluxes, α is a leakage coefficient (LT^{-1}) and $\underset{\sim}{T}$ is the transmisivity tensor.

3.2 TRANSPORT OF CONSERVATIVE SOLUTES

Dissolved species in saturated media are subject to various physical and chemical processes. The main transport processes are: (1) advection, (2) molecular diffusion and (3) hydrodynamic dispersion. Each of these processes produces a solute mass flux $\underline{F}$ (mass of solutes crossing a unit surface area of medium per unit time).

3.2.1 ADVECTION

Advection refers to solute migration associated to water flow. Solutes move with water. If water flows at a specific discharge $\underline{q}$ (volumetric water flux), the advective mass flux $\underline{F}_A$ is given by:

$$\underline{F}_A = \underline{q}c \tag{3.6}$$

where c is solute concentration, usually expressed as solute mass grams (or moles in reactive solute transport) per unit fluid volume. Solutes migrate at an average velocity $\underline{v}$ given by:

$$\underline{v} = \frac{\underline{q}}{\theta} \tag{3.7}$$

where θ is the volumetric water content which is equal to the porosity ϕ for saturated media. The advective mass flux can also be obtained as:

$$\underline{F}_A = \theta \underline{v}c \tag{3.8}$$

3.2.2 MOLECULAR DIFFUSION

Molecular diffusion is a transport mechanism related to the continuous Brownian motion of solute and fluid molecules. For pure water, molecular diffusion produces a mixing effect which obeys Fick's Law. This law states that the diffusive solute flux $\underline{F}_D$ is proportional to the concentration gradient ∇c :

$$\underline{F}_D = -D_0 \nabla c \tag{3.9}$$

where D_0 is the molecular diffusion coefficient in water. The diffusion coefficient of very small, near-spherical, particles in water is given by the Stokes-Eistein relation-

ship:

$$D_0 = \frac{kT}{6\pi\mu_w r} \tag{3.10}$$

where k is Boltzmann's constant, μ_w is the absolute viscosity of water and r is hydrodynamic radius of the particle. Although this relationship does not take into account chemical interactions between the solute and the solvent, it does provide a correct order of magnitude estimate of D_0 for many dissolved species in water. For hydrated ions, r is the radius of the hydration shell. Chemical species diffusing through the solution-filled pore spaces of a porous medium encounter along their path an irregular network of pore channels and frequently collide with the walls of these channels. Diffusion through this porous space is slower than it would be in the absence of the mineral framework. Based on these simple concepts of the diffusional process, the physical characteristics of the rock responsible for slowing down molecular diffusion are generally considered to be the water content θ itself, the pore size distribution and the tortuosity, τ, of the diffusional paths.

In a porous medium solutes can only diffuse along fluid pores following tortuous paths. This means that the effective molecular diffusion coefficient for a porous medium, D_e, is smaller than that for pure water. Usually is related to D_0 through:

$$D_e = \theta D_0 \tau \tag{3.11}$$

where τ is the medium tortuosity.

Therefore, the diffusive flux in porous media is given by:

$$\underline{F}_D = -D_e \nabla c \tag{3.12}$$

3.2.3 HYDRODYNAMIC DISPERSION

In addition to molecular diffusion there is a mixing phenomenon known as hydrodynamic dispersion which also produces both longitudinal and transverse solute spreading. This mixing effect is caused by medium heterogeneities. Actual flow paths are highly irregular. Some water particles move faster than the average velocity while others displace more slowly. The overall effect of all heterogeneities is a solute spreading in all directions. Laboratory and field evidence indicates that this phenomenon can also be described by Fick's Law, so that the hydrodispersive flux $\underline{F}_H$ can be described as:

$$\underline{F}_H = -\theta \underset{\sim}{D}_H \nabla c \tag{3.13}$$

where $\underset{\sim}{D}_H$ is the hydrodynamic or mechanical dispersion tensor. Its principal directions coincide with the flow direction and its normals. The component along the flow direction D_L is the largest and is given by:

$$D_L = \alpha_L |v| \tag{3.14}$$

while the smallest components D_T occur along the transverse directions and are given by:

$$D_T = \alpha_T |v| \tag{3.15}$$

where $|v|$ is the modulus of the velocity vector $\underline{v}$, and α_L and α_T are the longitudinal and transverse dispersivities which are characteristic parameters of the medium having dimensions of length which measure the scale of the spatial heterogeneities.

In general, $\underset{\sim}{D}_H$ is a symmetric tensor whose components in two dimensions are:

$$D_{xx} = \frac{\alpha_L v_x^2 + \alpha_T v_y^2}{|v|} \tag{3.16 a}$$

$$D_{yy} = \frac{\alpha_L v_y^2 + \alpha_T v_x^2}{|v|} \tag{3.16 b}$$

$$D_{xy} = D_{yx} = (\alpha_L - \alpha_T)\frac{v_x v_y}{|v|} \tag{3.16 c}$$

For practical purposes, the effects of molecular diffusion and hydrodynamic dispersion are usually lumped together in a single dispersion tensor $\underset{\sim}{D}$ which takes the form:

$$\theta \underset{\sim}{D} = \underset{\sim}{I} D_e + \theta \underset{\sim}{D}_H \tag{3.17}$$

where $\underset{\sim}{I}$ is the identity tensor.

3.2.4 SOLUTE TRANSPORT EQUATIONS

The equation governing solute transport through porous media is derived from the principle of mass conservation. This principle states that for any reference elementary volume of medium, the net flux plus sink/source terms must be equal to the time rate of change of the solute mass contained in the reference volume. Solute mass per unit volume of medium is equal to θc . The net mass flux is given by minus the divergence of the total flux vector. Therefore, mass conservation leads to the following equation:

$$-\nabla \cdot (\underline{F}_A + \underline{F}_D + \underline{F}_H) = \frac{\partial(\theta c)}{\partial t} \tag{3.18}$$

where $\nabla \cdot (\ )$ is the divergence operator which when applied to a vector $\underline{F}$ of

components (F_x,F_y,F_z) is equal to:

$$\nabla \cdot (\underline{F}) = \frac{\partial F_x}{\partial x} + \frac{\partial F_y}{\partial y} + \frac{\partial F_z}{\partial z} \tag{3.19}$$

Substitution of mass fluxes $\underline{F}_A$,$\underline{F}_D$ and$\underline{F}_H$ into the continuity Equation 3.18 leads to:

$$-\nabla \cdot (\theta \underset{\sim}{D} \nabla c) - c\nabla \cdot \underline{q} - \nabla c \cdot \underline{q} = \frac{\partial(\theta c)}{\partial t} \tag{3.20}$$

Possible solute sinks and sources are added to the left-hand-side of this equation. For a fluid source of water flux w (per unit volume of medium) having a concentration c', and a solute sink/source term R (solute mass added per unit time and unit fluid volume) the transport equation becomes:

$$-\nabla \cdot (\theta \underset{\sim}{D} \nabla c) - \underline{q} \cdot \nabla c + w(c' - c) + \theta R = \theta \frac{\partial(c)}{\partial t} \tag{3.21}$$

where the following identity, which derives from the flow equation, has been taken into account:

$$\left(-\nabla \cdot \underline{q} + w - \frac{\partial \theta}{\partial t}\right) c = 0 \tag{3.22}$$

The solution of the transient solute transport equation requires knowing:

(1) transport parameters which include: water content θ, molecular diffusion coefficient D_e , and dispersivities (α_L, α_T).

(2) sink/sources: w, c' and R.

(3) initial conditions: $c_0(x,y,z)$ at $t=t_0$

(4) boundary conditions

The initial condition c_0 is either known or may correspond to the solution of a steady-state transport problem such as:

$$-\nabla \cdot (\theta \underset{\sim}{D} \nabla c_0) - \underline{q} \cdot \nabla c_0 + w(c_0' - c_0) + \theta R_0 = 0 \tag{3.23}$$

At the boundary of the domain, either concentration or a function of its gradient must be known. Possible types of boundary conditions include:

(1) Dirichlet condition. The points lying at this part of the boundary Γ_1 satisfy the following condition:

$$c|_{\Gamma_1} = \tilde{c} \tag{3.24}$$

where $\tilde{c}$ is a specified concentration, which may vary in space and time.

(2) Neumann condition. Let $\underline{n}$ be the unit vector normal to Γ_2, the part of Γ at which the dispersive flux F'_D is known. This type of condition is:

$$-\theta \underset{\sim}{D} \nabla c \cdot \underline{n}\Big|_{\Gamma_2} = F'_D \tag{3.25}$$

This equation states that the component of the dispersive flux normal to the boundary is known. This condition is usually imposed at impervious boundaries where F'_D is equal to zero.

(3) Cauchy mixed condition. Some parts of the boundary Γ_3 may have a condition in terms of the total mass flux:

$$(-\theta \underset{\sim}{D} \nabla c + \underline{q} c) \cdot \underline{n}\Big|_{\Gamma_3} = F_0 \tag{3.26}$$

The imposed flux is given by F_0. Usually F_0 is taken equal to the advective flux $c\underline{q} \cdot \underline{n}$. At outflow boundaries it is usually assumed that the solute mass flux is given by the product of the water flux $\underline{q} \cdot \underline{n}$ times the concentration c of the flowing water. In this case, $c\underline{q} \cdot \underline{n} = F_0$ and therefore the boundary condition reduces to:

$$-\theta \underset{\sim}{D} \nabla c \cdot \underline{n}\Big|_{\Gamma_3} = F_0 \tag{3.27}$$

which is a particular case of the type (2) condition.

When the transport equation is integrated over aquifer thickness b, the result is:

$$-\nabla \cdot (\theta b \underset{\sim}{D} \nabla c) - b\underline{q} \cdot \nabla c + r(c' - c) + b\theta R = b\theta \frac{\partial c}{\partial t} \tag{3.28}$$

where r is the fluid source term per unit surface area.

4. NUMERICAL MODEL

4.1 NUMERICAL TOOL

The code used to solve the equations of the numerical model was TRANMEF-3 (Juanes, 1997) developed in the Hydrogeology Group of the University of La Coruña.

TRANMEF-3 is a general numerical code for solving groundwater flow, multi-component weakly-reactive solute transport and heat transport in heterogeneous (fractured) formations.

All the capabilities of the program are explained in the User's Manual (Juanes, 1997). TRANMEF-3 solves water flow, solute transport and heat transport simultaneously, or any of then separately. The Finite Element Method is used for discretization of space while a general Finite Difference scheme is used for time discretization.

The program performs an "exact" treatment of the Boundary Conditions, by fully integrating along boundaries. TRANMEF-3 handles 6 different type of elements, that can be used arbitrarily together in any simulation problem. Moreover, and here stays the most interesting point, these elements do not need to have the same dimensions (they can be either 1-D, 2-D or 3-D). This capability allows to simulate, for example, 1-D and 2-D fracture networks in a general 3-D porous medium. Numerical Integration through the elements and element faces is taken into account, using Gauss quadrature in any dimension varying from 1 to 3, and order of integration between 1 and 4 for any kind of element.

4.2 MODELLING APPROACH

4.2.1 INTRODUCTION

In order to deal with the wide variety of flow and transport problems in fractured media, a number of modelling approaches have been developed. Following the classification of modelling approaches proposed by Berkowitz (1994) there are tree main types categories for fractured hydrogeological models: (1) Discrete fracture models, (2) Continuum models and, (3) Hybrid models. Other approaches are possible, such as stochastic and hierarchical models.

Discrete fracture models consider flow and transport processes within isolated (and normally connected) fractures. Analysis of problems with this approach has provided fundamental understanding of behaviour of relevant processes (Berkowitz, 1994). The main problem of this approach is the geometrical definition of the system. A number of conceptualizations have been developed, which range from the simplest parallel plate model to 3-D fracture networks with variable aperture. Channelling models (Moreno et al., 1988) are also a particular type of this approach.

Continuum models consider the whole fractured medium as an equivalent porous medium. This approach is valid as long as it is possible to define a REV (Representative Elemental Volume) for the problem of interest. These models are applicable

when the system allows sufficient interaction between fractures and porous blocks to allow establishment of local equilibrium. This approach solves the geometrical problem, but usually it is very difficult to find an adequate REV in fractured media.

Hybrid models are in the middle of the two approaches described above. This approach combines continuum representation of the domain with a discrete representation of the primary fractures in the formation.

4.2.2 MODELLING APPROACH AND METHODOLOGY FOR THE ÄSPÖ SITE SCALE MODEL

As was mentioned before, the numerical tool used (TRANMEF-3) has the capability to handle multidimensional finite elements. This fact allows to simulate three-dimensional blocks of rock together with the main fractures defined as two-dimensional planes. The multidimensional capability is useful to reduce the number of elements and thus save CPU time and computer memory requirements.

The original plans of the ULC group for coping with the Äspö model were based on the use of a hybrid approach, including 3-D rock domains and 2-D conductor domains.

Methodologically, the numerical model was started as a continuum model (with 3-D elements) as a starting point before including the 2-D conductor domains. However, preliminary results obtained with the continuum model indicated the need to account for discrete fractures. Therefore, the discrete fracture approach was adopted. This decision was taken because:

1) The computed flow rate into the tunnel using the continuum model was less than a 7 % of the measured value, even with an equivalent permeability larger than the median of the measured permeability.
2) The analysis of the measured flow rates indicates that the sections containing no hydraulic conductor domains contribute very little to the total flow rate. In addition there are evidences that in the Äspö area, major fractures and fractures zones control the groundwater system (Smellie & Laaksoharju, 1992).
3) Using a discrete fracture network approach allows us to save a lot of CPU time and memory. This is an important point due to the large number of calibration runs that are foreseen.

4.3 SPATIAL DISCRETIZATION

4.3.1 GEOMETRY

The model domain consists in a three dimensional block of 2 x 2 km on the upper surface and 1 km depth (Figure 4.1). Inside this volume 19 of the 20 hydraulic conductor domains (HCD) have been considered (Figure 5.1). SFZ-14 is not considered because it is not crossed by the tunnel and neither connected with any other HCD. Then, in a Discrete Fracture Networks model this HCD is not playing any role. On the other hand, 11 out of the 19 HCD cross the Äspö HRL tunnel and elevator (Figure 4.1).

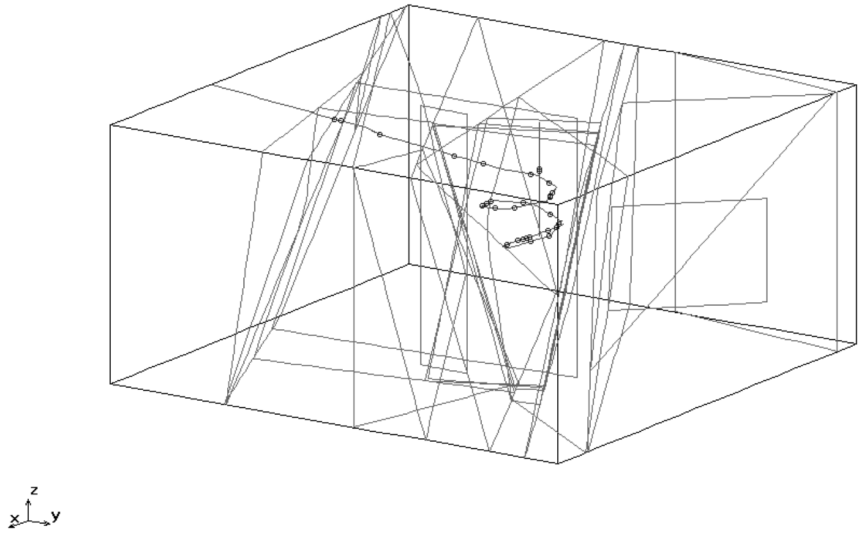

Figure 4.1 Model domain considered in the numerical model with the 20 major hydraulic conductor domains, the Äspö HRL tunnel and the elevator. The points represent the intersection between the tunnel-elevator and the hydraulic conductor domains.

4.3.2 FINITE ELEMENT MESH

The finite elements mesh generated for the Discrete Fracture Networks Models consists on 12,847 nodes and 14,273 elements. Most of them are 2-D quadrilateral and triangular elements for the hydraulic conductor domains discretization but, there are also 1-D linear elements to represent intersections between HCD and between de conductors and the external boundaries. HRL tunnel and elevator have been also discretized by means of 1-D linear elements.

Figures 4.2 and 4.3 show the details of the spatial discretization for the Discrete Fracture Networks Model.

4.4 TIME DISCRETIZATION

For the Task #5 exercise the proposed model was specified to start on 1990-10-01. Instead of this date, the Discrete Fracture Networks model starts on 1991-06-27, because this is the date in which the tunnel crossed the first Hydraulic Conductor Domain (EW-7). The final time for the model is the 1997-01-01. Therefore, the numerical model covers a period of 2013 days.

Time discretization (Δt) are equal to 1 day, except for the dates when the tunnel crosses a HCD when Δt is ten times smaller. This discretization criterion for the time leads to a total of 2275 time steps.

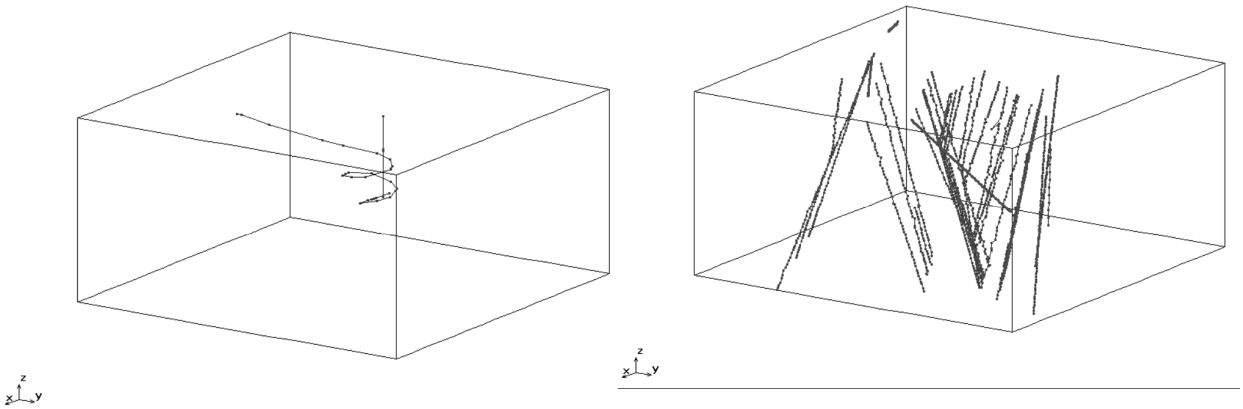

Figure 4.2. 1D finite elements representing the HRL tunnel and elevator, and hydraulic conductor domains intersections.

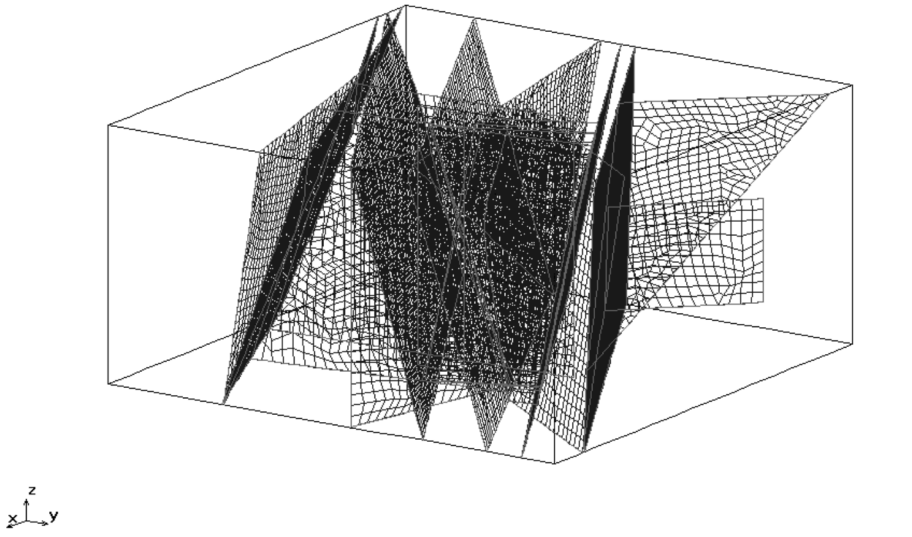

Figure 4.3. Spatial discretization used for the hydraulic conductor domains, using 2D (quadrilateral and triangular) finite elements.

A key point of the model is the simulation of the tunnel construction process. There are two decisions to be taken concerning with this issue:

1) How many stages must be considered to simulate de tunnel front movement.
2) How to represent the tunnel advance in the numerical model.

To simulate the tunnel advance there are two possibilities: (1) to simulate each stage with a single computer run, using as initial conditions the results computed by the previous run and, (2) to simulate the whole tunnel construction (all the stages)

within a single run. A single run for the whole tunnel construction is a time-saving option which avoids reading and writing intermediate computed results. In addition, this is a better option in order to prevent possible mistakes. However, to model the entire construction in a single run the code must be able to handle with time varying boundary conditions.

In the numerical model presented in this report a mixed condition was adopted for the tunnel internal boundary. Using the mixed boundary condition, a minor change in the numerical code must be done in order to be able to model the whole process of the tunnel advance using just a single computer run. The change consists on implement the capability of handle with leakage coefficients values variable in time. In this way, the leakage coefficient of a node will have a zero value (no boundary condition) for the time before the tunnel arrive to the node location, and will have a non-zero value after this time.

The tunnel front movement has been simulated by using 29 stages, one stage for each time that the tunnel crossed a Hydraulic Conductor Domain. Figure 4.4 compares the real advance of the tunnel front with the 29 stages considered in the numerical model

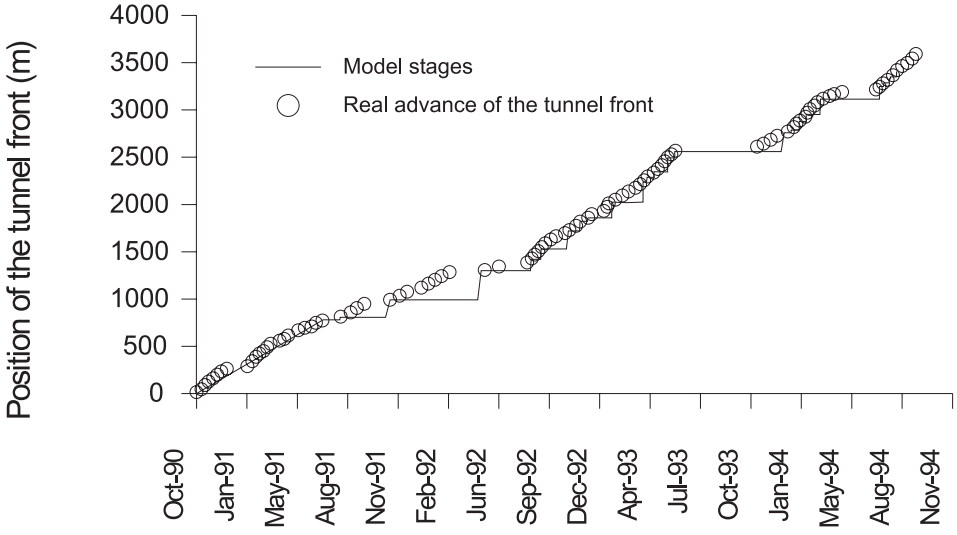

Figure 4.4 Representation of real tunnel front advance and model stages used to simulate the tunnel construction.

4.5 BOUNDARY AND INITIAL CONDITIONS

4.5.1 GROUNDWATER FLOW

- Side boundaries: Dirichlet condition with h* = 1000 m.
- Bottom boundary: Neumann condition (impervious, Q* = 0).
- Upper boundary I (Baltic sea):Dirichlet condition with h* = 1000m.
- Upper boundary II (Lands): Specified groundwater recharge R = 5 mm/year.
- Inner Boundaries (tunnel & elevator): Dirichlet condition with a prescribed pressure head equal to atmospheric pressure.

Figure 4.5 shows the 1-D elements used to represent the intersections between HCD and the upper external boundary. In this figure it is possible to distinguish the elements corresponding to emerged lands (with surface recharge) and the elements under the Baltic sea (prescribed head pressure).

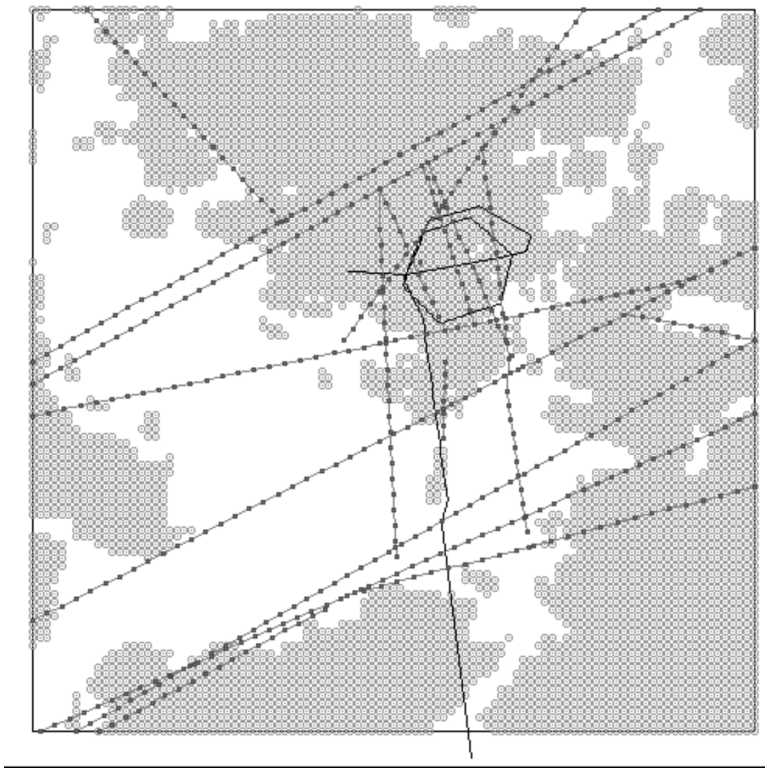

Figure 4.5 1D elements used to represent the intersection between H.C.D. and the upper boundary. In the figure it is represented the emerged land (grey) and the Baltic sea (white). Elements on the land have recharge boundary condition while elements on the sea have Dirichlet condition.

An initial hydraulic head of 1000 m was assigned to the whole domain.

4.5.2 TRANSPORT OF SOLUTES

- Side boundaries: Solute Flux associated to water flux (no dispersion).
- Bottom boundary: No flux.
- Upper boundary I (Baltic sea): Dirichlet condition with Baltic sea water concentration.
- Upper boundary II (Lands): Dirichlet condition with meteoric concentration.
- Inner Boundaries (tunnel & elevator): Solute flux associated to water flux.

To define the initial conditions of solute transport it is needed to interpolate from the 3-D data grid provided by Task #5 data deliveries to the nodes of the finite element mesh. For finding out the values to use in the finite element mesh, the first adopted solution (the easiest) was to find the closest point of the data grid to each one of the nodes and use that concentration value. This is a very poor approach, because it

is possible to find in the data grid two neighbour points having very different solute concentrations (even 15000 times different for the case of chlorides).

A better solution consists on using an interpolation method based on the concentration values (c_1) of the 3-D data grid. One can calculate the solute concentration (c_2) at any point of co-ordinates (x,y,z) as:

$$c_2(x,y,z) = \sum_{i=1}^{8} c^i{}_1 \cdot N_i(x,y,z) \tag{4.1}$$

where $N_i(x,y,z)$ are the interpolation functions of concentration.

The same shape functions used by the code TRANMEF-3 (Juanes, 1997) have been used as interpolation functions. The shape functions use local co-ordinates (Figure 4.6) so, it is needed to make a transformation:

$$\xi = \frac{(x_2 - x_c)}{\Delta x_1}$$

$$\eta = \frac{(y_2 - y_c)}{\Delta y_1} \tag{4.2}$$

$$\zeta = \frac{(z_2 - z_c)}{\Delta z_1}$$

where:

(ξ, η, ζ) are local co-ordinates of the cube

(x_2, y_2, z_2) are global co-ordinates of the point in which we want to calculate the solute concentration

(x_c, y_c, z_c) are global co-ordinates of the centre of the cube

$(\Delta x_1, \Delta y_1, \Delta z_1)$represent the length of the three sides of the cube (distance between the data grid points).

Knowing the local co-ordinates of the interpolation point, the values of the interpolation functions at that point can be computed according to (4.3) and, using this interpolation functions (4.3) and with the equation (4.1) the solute concentration in each node of the finite elements mesh can be obtained.

$$
\begin{aligned}
N_1(\xi,\eta,\zeta) &= \frac{1}{8}\cdot(1-\xi)\cdot(1-\eta)\cdot(1-\zeta)\\
N_2(\xi,\eta,\zeta) &= \frac{1}{8}\cdot(1+\xi)\cdot(1-\eta)\cdot(1-\zeta)\\
N_3(\xi,\eta,\zeta) &= \frac{1}{8}\cdot(1+\xi)\cdot(1+\eta)\cdot(1-\zeta)\\
N_4(\xi,\eta,\zeta) &= \frac{1}{8}\cdot(1-\xi)\cdot(1+\eta)\cdot(1-\zeta)\\
N_5(\xi,\eta,\zeta) &= \frac{1}{8}\cdot(1-\xi)\cdot(1-\eta)\cdot(1+\zeta)\\
N_6(\xi,\eta,\zeta) &= \frac{1}{8}\cdot(1+\xi)\cdot(1-\eta)\cdot(1+\zeta)\\
N_7(\xi,\eta,\zeta) &= \frac{1}{8}\cdot(1+\xi)\cdot(1+\eta)\cdot(1+\zeta)\\
N_8(\xi,\eta,\zeta) &= \frac{1}{8}\cdot(1-\xi)\cdot(1+\eta)\cdot(1+\zeta)
\end{aligned}
\qquad (4.3)
$$

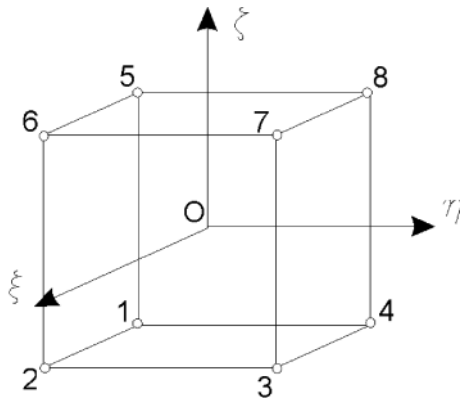

Figure 4.6 Local co-ordinate system of the shape functins used as interpolation functions to generate initial conditions of solute transport.

4.6 PARAMETERS

The main material parameters for the numerical model are hydraulic conductivity (K) and specific storage coefficient (S_s) concerning to the groundwater flow, and kinematic porosity (n_e) and dispersivity (α) concerning to the transport of solutes.

Groundwater parameters were collected from the hydrogeological conceptual model proposed by Rhén et al. (1997 b). Solute transport parameters were collected from Holmquist & Andersson (1999) and Rhén et al. (1997 b). Initial parameters and those adjusted by hand calibration of the numerical model are shown in Appendix 1.

5 CALIBRATION I: GROUNDWATER FLOW

5.1 STEADY-STATE GROUNDWATER FLOW

The steady-state groundwater flow numerical model corresponds to a set of computation runs called Run_2. These runs were the first attempt to calibrate the hydraulic conductivity field of the HCD. The starting values of the hydraulic conductivity field are shown in Appendix 1 and correspond to the geometric mean of the measured values (Rhén et al., 1997 b).

One of the important points extracted from the study of the Run_2 results is the role of transmissivities of the Hydraulic Conductors Domains in the numerical model. A sensitivity analysis of this parameter was done, and the results can be seen in the Figure 5.1. This figure shows a comparison of measured and computed flow rates into the tunnel for Run_2a and Run_2b. Transmissivities used in both runs coincide with those values provided by (Rhén et al., 1997 b), but the difference arrives in the values used for the intersections.

In Run_2a the transmissivities of the intersections take a value equal to the arithmetic mean values of the intersected domains, while in Run_2b they are equal to 1000 m^2/day for each intersection.

Figure 5.1 illustrates that the model is not sensitive to the value of the transmissivities of these intersections, at least in terms of flow rates into the tunnel. Of course, the computed pressure head distribution around the intersections is different for both runs.

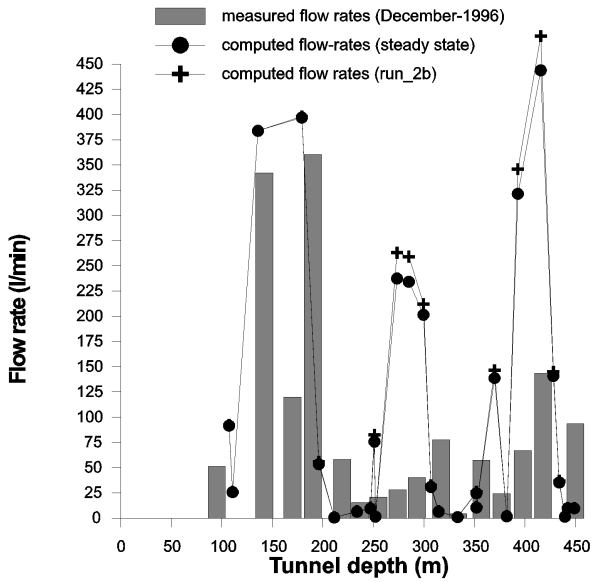

Figure 5.1 Results of Run_2a and Run_2b. Sensitivity analyses with respect to the intersections of transmissivity.

Due to the relatively small computational requirements needed to solve for steady-state flow (in comparison with transient flow), the set of computations run_2 was used to debug and check the model, looking for anomalies, mistakes in input data files, and specially for checking the behaviour of the intersections among HCD.

Figure 5.2 shows the computed drawdowns on HCD NE-1, NNW-3 and NNW-7. It must be noticed that the tunnel cross all these three domains. Figure 5.3 shows the computed drawdowns on the HCD NNW-4 and EW-1S. The important point in the last figure is that only the NNW-4 HCD is crossed by the tunnel and then, the computed drawdowns on EW-1S are due to the connection with other domains. In Figure 5.3 it is possible to see the expected pattern of pressure head around the intersection.

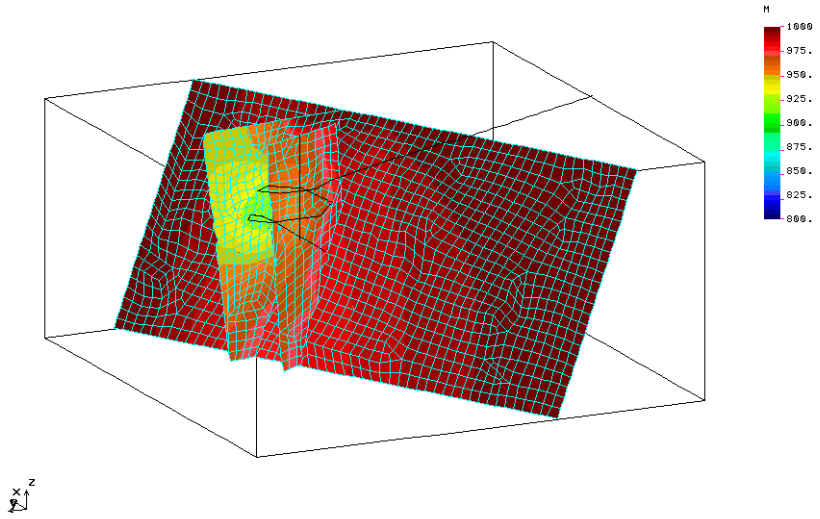

Figure 5.2 Computed steady-state pressure heads on HCD NE-1, NNW-3 and NNW-7.

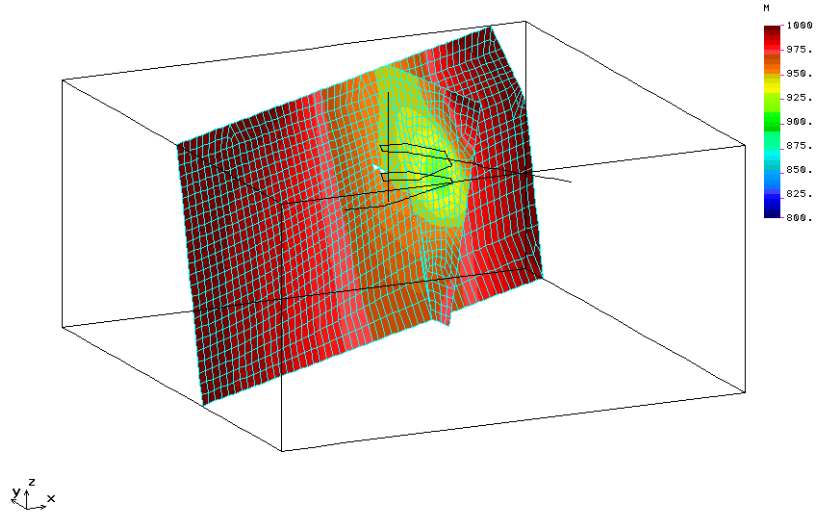

Figure 5.3 Computed steady-state pressure heads on HCD NNW-4 and EW-1S. Notice that EW-1S domain is not crossed by the tunnel.

5.2 TRANSIENT GROUNDWATER FLOW

The transient groundwater flow numerical model corresponds to a set of computation runs called Run_3. In this report the results of the Run_3ZG are presented. Run_3ZG corresponds to the best calibration run reached.

It must be recalled that a mixed flow condition has been used for the inner boundary of the tunnel and elevator. This means that the flow rates into the tunnel are computed by the model and not prescribed as a boundary condition. Thus, measured flow rates into the tunnel can be compared to computed values. Finally the model is able to reproduce flow rates and heads and then, it has more confidence than a model fitting only one of them separately.

The control points used to compare measured values against model results are listed in the Appendix 2. In terms of head pressure the observation points are the sections of the boreholes KAS02 to KAS09, KAS12 and KAS14 crossing al least one HCD. In terms of flow rates the observation points are all the tunnel sections crossing at least one HCD. Despite the numerical model takes into account also the elevator, computed flow rates in the shafts have not been compared.

5.2.1 FLOW RATES INTO THE TUNNEL

Figures 5.4 and 5.5 show the comparison between measured and computed flow rates into the tunnel at observation points. The analysis of these results indicates that there is an excellent agreement between computed and measured values. The main discrepancy (and could be said that the unique one) can be found in section MA3179G (Figure 5.5-E) where the model is not able to reproduce the pattern of the evolution of the measured flow rate. In this control point the model underpredicts by around 70 l/min the measured flow rates.

Figure 6.5-G shows the evolution of total amount of water flowing into the tunnel. The model is able to reproduce the patterns of measured data and the largest discrepancy is on the order of 20% of the total water inflowing into the tunnel, for the transient intermediate stage. Must be noticed again that the model is not accounting for the contribution of the rock domains so, it is reasonable to expect a computed flow rate smaller than the measured values. Once steady-state is reached, the model reproduce perfectly the measured data.

Figure 5.5-H shows the evolution of the flow rate average residuals. The average residuals (dh) have been computed by the equation:

$$dh = \frac{\sum_{i=1}^{n} (q_i^m - q_i^c)}{n} \qquad (5.1)$$

and the average of absolute value of residuals (dh_abs):

$$dh(abs) = \frac{\sum_{i=1}^{n} \left| q_i^m - q_i^c \right|}{n} \qquad (5.2)$$

where:
n is the number of points with measured data to be compared against computed values.
q is the flow rate (l/min).
the index m represents the measured value.
the index c represents the computed value.

In Figure 5.5-H can be observed that the average of absolute value of residuals for the tunnel inflows, *versus* the time, take a constant value around 40 l/min after 1000 days, and it shows a maximum (lower than 70 l/min) during the transient period. No systematic errors have been detected in the computed flow rates along the modelled time.

5.2.2 GROUNDWATER PRESSURE HEADS

As was mentioned before, the calibration of the transient groundwater flow model was done by comparison of computed values against measured flow rates and groundwater pressure heads. Totally, 15 control points were selected for pressure heads, corresponding to those isolated sections of boreholes KAS02 to KAS09, KAS12 and KAS14 crossed by, at least, one HCD (Appendix 2).

After running the transient groundwater flow numerical model more than 40 times it could be said that the groundwater pressure head distribution into the modelled domain is sensitive to transmissivity and storage coefficient fields. By hand calibration of the numerical model, it has been possible to obtain a solution able to reproduce, in general, the pressure head evolution at the 15 selected control points. This solution (Run_3ZG) is also consistent with measured flow rates into the tunnel as was shown previously (figures 5.4 and 5.5). The flow parameters used in the final calibrated model are shown in Appendix 1.

Figures 5.6, 5.7 and 5.8 show the groundwater pressure head distribution into the modelled domain after 313, 525 and 2013 days, respectively. Looking at these 3 figures it is possible to observe a detail of the pressure heads transient evolution as a response of the impact of the tunnel construction in the Äspö groundwater system.

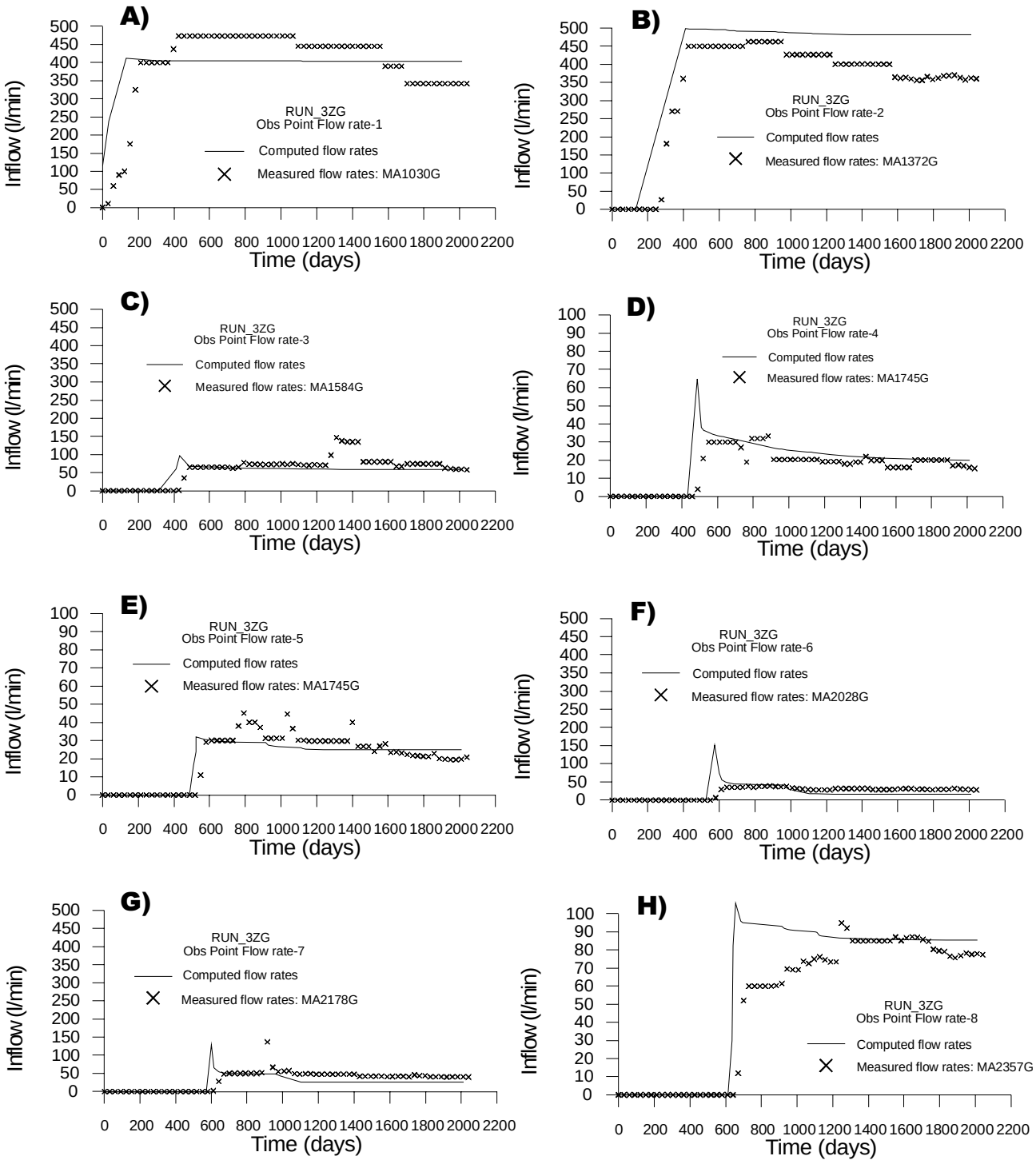

Figure 5.4 Computed and measured flow rates at tunnel section: A) MA1030G, B) MA1372G, C) MA1584G, D) MA1754G, E) MA1745G, F) MA2028G, G)MA2178G and H) MA2357G.

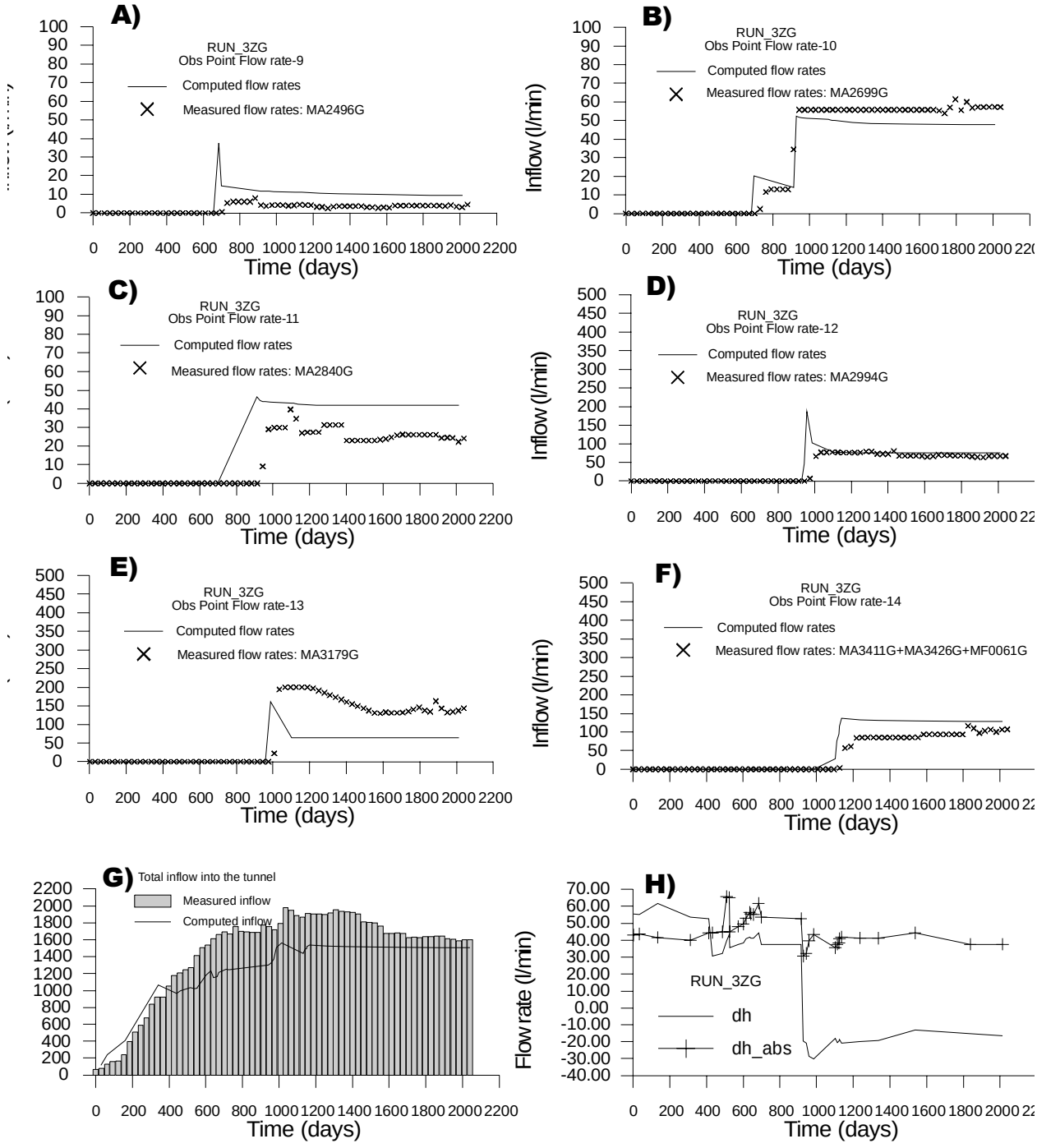

Figure 5.5 Computed and measured flow rates at tunnel section: A) MA2496G, B) MA2699G, C) MA2840G, D) MA2994G, E) MA3179G and F)MA3411G+MA3426G+MF0061G. G) Computed and measured flow rates in the total tunnel length. H) Accuracy of the model: time evolution of the average residuals (dh) and average of absolute value of residuals (dh_abs) of the flow rates.

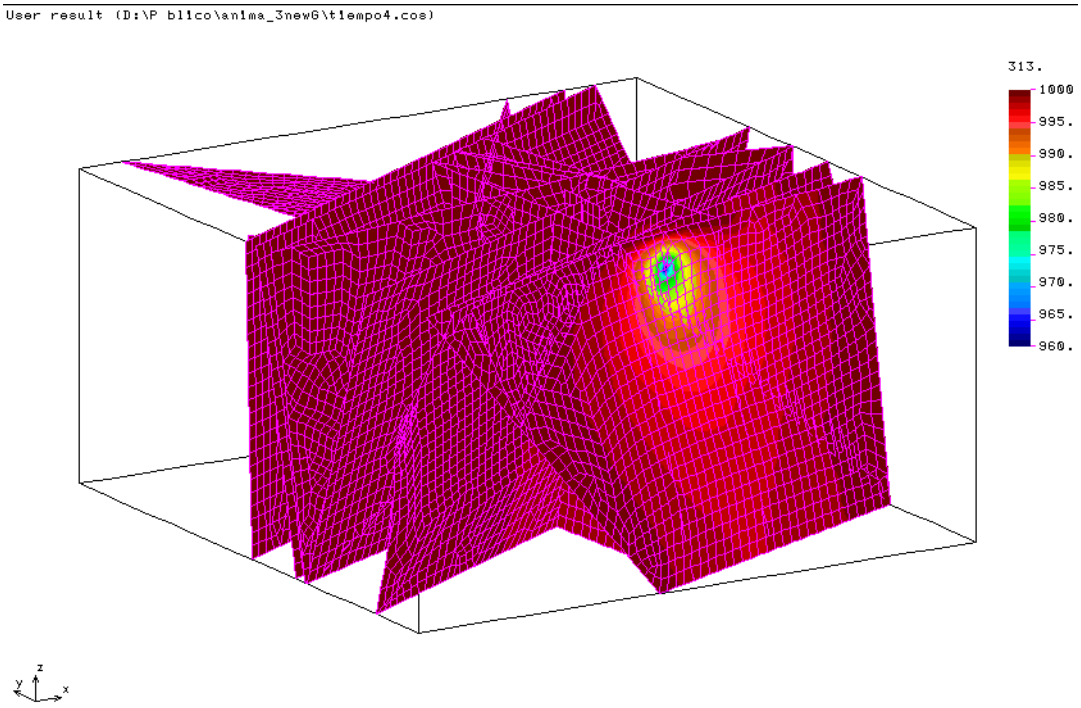

Figure 5.6 Computed pressure head distribution after 313 days.

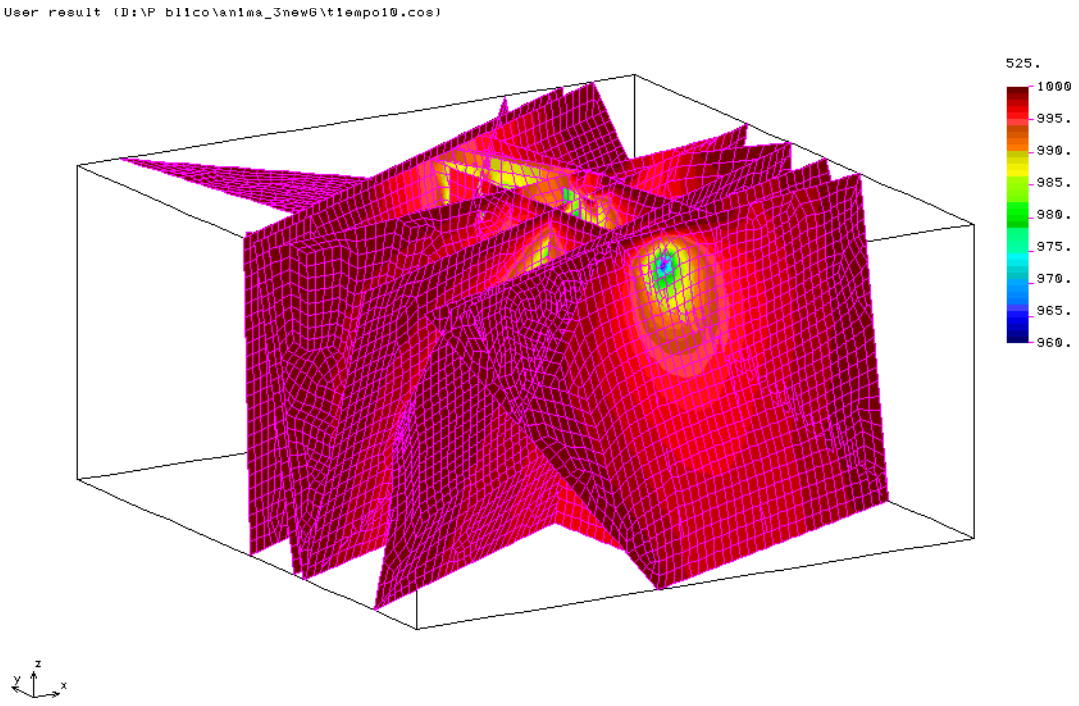

Figure 5.7 Computed pressure head distribution after 525 days.

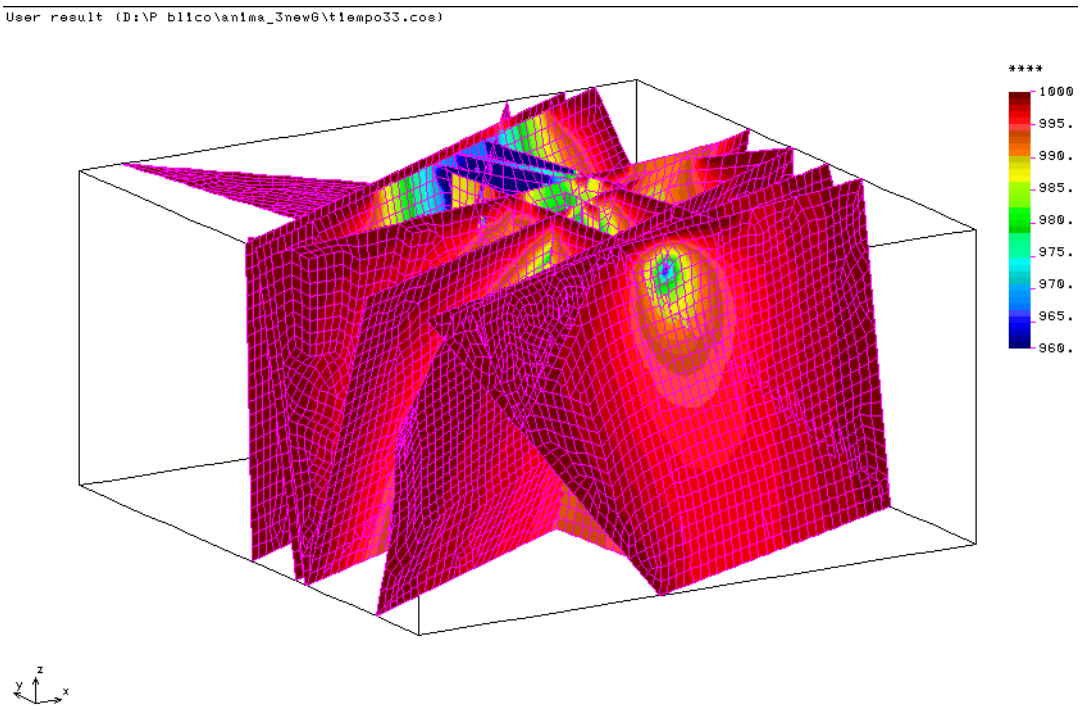

Figure 5.8 Computed pressure head distribution after 2013 days.

Figures 5.6, 5.7 and 5.8 approximately correspond to the contrary point of view of that used in figures 4.2 and 4.3 so, the tunnel ramp starts from the figure front and goes down towards the central zone of the cube, where the tunnel spiral is located.

As expected, the tunnel acts as a groundwater sink and the piezometric isolines show a more or less concentric pattern around the tunnel-fracture intersections (figures 5.6, 5.7 and 5.8). The piezometric isolines become paralel to the 4 side boundaries and to the Baltic sea upper boundary, because a prescribed head condition was imposed over these boundaries. On the contrary, on the bottom and land (upper) boundaries the isolines pattern shows a normal behaviour because a no flow and recharge condition was adopted, respectively.

Figures 5.9 and 5.10 show the comparison between computed and measured pressure heads at the 15 selected control points. Prior to mesh generation, all monitored intervals (each packed borehole interval crossing a HCD) were identified. Then, the middle point of each interval was defined within the geometrical model. All this points were prescribed as being nodes of the numerical finite element grid, in order to compare computations and measurements. In summary, no interpolation was made to compare results to measured data. Looking at these figures it can be stated that numerical model computations have a good agreement with measured data. The numerical computations predict reponses for transient head stepper tan those measured. We think this is due to the role of the rock mass domains, which are not considered in the model. A better fit of the transient head evolution could possibly be achieved by calibrating/adjusting storativity values. However, neglecting rock mass domains

allows to save CPU time in order to perform a fully transient treatment of the tunnel construction process. Moreover, as has been shown, the model is able to reproduce very good groundwater inflows into the tunnel.

Figure 5.10-H shows the time evolution of the groundwater pressure heads residuals and mean square errors. The residuals have been computed with equations 5.1 and 5.2, but using heads instead of flow rates. For computing the mean square errors (Dh) the following equation was used:

$$Dh = \sqrt{\frac{\sum_{i=1}^{n} (h_i^m - h_i^c - dh)^2}{n-1}} \qquad (5.3)$$

with the same notation than in equations 5.1 and 5.2, and being h the groundwater pressure head.

The residuals and errors where computed for the first 788 days (the time with available measured data). Figure 5.10-H shows that there is a systematic increase of the residuals during the first 300 days and, for the next 200 days the residuals move drastically to almost zero. An instantaneous increase occurs around day 500, reaching a maximum value of 8.27 m (dh_abs), followed by a final decreasing stage for the last 150 days.

The average of the absolute value of residuals is 2.99 m and, the average mean square error of the model goes to 4.32 m.

The most relevant discrepancies between computed and measured values can be observed in figures 5.9-H and 5.8-B. Both figures show a drastic drawdown around day 500 that the model do not reproduce. Observation point 8 (figure 5.9-H) is located on the NNW-1 HCD and point 10 (figure 5.10-B) is situated on NNW-7 HCD. These fracture zones were crossed by the tunnel construction during days 509 and 486 respectively. Nevertheless, there are other control points located on those 2 HCD that show a good agreement with measured data (such as those shown in figures 5.9-A, 5.9-B and 5.10-C), in addition of the agreement shown in the computed flow rates on the sections crossed by these HCD. A possible explanation for these 2 main discrepancies can be found on the possibility of the occurrence of heterogeneity inside an individual fracture zone. In spite of the numerical preproccesing has been extensively verified, the existence of mistakes in the finite element mesh (specially in the fracture and tunnel connections), even very unprobable, could also be responsible of the observed discrepancies.

To compute the residuals and mean square errors no filtering of data have been done, although there are clear anomalies in measured data at some boreholes (i.e. observation points 9 and 11, figures 5.10-A and 5.10-C). Taking these abnormal data out, the accuracy of the model will improve.

The observation point 1 (Figure 5.9-A) corresponds to a borehole section crossed by 2 HCD. Figure 5.9-A shows the pressure head evolution computed at 2 nodes (one for each HCD) and, it can be noticed how the measured data are in the middle of the computed values. Therefore, the borehole section KAS02 (346-799) could be behaving as an artificial connection between NE-2 and NNW-7 domains.

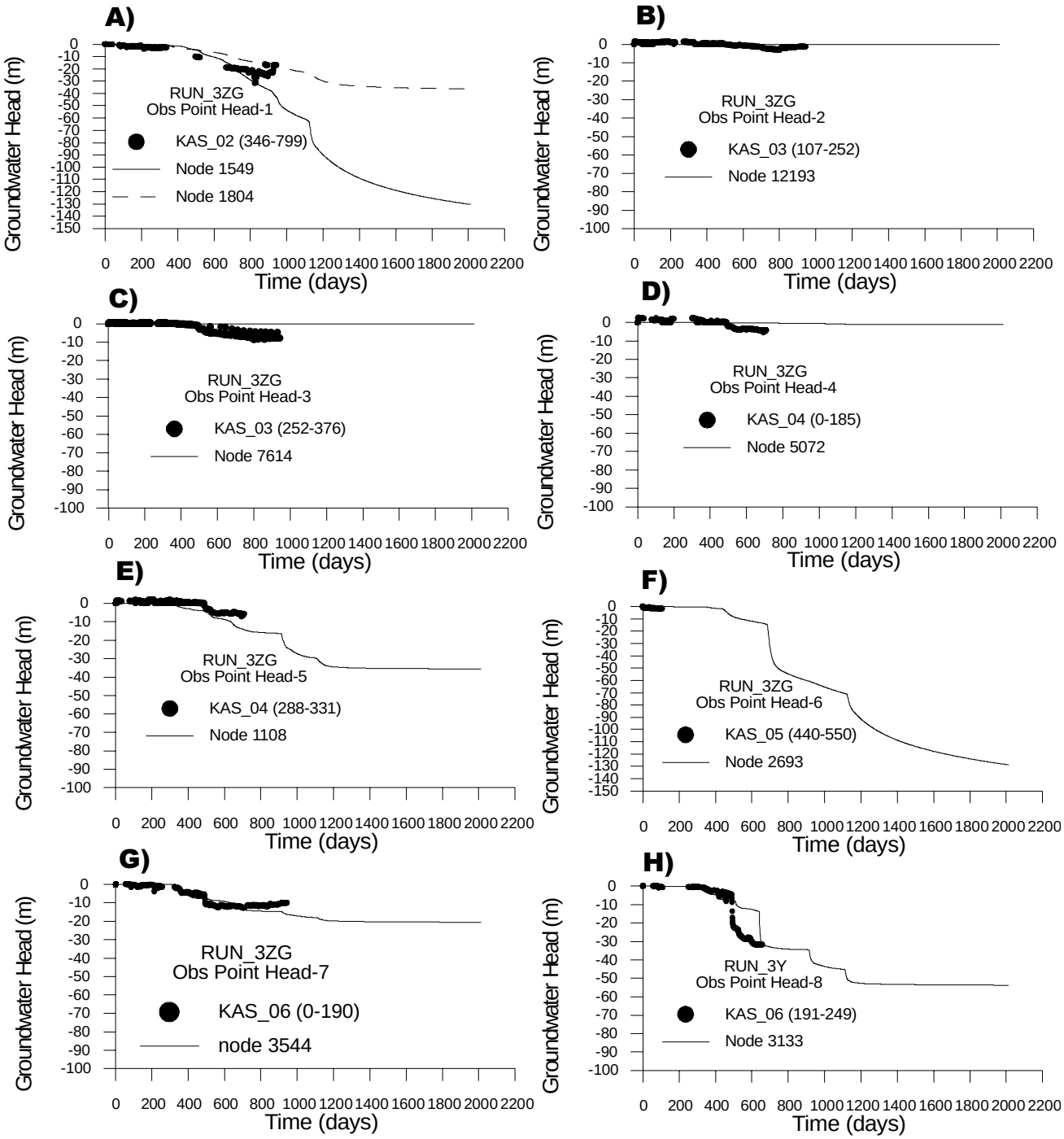

Figure 5.9 Computed and measured groundwater pressure head evolution at the first 8 selected control points.

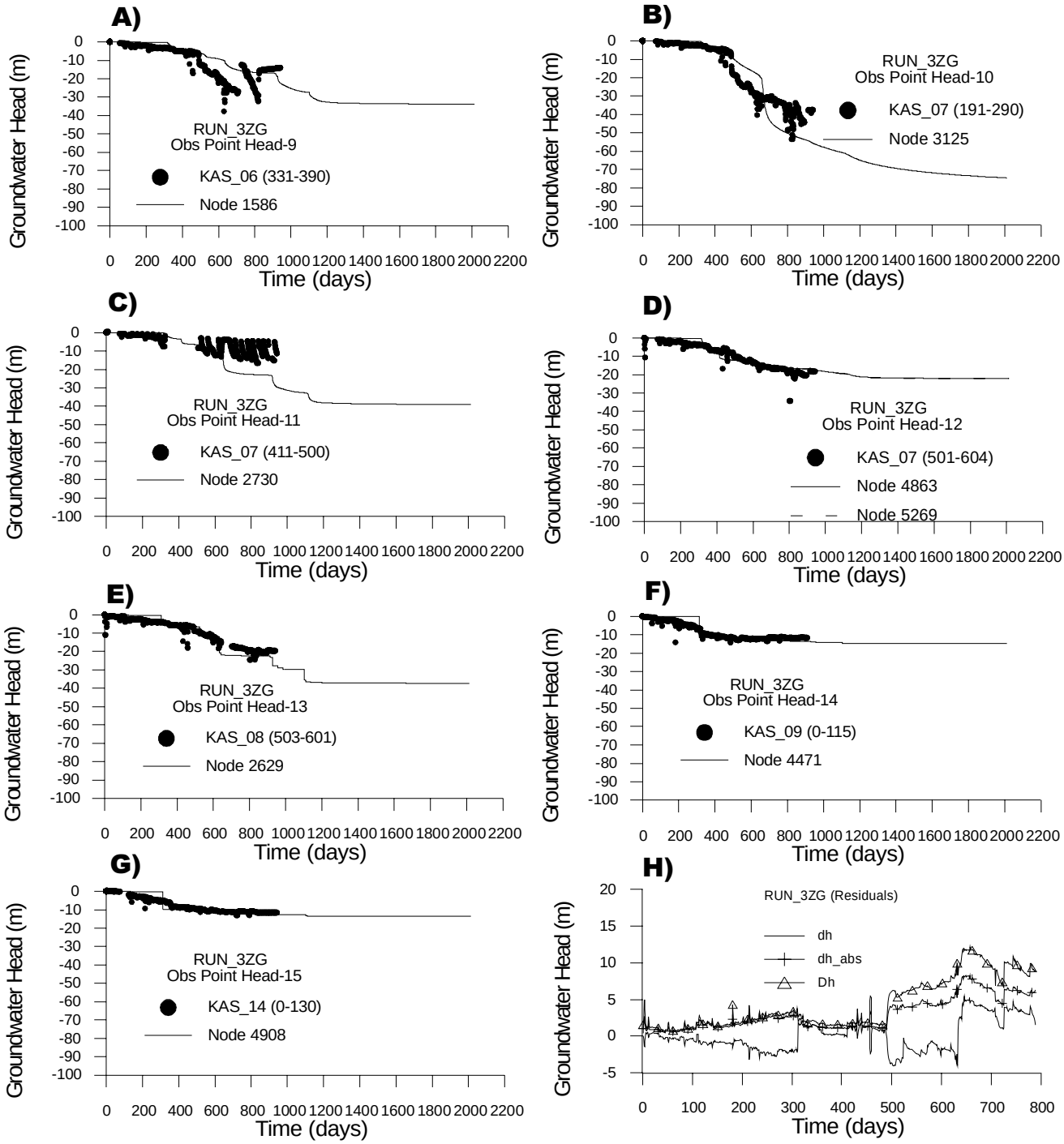

Figure 5.10 Computed and measured groundwater pressure head evolution at the last 7 selected control points. Figure 5.10-H shows the time evolution of the average residuals (dh and dh_abs) and the mean square error (Dh).

6 CALIBRATION II: TRANSPORT OF SOLUTES

6.1 INTRODUCTION

In this chapter the results of a hydrodynamic numerical model for solute transport are shown. Once calibrated the transient groundwater flow numerical model (Chapter 5), mass transfer processes have been considered. Solute transport model accounts for advection, mechanical dispersion and molecular diffusion as were defined in Chapter 3.

Due to the fact that hydrochemical reactions are not considered into the numerical model, conservative species (chlorides and ^{18}O) were the unique species taken into account. Numerical model results were compared against field data, in terms of concentration at 15 control points (Appendix 2).

6.2 TRANSPORT OF CONSERVATIVE SOLUTES

As was shown in Chapter 5, tunnel construction modified drastically the groundwater system at the Äspö site and then, groundwater chemical composition will also be affected by the impact of the tunnel construction. The groundwater chemical evolution of a hydrodynamic system reflects the action of coupled physical and chemical processes. In order to understand and characterize mass transfer processes in such a systems it is well known that attention must be focussed in conservative (nonreactive) chemical species behaviour.

Chloride are the most typical conservative solute in groundwaters. In this work, initially chlorides in addition to $\delta^{18}O$ and ^{3}H were considered in the model as conservative species. However, tritium activities field data show a great dispersion when measured breakthrough curves are displayed. There are evidences of analitical measurement errors (Wikberg, personal communication) and, finally it was decided to neglect tritium data.

Contrary to the groundwater flow numerical model, almost no calibration has been made for the transport model. Parameters concerning mass transfer processes have been collected from Rhén et al. (1997 b) and Holmquist & Andersson (1999), and are shown in Appendix 1.

Figure 6.1 shows the initial conditions used in the numerical model for chloride concentrations. This initial distribution of chlorides was obtained by interpolation of the data grid provided by Task 5 (Gurban et al., 1998). Interpolation method was explained in Chapter 4. Initial chloride concentrations range between 0 (meteoric) and 20 g/l (deeper water) following a more or less stratified pattern (Figure 6.1).

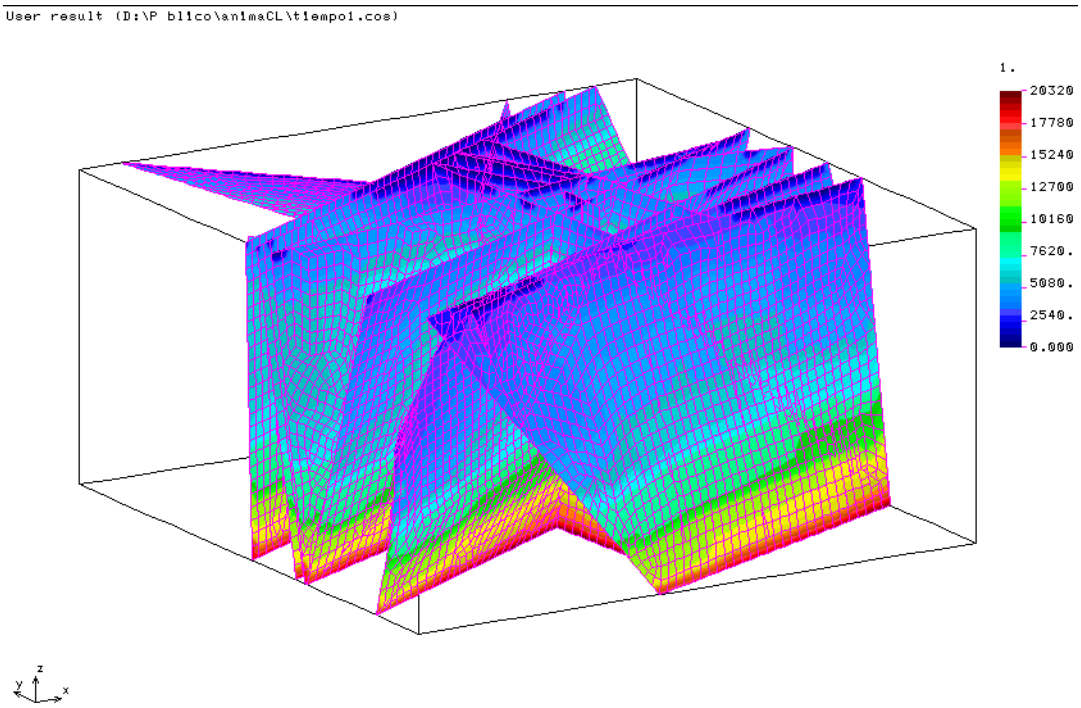

Figure 6.1 Initial chlorides distribution in the modelled domain (mg/l).

Figure 6.2 shows the computed final chlorides distribution (1997/01/01). Comparison of figures 6.1 and 6.2 allows to realize that meteoric and baltic water flow from the surface to the tunnel location, at the same time that an upconing of deeper saline groundwater is produced towards the tunel.

The initial distribution of $\delta^{18}O$ shows quite a different pattern in comparison with the initial distribution of chlorides. Initial values of $\delta^{18}O$ show a clear maximum (heaviest waters) located at an intermediate depth (Figure 6.3). These maximum values of $\delta^{18}O$ are a signature of old glacial waters and then, they correspond to a relict (fossil) water.

Figure 6.4 show the final computed distribution of $\delta^{18}O$ after 2013 days (1997/01/01). The Äspö HRL tunnel acts as a sink of groundwater and by comparison of figures 6.3 and 6.4 it can be observed how light waters flowing from the upper and lower boundaries replace heavy waters.

Although side boundaries contribute heavy water to the system[1], contribution of light water from islands, sea and deeper parts are large enough to replace most of the heavy water initially located in the tunnel surrondings.

1. A Dirichlet conditon was used for each side boundary and each modelled solute.

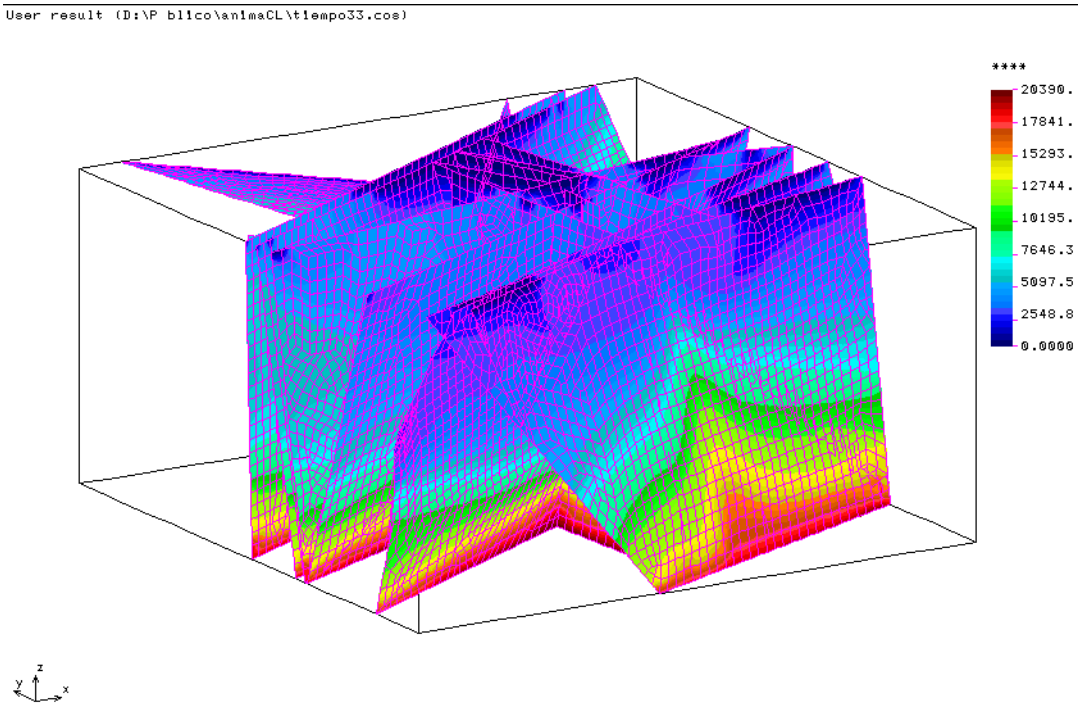

Figure 6.2 Computed chlorides distribution after 2013 days (1997/01/01).

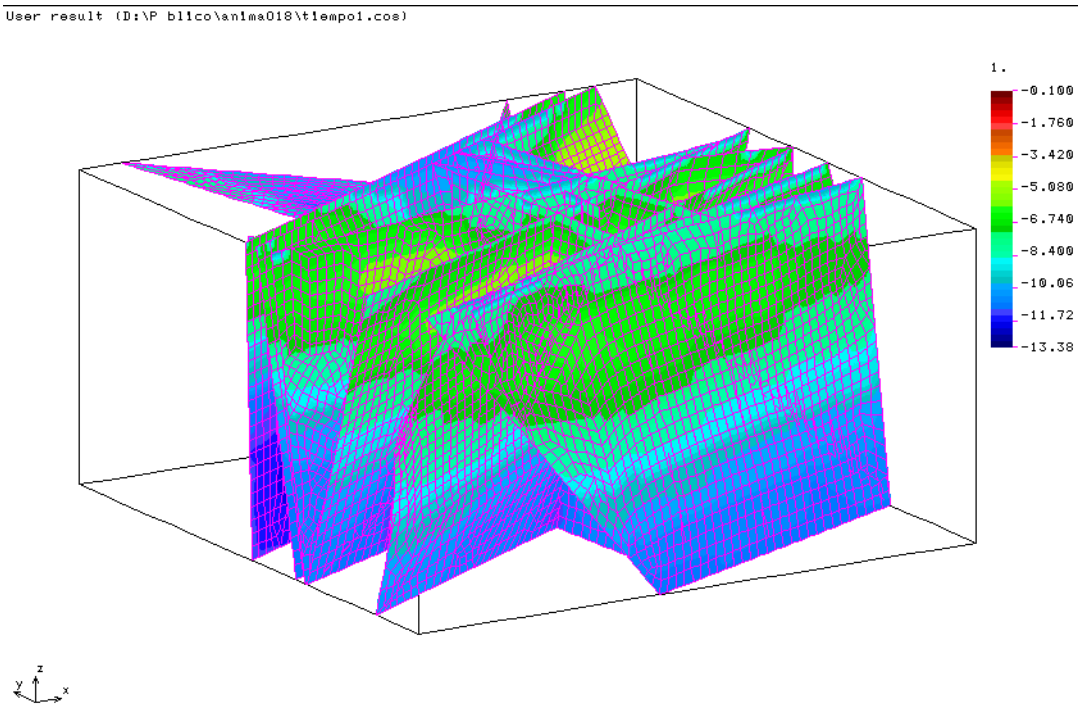

Figure 6.3 Initial $\delta^{18}O$ distribution in the modelled domain (deviation SMOW).

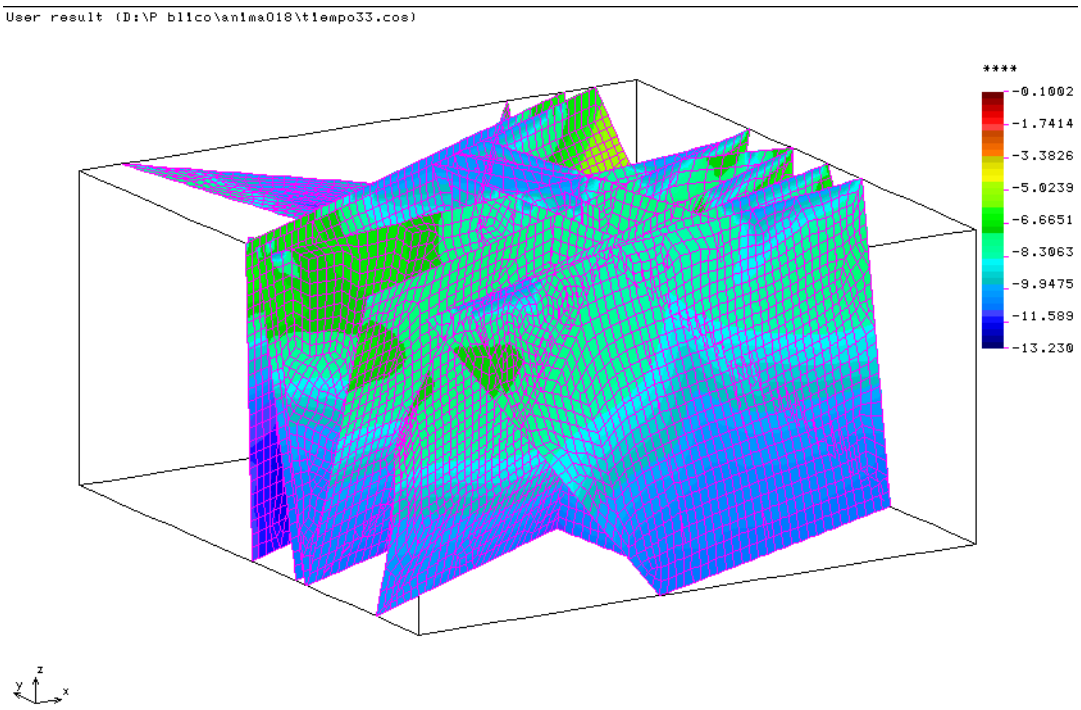

Figure 6.4 Computed $\delta^{18}O$ distribution after 2013 days (1997/01/01).

Figures 6.5 through 6.19 show measured values and computed results of the considered conservative species at the selected control points. The 15 control points correspond to all the borehole sections crossing a Hydraulic Conductor Domain and located in the tunnel surroundings, with available chemical time series (Appendix 2).

In general, a very good agreement exists between model computations and measured values. This kind of very good agreement can be observed in most of the control points (i.e figures 6.5, 6.6, 6.7, 6.8, 6.9, 6.10, 6.14, 6.15, 6.16 and 6.18). There are other control points showing a little worse fitting between measured and computed values, but with an acceptable behaviour of the model, getting perfectly measured trends (figures 6.13, 6.17 and 6.19).

Control points 7 and 8 (figures 6.11 and 6.12) constitute the worse comparison between computed and measured values. As in the rest of the control points (located backwards and ahead these 2 points) the numerical model predicts a chloride dilution along the time, but measured values show a very strong increase of chlorides concentrations. Control point 8 (Figure 6.12) constitute a clear example of inadequate initial conditions. The first available measured value shows a concentration of chlorides less than 1500 mg/l and, the initial value used by the model, at the same point, was more than 5000 mg/l. It is difficult to think about such a drastic dilution followed by an even more spectacular chlorides increase (at least this kind of drastic behaviour is not observed at any other control point).

A very remarkable fact can be observed at control point 15 (borehole SA2783A, Figure 6.19). This point corresponds to the unique available control point recording a constant chlorides increase. Although numerical model underpredicts chlorides concentrations it is able to reproduce the increasing trend.

In fact, borehole SA2783A is the last available control point before starting the prediction section. This point shows a clear change in the chlorides behaviour, with respect to the previous 14 points. Looking at all these figures it is possible to realize that comparisons of $\delta^{18}O$ have much less significance for model evaluation than chloride evolutions.

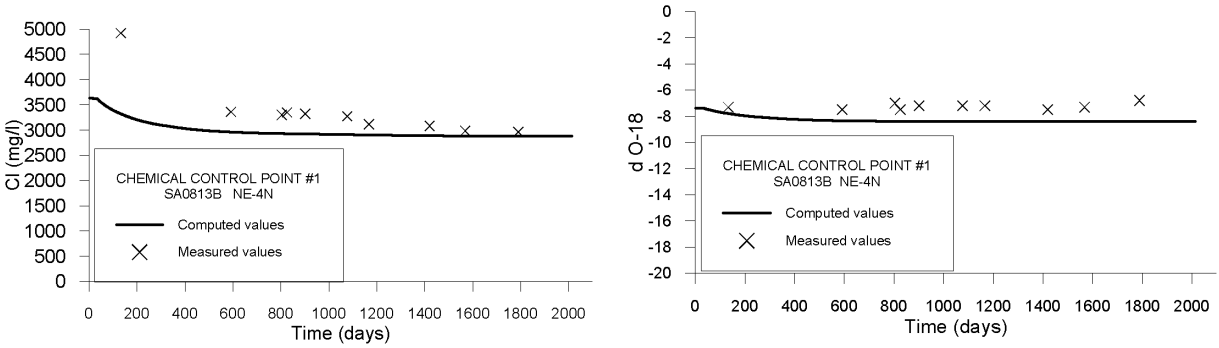

Figure 6.5. Fiel data and computed values of chlorides and 18-O at SA0813B borehole.

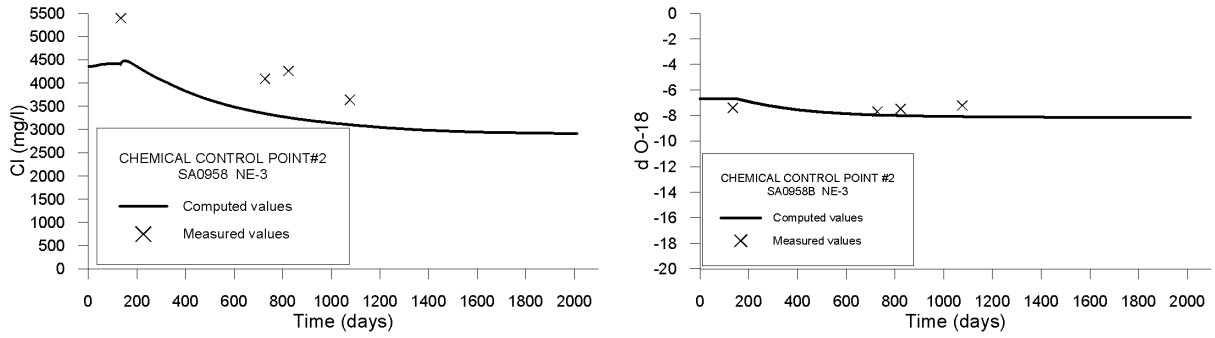

Figure 6.6. Fiel data and computed values of chlorides and 18-O at SA0958B borehole.

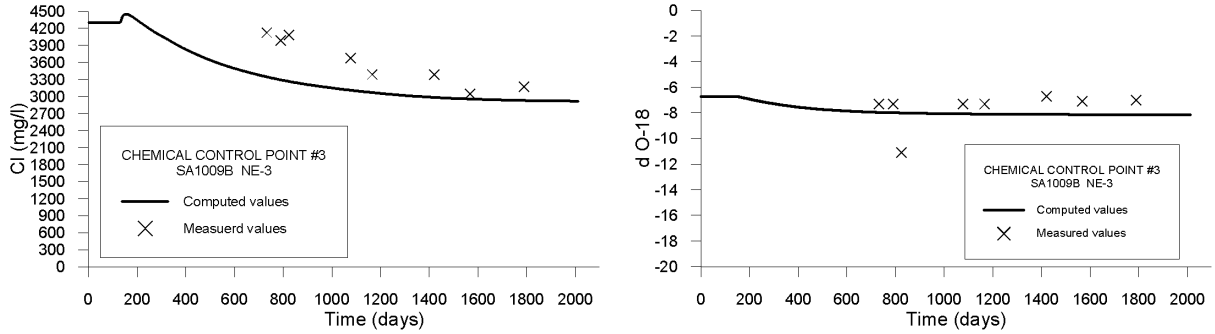

Figure 6.7. Fiel data and computed values of chlorides and 18-O at SA1009 borehole.

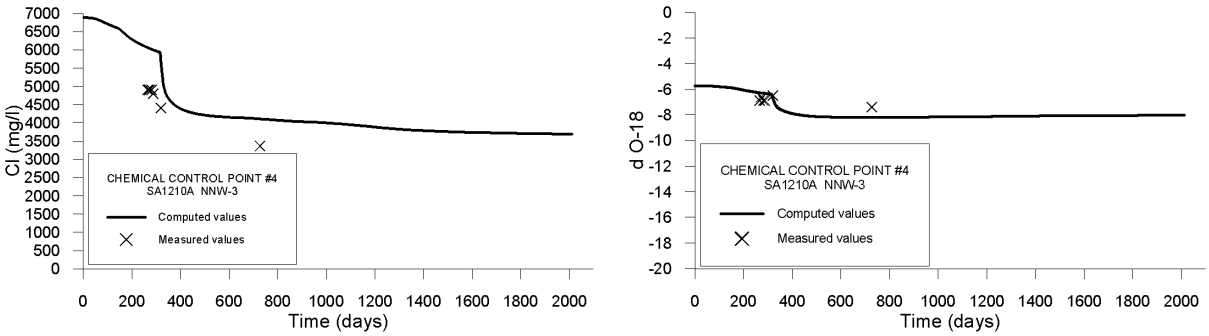

Figure 6.8. Fiel data and computed values of chlorides and 18-O at SA1210A borehole.

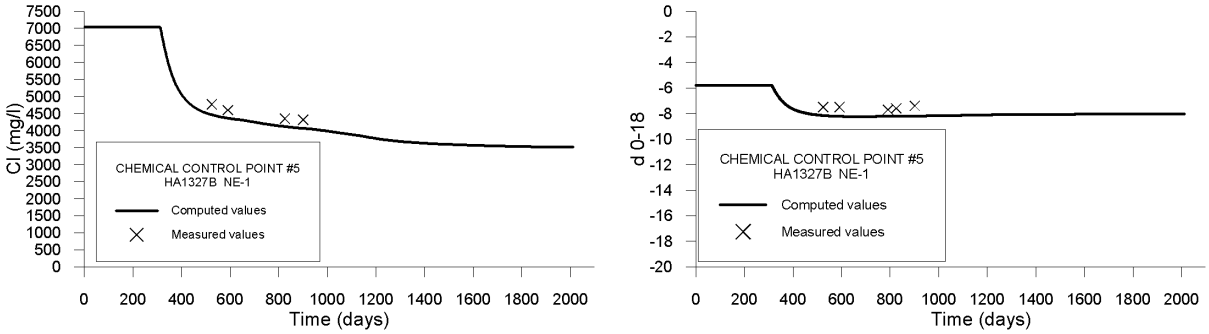

Figure 6.9. Fiel data and computed values of chlorides and 18-O at HA1327B borehole.

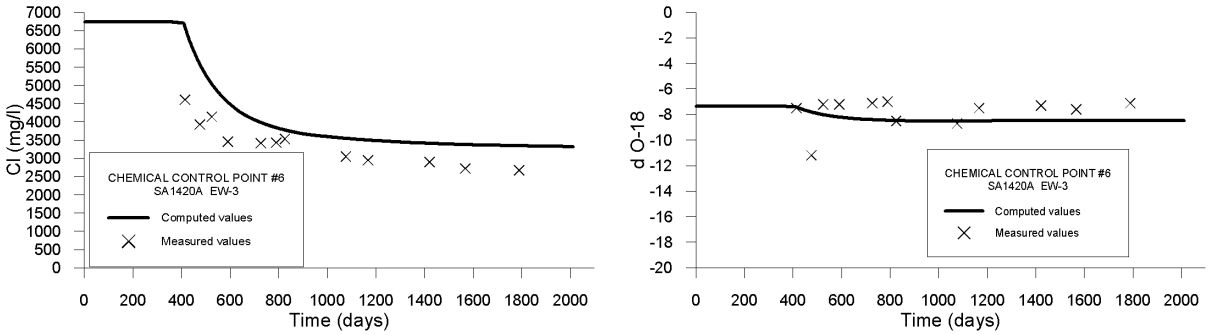

Figure 6.10. Fiel data and computed values of chlorides and 18-O at SA1420A borehole.

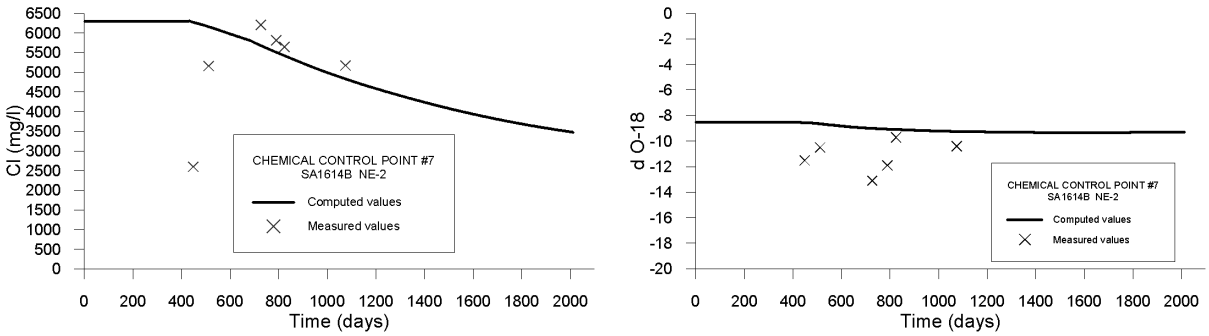

Figure 6.11. Fiel data and computed values of chlorides and 18-O at SA1614B borehole.

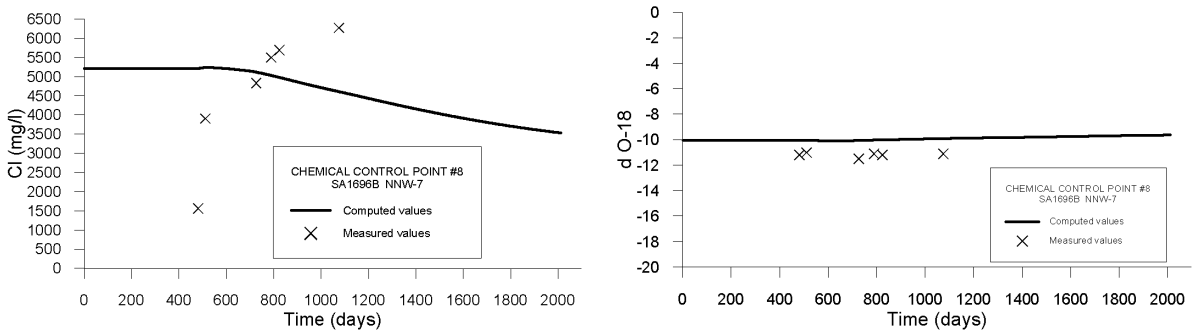

Figure 6.12. Fiel data and computed values of chlorides and 18-O at SA1696B borehole.

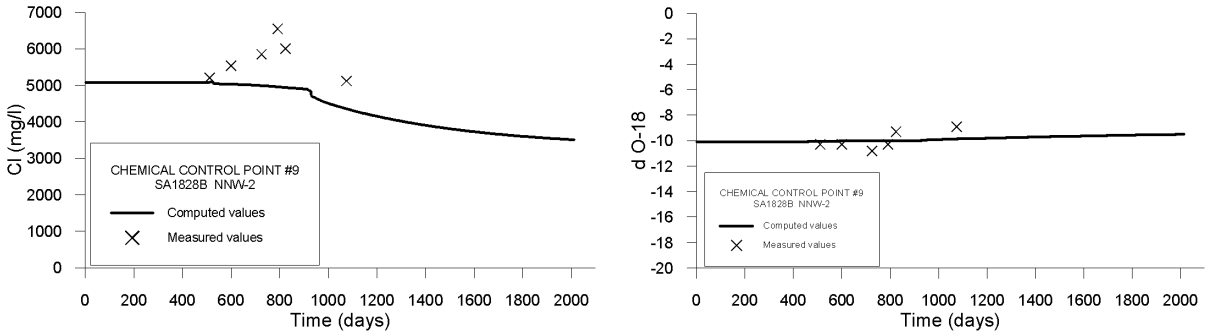

Figure 6.13. Fiel data and computed values of chlorides and 18-O at SA1828B borehole.

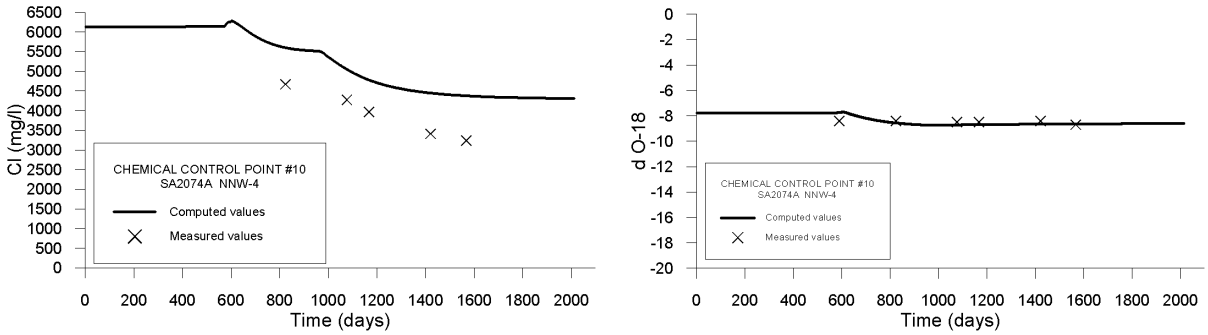

Figure 6.14. Fiel data and computed values of chlorides and 18-O at SA2074A borehole.

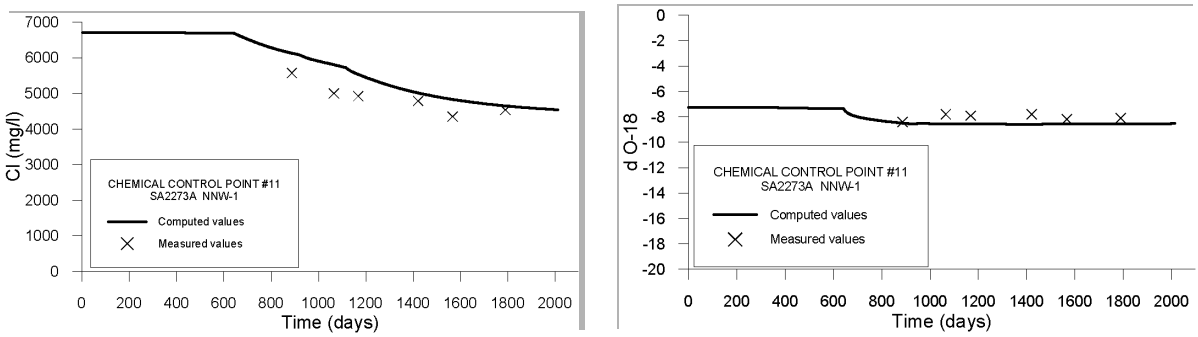

Figure 6.15. Fiel data and computed values of chlorides and 18-O at SA2273A borehole.

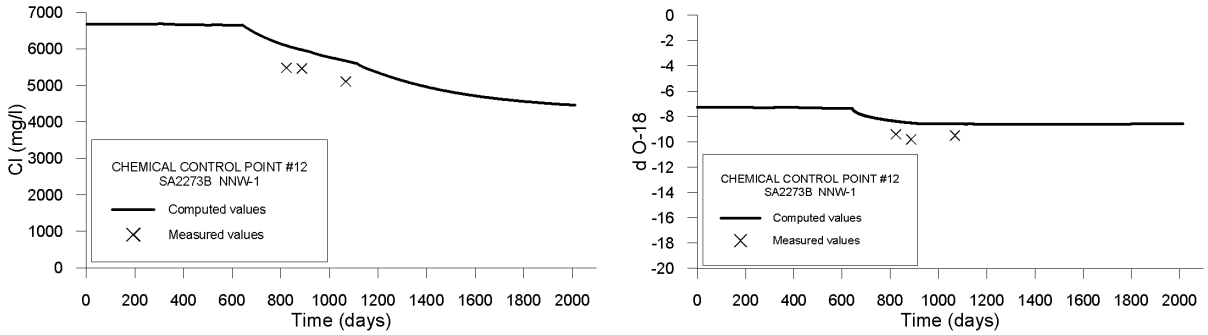

Figure 6.16. Fiel data and computed values of chlorides and 18-O at SA2273B borehole.

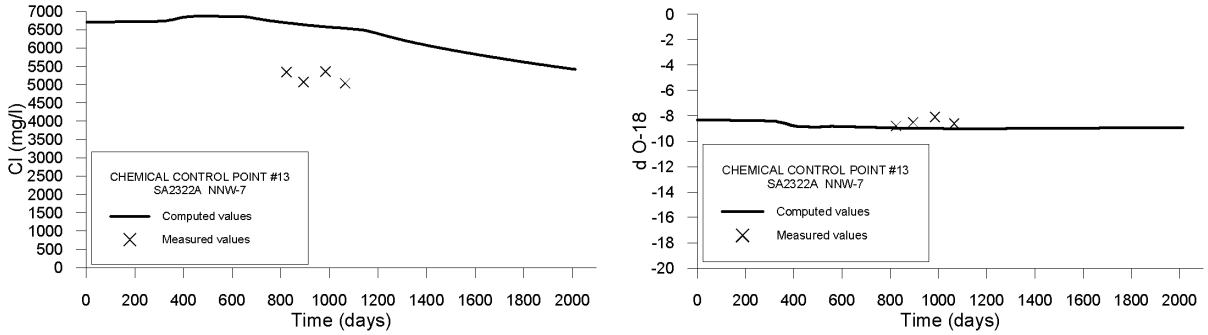

Figure 6.17 Fiel data and computed values of chlorides and 18-O at SA2322A borehole.

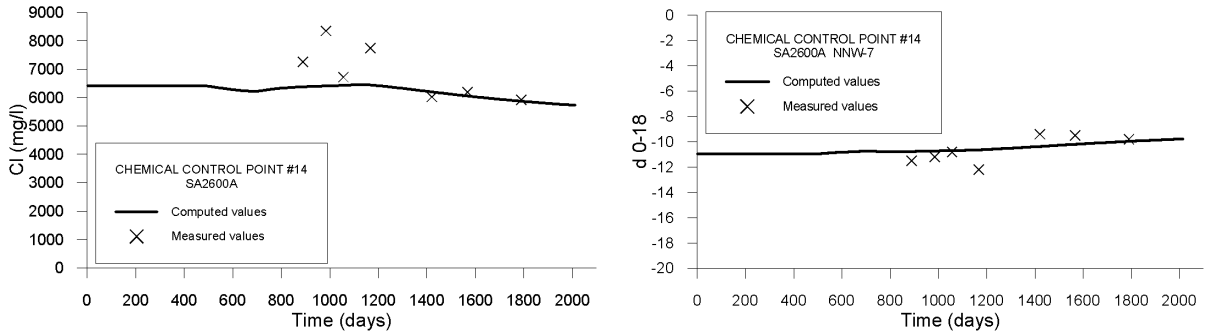

Figure 6.18. Fiel data and computed values of chlorides and 18-O at SA2600A borehole.

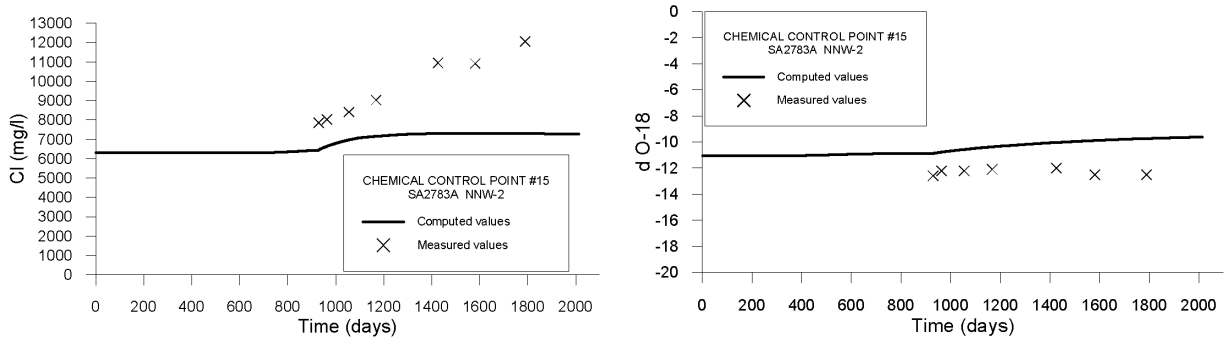

Figure 6.19. Fiel data and computed values of chlorides and 18-O at SA2783A borehohole.

7 SENSITIVITY ANALYSES

7.1 INTRODUCTION

As shown in previous chapters, the flow model of the Äspö site was thoroughly calibrated by comparison of computed and measured values. Calibration results indicate that the model provides a good representation of the hydrogeology of the site.

A model always entails a simplification of the real system. Computed results depend on the assumptions, boundary and initial conditions and model parameters all of which contain uncertainty. In order to know the confidence of the numerical model these uncertainties must be quantified. This can be done by sensitivity analyses. Finding out the main assumptions, the different plausible boundary and initial conditions and the variation ranges of the main parameters is the first stage of a sensitivity analysis. Uncertainties identified during the calibration process must be considered in the predictions, leading to an evaluation of prediction uncertainties.

A model is said to be sensitive to a given parameter or condition if reasonable variations of that parameter lead to significant changes in computed results.

7.2 GROUNDWATER FLOW SENSITIVITY ANALYSIS

Given the lack of data on some relevant parameters and conditions, the calibration is complemented with a sensitivity analysis with respect to some selected parameters as well as with respect to boundary and initial conditions.

A main source of uncertainty regarding to groundwater flow arises from boundary and initial conditions of groundwater heads. This uncertainty is mainly due to the fact that geometry of the model does not coincide with natural hydrogeological boundaries of the system. Therefore, some assumptions were needed to set up the numerical model.

The calibrated reference flow model was based on assuming hydrostatic initial heads and constant prescribed heads along the boundaries, except for the bottom boundary which was assumed impervious. These assumptions about initial and boundary conditions, however, may not hold at the Aspo site. An alternative and attractive assumption for initial and boundary conditions consists on using the results of the regional model proposed by Svensson (1997).

In addition to boundary and initial conditions, other sources of uncertainty arise from flow parameters. Fracture zone transmissivities and storativities are expected to have a strong influence on model results.

7.2.1 Sensitivity analysis with respect to boundary and initial conditions

Several runs of the numerical model were performed with different initial and boundary conditions (see Table 7.1).

Table 7.1. Model runs for sensitivity analyisis with respect to the groundwater flow boundary and initial conditions.

Name of the run	Characteristics
Flujo-0	Calibrated base reference run.
Flujo-1	Boundary conditions were interpolated linearly based on the results of the Regional Model both prior and after tunnel construction.
Flujo-2	Same as Flujo-1, but with initial conditions from the Regional Model prior to tunnel construction. Initial and boundary heads were corrected for salinity
Flujo-3	Same as Flujo-2 with impervious bottom boundary
Flujo-4	Same as Flujo-3 without salinity corrections in groundwater heads

To evaluate the sensitivity of the model with respect to initial and boundary conditions, a comparison of computed flow rates into the tunnel and groundwater heads at the control points was made. In fact, the comparison was made in terms of the average absolute values of residuales between computed and field data (equation 5.1). In this manner, in addition to evaluate the sensitivity of the model, it is possible to evaluate whether the results of different runs improve or get worse compared to the reference model. Sensitivity analyses results have been always displayed against the calibrated base run results (in terms of the average absolute values of residuals). Figures 7.1 to 7.5 show the comparison between the sensitivity runs with respect to the initial and boundary conditions. In the graphics, the X-axis represents the base run and the Y-axis represents the sensitivity run. Thus, symbols along the 45º-slope line mean no variation of the model results (in this case the model would not be sensitive with respect to the performed variation made in the sensitivity run). If the model is sensitive to a given variation, symbols will move outside of the 45º-slope line. A displacement of the symbols below the line indicates an improvement of the new computed results, with respect to the base run, and vice versa.

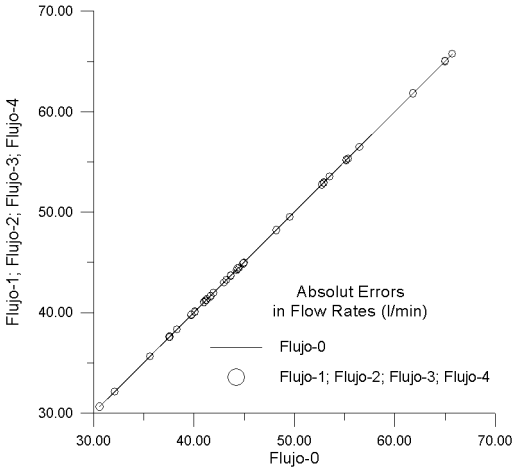

Figure 7.1. Absolute errors in computed flow rates into the tunnel: Comparison of sensitivity runs with respect to the reference model (Flujo 0).

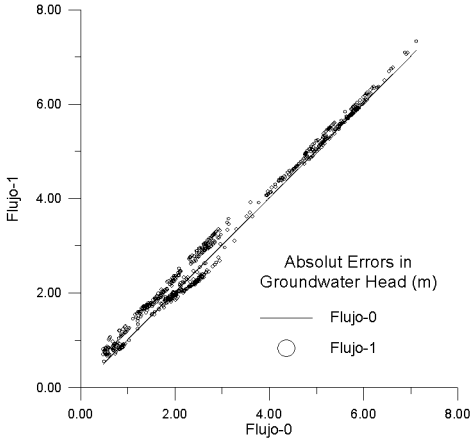

Figure 7.2. Absolute errors in computed groundwater heads. Comparison of sensitivity run Flujo-1 with respect to the reference model (Flujo 0).

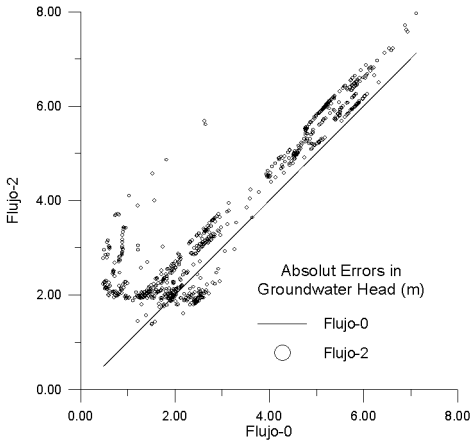

Figure 7.3. Absolute errors in computed groundwater heads. Comparison of sensitivity run Flujo-2 with respect to the reference model (Flujo 0).

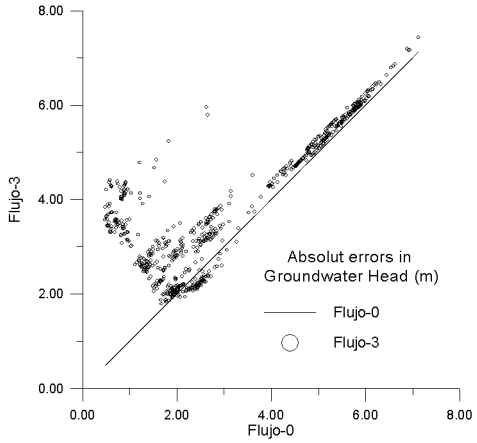

Figure 7.4. Absolute errors in computed groundwater heads. Comparison of sensitivity run Flujo-3 with respect to the reference model (Flujo 0).

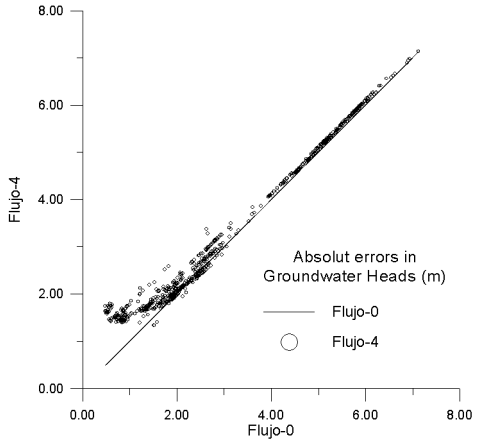

Figure 7.5. Absolute errors in computed groundwater heads. Comparison of sensitivity run Flujo-4 with respect to the reference model (Flujo 0).

A remarkable conclusion is that computed flow rates into the tunnel are not sensitive with respect to the boundary and initial conditions used in the numerical model (Figure 7.1).

In terms of groundwater heads, the model lacks sensitivity to the selected boundary conditions (figure 7.2), but, on the contrary, it is more sensitive with respect to the initial values of groundwater heads (figures 7.2 to 7.5). Computed head differences due to changes in initial conditions are greater at initial times and reduce rapidly towards zero along the simulated time. As has been said before, the comparison between different sensitivity runs was performed using the nodes of the numerical grid where we could compare to measured data. The objective of this exercise is to evaluate both, the sensitivity and the improvement (or not) of each run. However, there is really no control about each one of the individual points in each figure. It will be certainly interesting to identify what are the particular structures influencing each control point but this will require an amount of work that was initially too far beyond the scope of this work.

The observed differences between runs 2 and 3 (figures 7.3 and 7.4) are due to the variation of the lower boundary condition, so it can be stated that the numerical model is relatively sensitive to the type of chosen bottom boundary condition.

The reason why the Regional Model results (Svensson, 1997) provide worse initial conditions for our model is the larger scale of the Regional Model. For instance, some of the points in the top surface of the Regional Model corresponding to the Äspö Island, they correspond to the Baltic Sea in our site-scale model... This is a matter of having different space resolution in two different scale models.

7.2.2 Sensitivity analysis with respect to flow parameters

Several runs were performed to evaluate the sensitivity of the model to changes in transsmissivity and storativity. In the numerical model 19 hydraulic conductor domains were considered, in addition to all the existent conections between them. Table 7.2 show the characteristics of the performed runs to evaluate the sensitivity of the numerical model with respect to the transmissivities.

Table 7.2. Model runs for sensitivity analyisis with respect to the transmissivities.

Name of the run	*Characteristics*
Flujo-0	Calibrated base run.
Flujo-5	Transmissivity of all the intersections between H.C.D. reduced in 1 order of magnitude.
Flujo-6	Transmissivity of all the intersections between H.C.D. reduced in 1 order of magnitude, except for 2 intersections which are located close to some control (observation) points.
Flujo-7	Transmissivity of EW-7, NE-4S, NNW-4, NNW-5 and NE-3 equals to the minimum measured values.
Flujo-8	Transmissivity of NE-4N equals to the minimum measured value.
Flujo-9	Transmissivity of NE-1 equals to the minimum measured value.
Flujo-10	Transmissivity of EW-1N equals to the minimum measured value.
Flujo-11	Transmissivity of EW-1S equals to the minimum measured value.
Flujo-12	Transmissivity of NE-1 and NNW-7 equals to the minimum measured value.

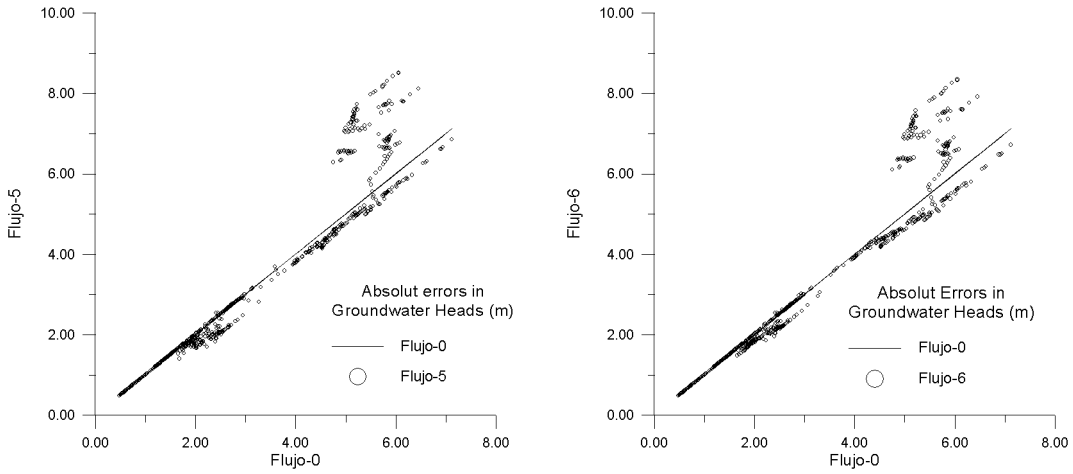

Figure 7.6. Absolute errors in computed groundwater heads. Comparison of the reference run (Flujo-0), run Flujo-5 and run Flujo-6.

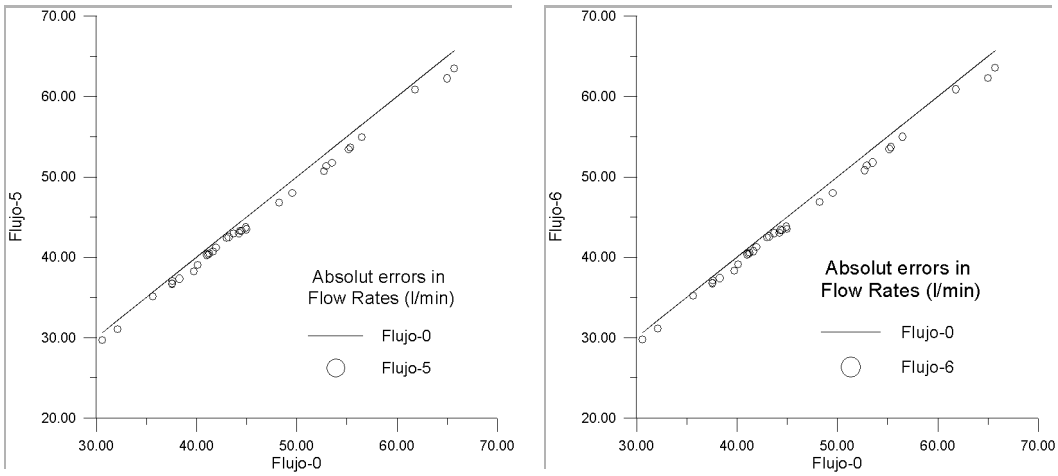

Figure 7.7. Absolute errors in computed flow rates into the tunnel. Comparison of the reference run (Flujo-0), run Flujo-5 and run Flujo-6.

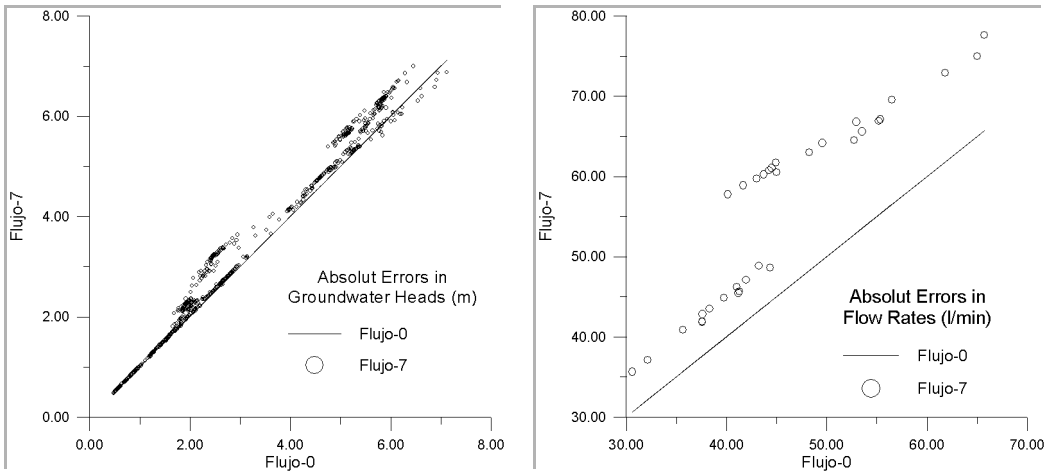

Figure 7.8. Absolute erros in computed groundwater heads and flow rates into the tunnel. Comparison of the reference run (Flujo-0) and run Flujo-7.

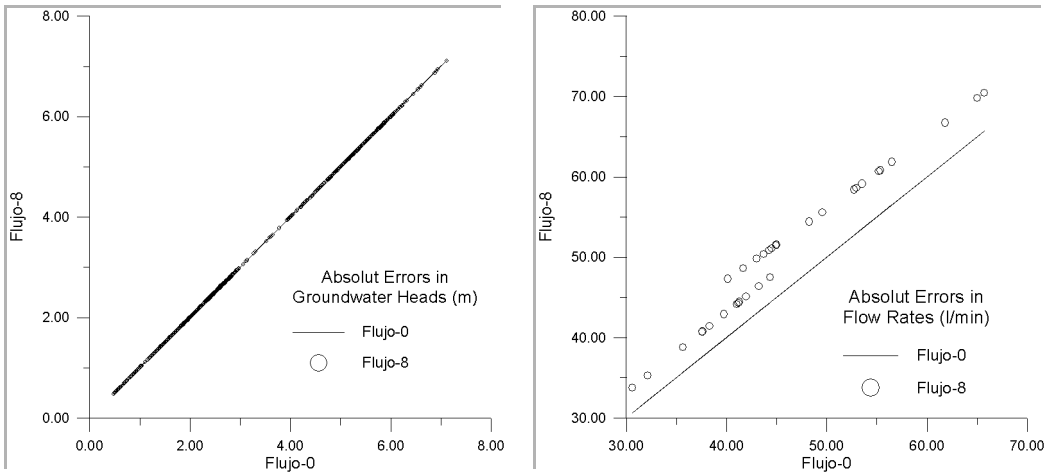

Figure 7.9. Absolute erros in computed groundwater heads and flow rates into the tunnel. Comparison of the reference run (Flujo-0) and run Flujo-8.

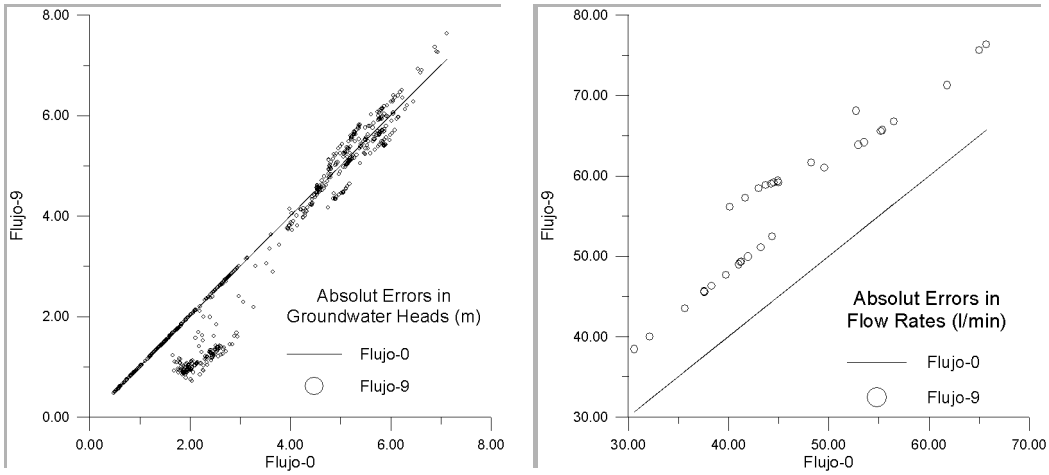

Figure 7.10. Absolute erros in computed groundwater heads and flow rates into the tunnel. Comparison of the reference run (Flujo-0) and run Flujo-9.

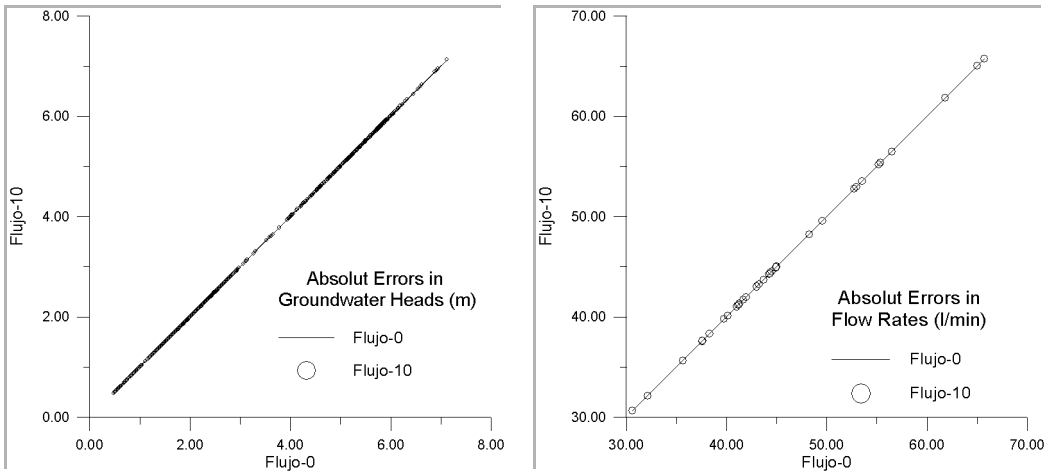

Figure 7.11. Absolute erros in computed groundwater heads and flow rates into the tunnel. Comparison of the reference run (Flujo-0) and run Flujo-10.

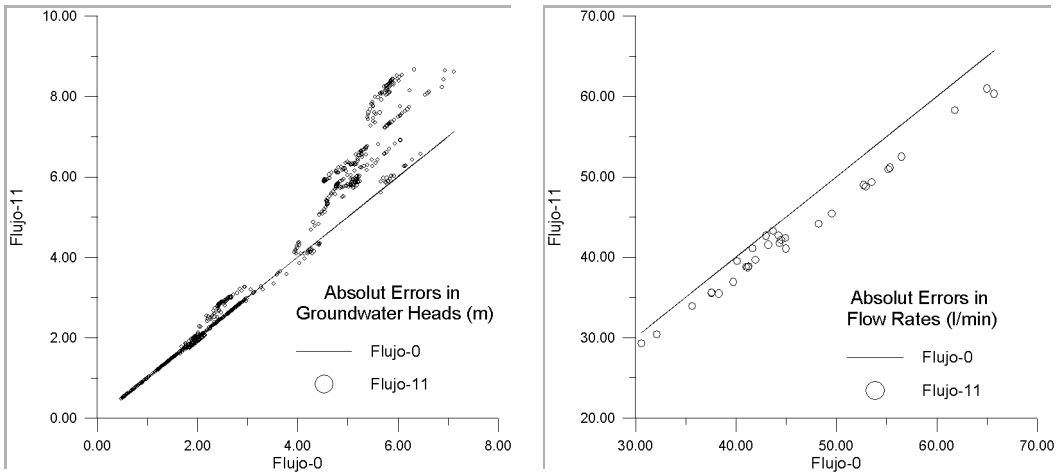

Figure 7.12. Absolute erros in computed groundwater heads and flow rates into the tunnel. Comparison of the reference run (Flujo-0) and run Flujo-11.

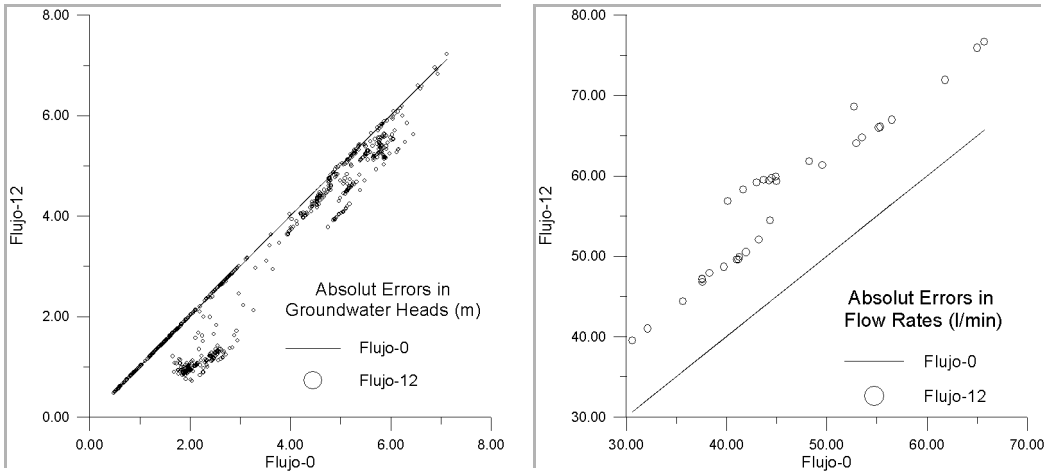

Figure 7.13. Absolute erros in computed groundwater heads and flow rates into the tunnel. Comparison of the reference run (Flujo-0) and run Flujo-12.

The comparison between measured and calibrated hydraulic conductivities of the hydralic conductor domains is shown in Appendix 1. As commented in chapter 5, most of the calibrated hydraulic conductivities are within the range of measured values, except for NE-1 and NNW-7 hydraulic domains, which have calibrated values a little lower than those measured.

The results of the sensitivity runs to the transmissivity values are shown in Figures 7.6 through 7.13. Figures 7.6 and 7.7 illustrate that the permeability of the intersections between hydraulic conductor domains have just a small influence on the computed groundwater heads, and in terms of the flow rates into the tunnel, the numerical model is not sensitive with respect to this parameter. In these particular runs seems to be group of data from one or may be two control points that have significantly greater errors. Again, we have no control about each individual control point. The objective is to evaluate the overall sensitivity of the whole model to each parameter. It could be possible to detect the control points with larger errors but it would not be

trivial.

Looking at the figures 7.8 through 7.13 it is possible to notice that as expected, the numerical model is very sensitive with respect to the transsmissivities of conductor domains. The best global solution (heads and inflows) is obtained with the calibrated reference run. There are some runs in which groundwater heads does not show variations, but this is because there are not availbale observation points at this fracture zones where the transmissivity values were changed (Figures 7.9 and 7.11). Figure 7.12 illustrates that with run Flujo-11 an improvement in computed flow rates was achieved but, by the contrary, the residuals of groundwater heads increase importantly. Run Flujo-12 was the unique sensitivity run in which an improvement of computed groundwater heads was reached (Figure 7.13). In this run the used transmissivity values for NE-1 and NNW-7 were changed to be within the range of the field measurements. One can observe at Figure 7.13 that in spite of computed groundwater heads improve, computed flow rates into the tunnel get worse.

To evaluate the sensitivity of the numerical model with respect to the storativity a number of runs were performed. Table 7.3 summarizes the characteristics of these sensitivity runs.

Table 7.3 Model runs for sensitivity analyses with respect to the storativity.

Name of the run	*Characteristics*
Flujo-0	Base calibrated run
Flujo-13	Storativity of all the hydraulic conductor domains increased in 1 order of magnitude
Flujo-14	Storativity of all the hydraulic conductor domains decreased in 1 order of magnitude
Flujo15	Storativity of all the hydraulic conductor domains increased in 2 orders of magnitude
Flujo-16	Storativity of all the hydraulic conductor domains decreased in 2 orders of magnitude

For the sensitivity analyses of the storativity, the base calibrated values (Appendix 1) were modified in 1 and 2 orders of magnitude. Figures 9.14 through 9.17 show the computed results for the sensitivity analyses with respect to the storativity values.

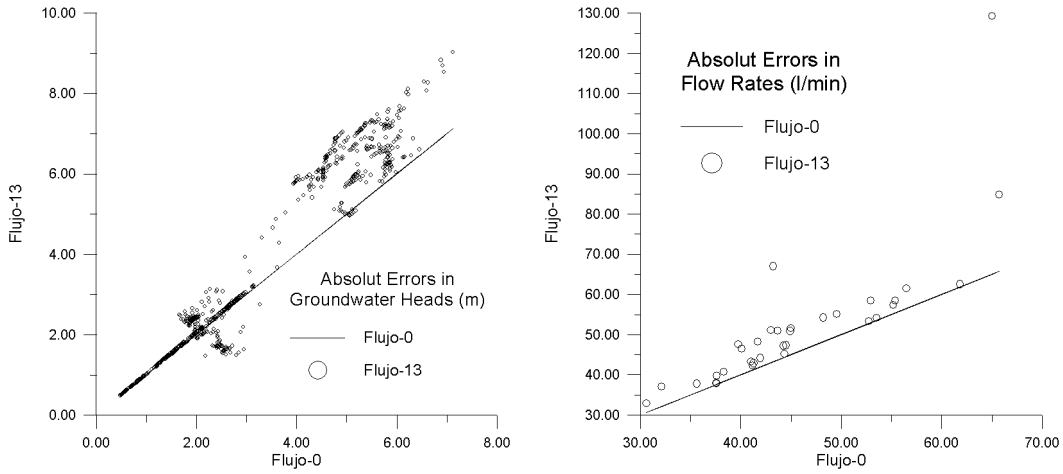

Figure 7.14 Absolute erros in computed groundwater heads and flow rates into the tunnel. Comparison of the reference run (Flujo-0) and run Flujo-13.

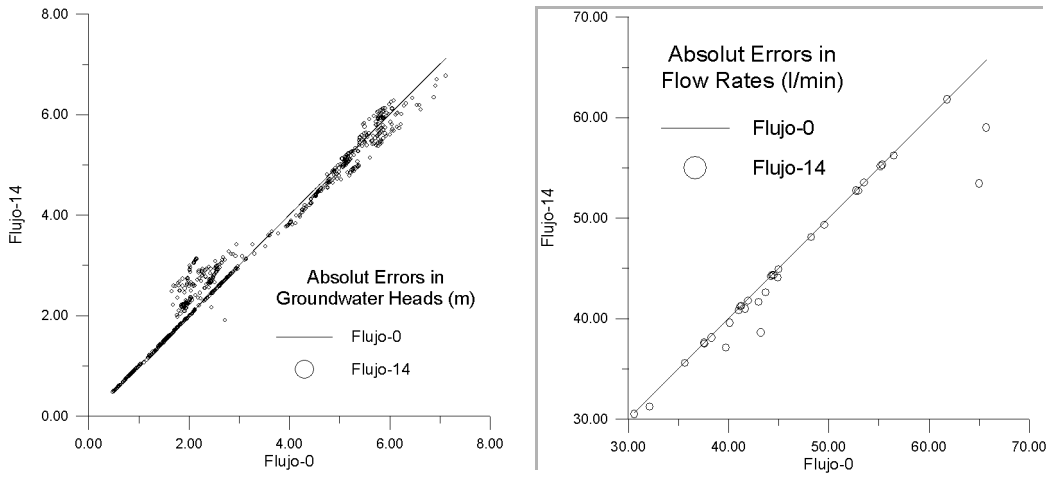

Figure 7.15 Absolute erros in computed groundwater heads and flow rates into the tunnel. Comparison of the reference run (Flujo-0) and run Flujo-14.

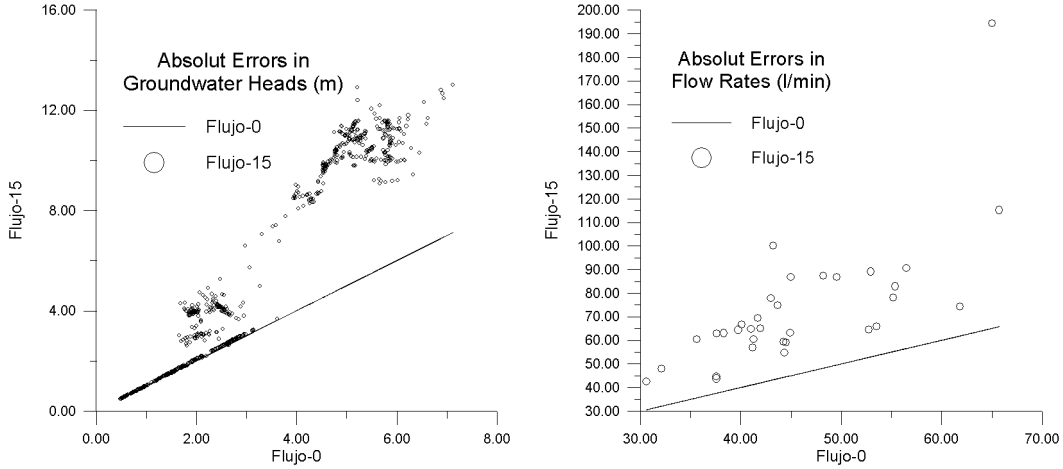

Figure 7.16 Absolute erros in computed groundwater heads and flow rates into the tunnel.

Comparison of the reference run (Flujo-0) and run Flujo-15.

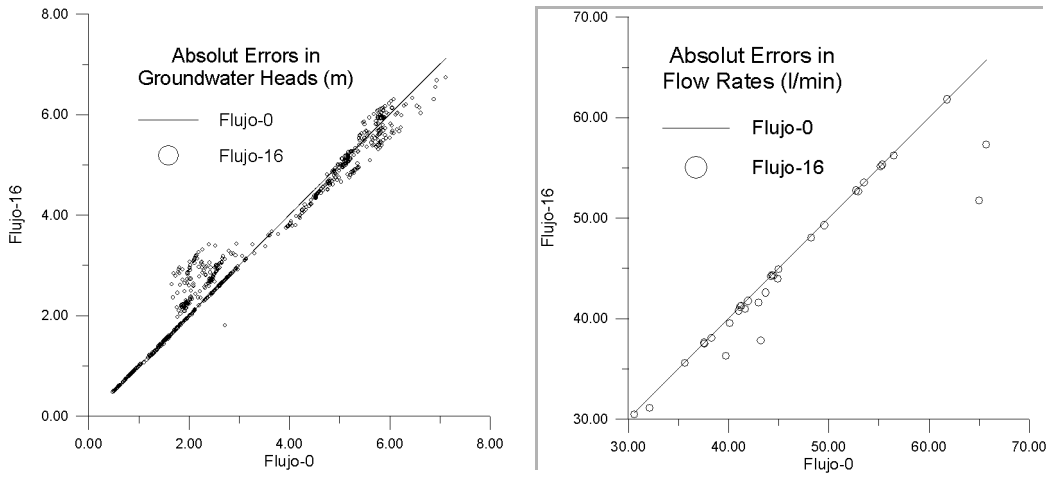

Figure 7.17 Absolute erros in computed groundwater heads and flow rates into the tunnel. Comparison of the reference run (Flujo-0) and run Flujo-16.

Figures 7.14 and 7.16 show that increasing storage coefficients of conductor domains leads to an increase in computed errors for both groundwater heads and flow rates into the tunnel. On the contrary, the numerical model is not sensitive to reductions of the storage coefficients (figures 7.15 and 7.17). It can be concluded that the order of magnitude for the storativities used in the calibrated model is optimum. It must be recalled that the numerical model does not account for rock mass domains, so the storativity values we evaluate are just for the HCD. Increasing the storativity values leads to a less stepper head responses (probably closer to measured trends).However, as shown in Figures 7.14 and 7.15, it also leads to larger errors between computations and measured data, both for tunnel inflows and potentiometric heads. We think that the “stepper” responses computed with the numerical model is a resut of neglecting the role of the rock domains and then a limitation of the adopted approach.

7.3 SENSITIVITY ANALYSIS OF SOLUTE TRANSPORT

As previously shown, from the sensitivity analysis of groundwater flow several posibilities were tested in the case of boundary and initial conditions. In the same manner, different scenarios for initial distribution of concentrations can be found.

Table 7.2 shows a summary of the runs performed to evaluate the sensitivity of the numerical model in terms of solute transport.

Three different initial conditions have been generated for the sensitivity analysis:

a) Initial chloride distribution as provided by the Task #5 data delivery (Gurban et al.; 1998)

b) Interpolation from the Regional Model (Svensson, 1997) salinity results. This interpolation contains an intermediate step because a transformation of salinity into chloride concentration is needed.

c) A new generation of initial chloride concentations by interpolation of the 32 available measured values of the pre-investigation phase. In addition to measured values, a guess of the initial concentration at the 15 control points location were included as "measured data". Besides, 353 points were also included in order to represent island and Baltic Sea values. The kriging method was used to generate the spatial interpolation of the data. Actual kriging was performed with the program GEOS developed by Samper (1990).

Table 7.2. Runs for solute transport sensitivity analyses.

Name of the run	*Characteristics*
Transporte-0	Base calibrated run
Transporte-1	Initial chloride concentrations from Svensson (1997) Regional Model
Transporte-2	Same as *Transporte-1* with Svensson (1997) Regional Model flow conditions
Transporte-3	Svensson (1997) Regional Model flow conditions with the initial chloride concentrations from *Transporte-0*
Transporte-4	Initial flow conditions (base run) with an alternative kriging interpolation of initial chloride concentrations.

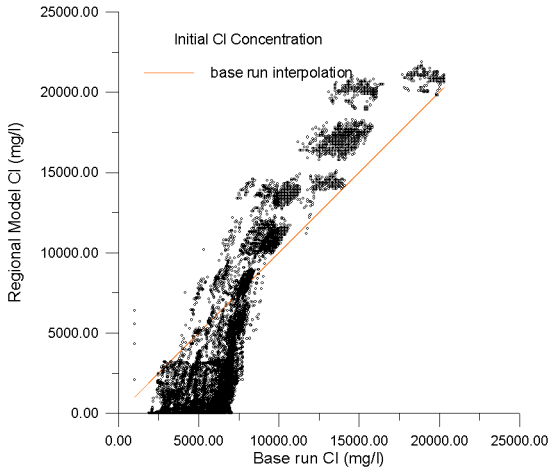

Figure 7.18. Regional Model initial concentrations (X) versus base run initial concentrations (Y).

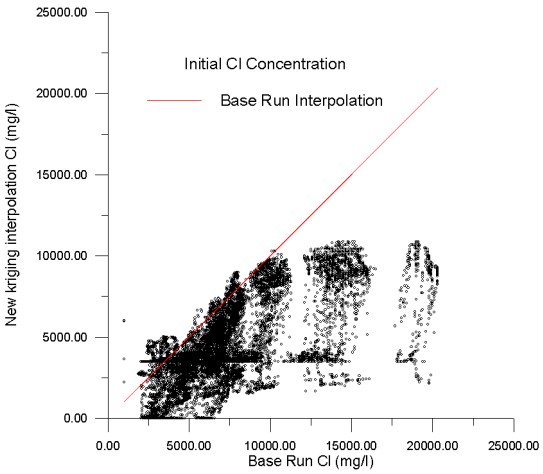

Figure 7.19. The new kriging interpolation of initial chloride concentrations (X) versus base run initial concentrations (Y).

Figures 7.18 and 7.19 show a comparison between the three different initial conditions considered in the sensitivity analysis. One can observe in Figure 7.19 that the new initial conditions generated by kriging interpolation are more dilute than the initial conditions of the base run. Initial condition generated with Regional Model results are both more diluted in some parts and more concentrated in others (figure 7.18). Figure 7.20 through 7.24 show the computed results obtained with the 5 sensitivity runs of the numerical model, as were defined in table 7.3. Computed results are compared against measured data at the tunnel weirs in terms of electrical conductivity. These figures illustrate that computed results are very sensitive with respect to the initial concentration field used as initial condition for solute transport. The best agreement with measured data were obtained with runs 0 and 4. The worse results of runs 2 and 3 are probably due to the fact that these runs include Regional Model groundwater heads as initial conditions for groundwater flow, so it can be concluded that transport result of the numerical model are sensitive to groundwater flow initial conditions.

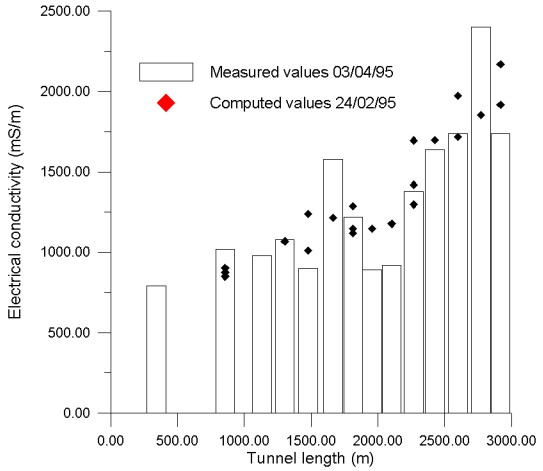

Figure 7.20 Measured and computed values (Run Tranporte-0) of electrical conductivity at the tunnel weirs.

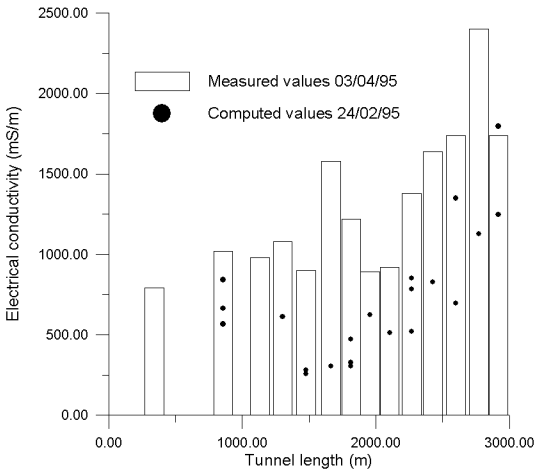

Figure 7.21 Measured and computed values (Run Tranporte-1) of electrical conductivity at the tunnel weirs.

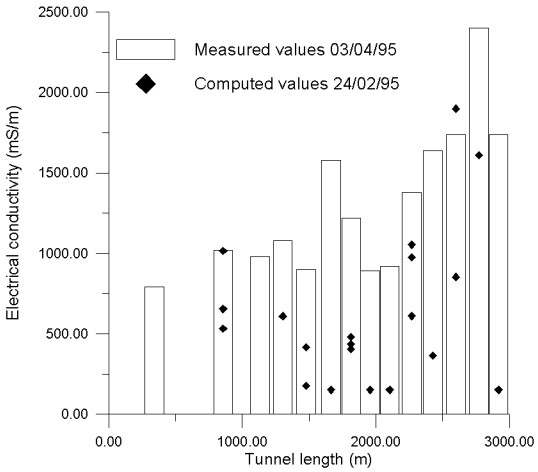

Figure 7.22 Measured and computed values (Run Tranporte-2) of electrical conductivity at the tunnel weirs.

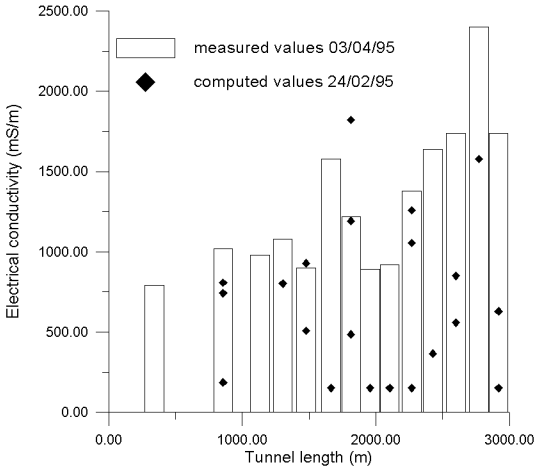

Figure 7.23 Measured and computed values (Run Tranporte-3) of electrical conductivity at the tunnel weirs.

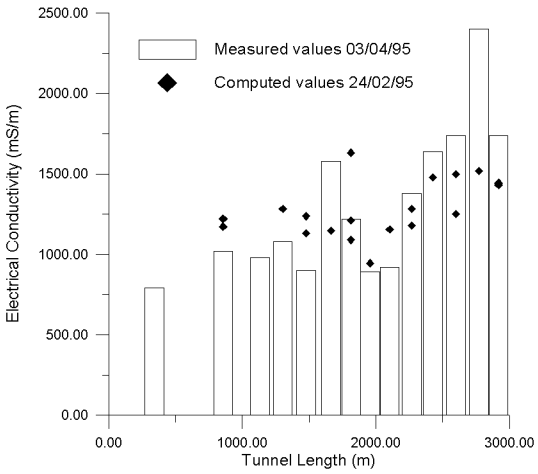

Figure 7.24 Measured and computed values (Run Tranporte-4) of electrical conductivity at the tunnel weirs.

Run Transporte-4 (figure 7.24) shows a good agreement with measured data in the intermediate section of the tunnel. For this section, the computed results using the new initial conditions generated by kriging improve the results of the base run. This improvement is due to the fact that we use 15 additional "measured data" which were estimated by using the first available concentration at each control point. In spite that these additional data do not correspond to the pre-investigation phase, they were measured at the very early stages of the construction phase.

Figures 7.25 to 7.39 show the comparison between measured and computed values for chloride concentrations at the 15 selected control points. Computed values with run Tranporte-0 and run Transporte-4 are included because they provide the best results at the tunnel weirs. Looking at these figures one can realize that the numerical model is highly sensitive to the initial conditions of concentrations. An alternative generation of the initial concentrations field provides as good results as those provided by using the initial distribution delivered by the Task 5 (Gurban et al., 1998).

Here, the strong conclusion is that by using two different initial conditions we get very different computed concentrations. Therefore, the greatest source of uncertainty in the Äspö site-scale model are the initial concentrations. Numerical model results are highly constrained by these initial conditions.

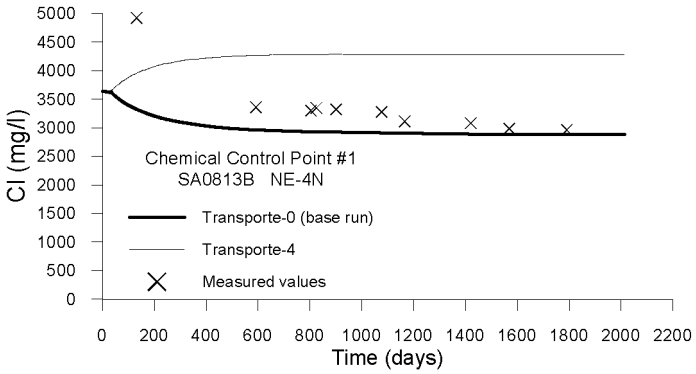

Figure 7.25 Chloride concentrations at control point 1: Measured values and computed results with run Transporte-0 (base run) and run Transporte-4 (new initial conditions generated by kriging).

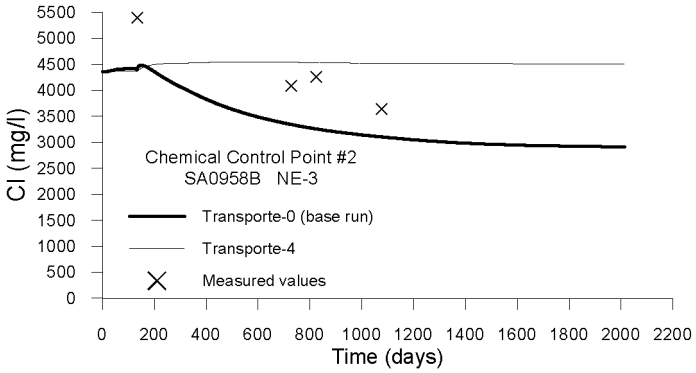

Figure 7.26 Chloride concentrations at control point 2: Measured values and computed results with run Transporte-0 (base run) and run Transporte-4 (new initial conditions generated by kriging).

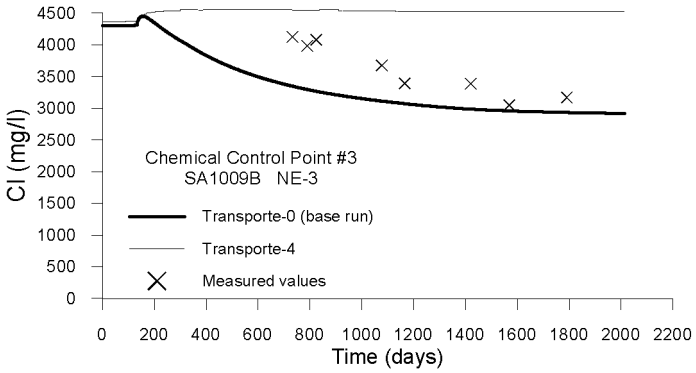

Figure 7.27 Chloride concentrations at control point 3: Measured values and computed results with run Transporte-0 (base run) and run Transporte-4 (new initial conditions generated by kriging).

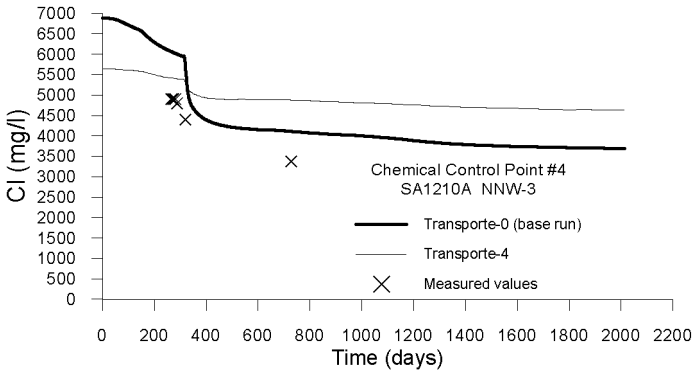

Figure 7.28 Chloride concentrations at control point 4: Measured values and computed results with run Transporte-0 (base run) and run Transporte-4 (new initial conditions generated by kriging).

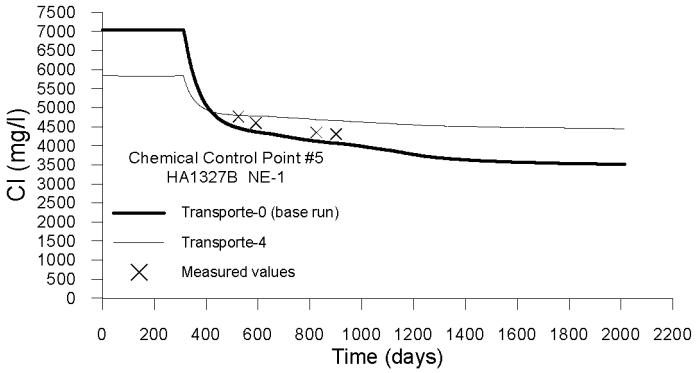

Figure 7.29 Chloride concentrations at control point 5: Measured values and computed results with run Transporte-0 (base run) and run Transporte-4 (new initial conditions generated by kriging).

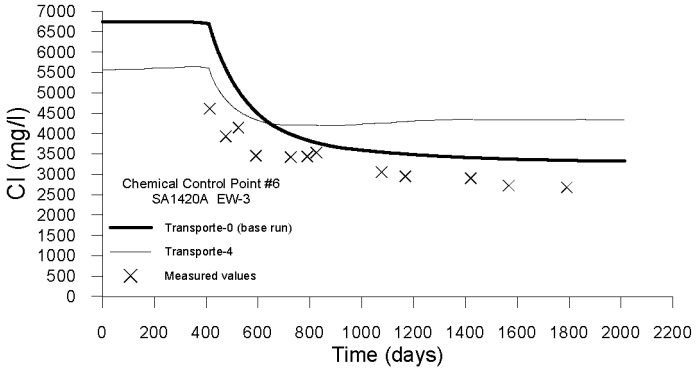

Figure 7.30 Chloride concentrations at control point 6: Measured values and computed results with run Transporte-0 (base run) and run Transporte-4 (new initial conditions generated by kriging).

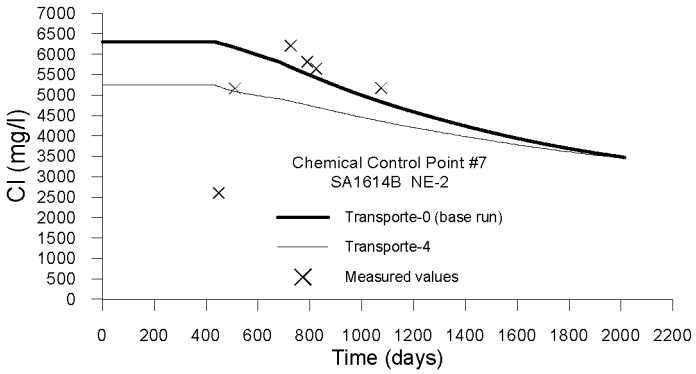

Figure 7.31 Chloride concentrations at control point 7: Measured values and computed results with run Transporte-0 (base run) and run Transporte-4 (new initial conditions generated by kriging).

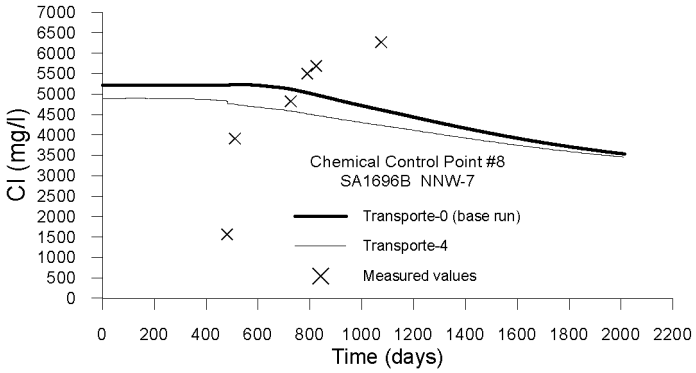

Figure 7.32 Chloride concentrations at control point 8: Measured values and computed results with run Transporte-0 (base run) and run Transporte-4 (new initial conditions generated by kriging).

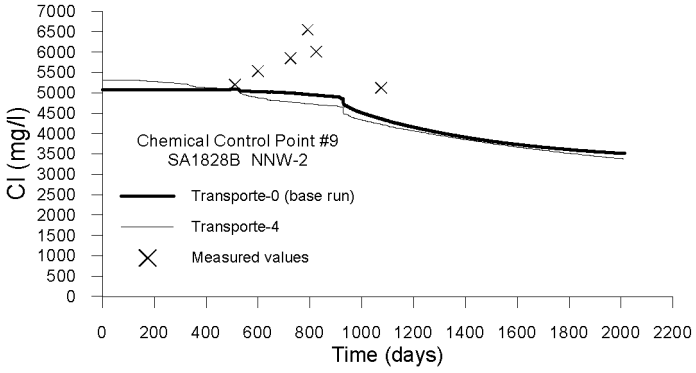

Figure 7.33 Chloride concentrations at control point 9: Measured values and computed results with run Transporte-0 (base run) and run Transporte-4 (new initial conditions generated by kriging).

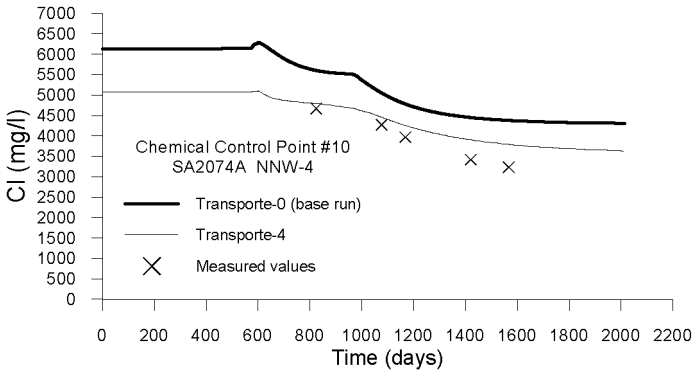

Figure 7.34 Chloride concentrations at control point 10: Measured values and computed results with run Transporte-0 (base run) and run Transporte-4 (new initial conditions generated by kriging).

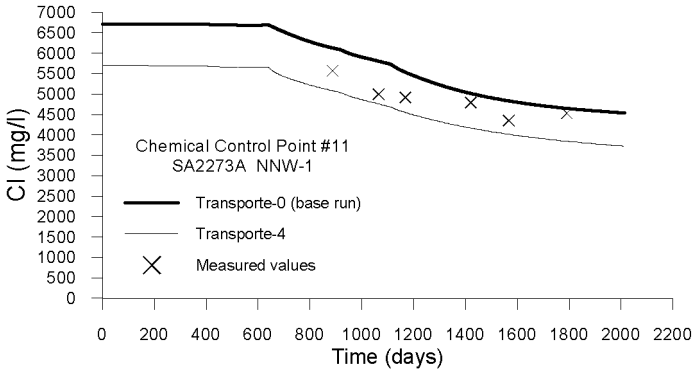

Figure 7.35 Chloride concentrations at control point 11: Measured values and computed results with run Transporte-0 (base run) and run Transporte-4 (new initial conditions generated by kriging).

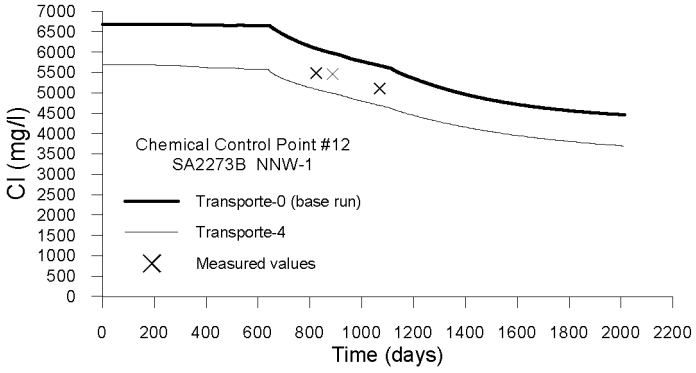

Figure 7.36 Chloride concentrations at control point 12: Measured values and computed results with run Transporte-0 (base run) and run Transporte-4 (new initial conditions generated by kriging).

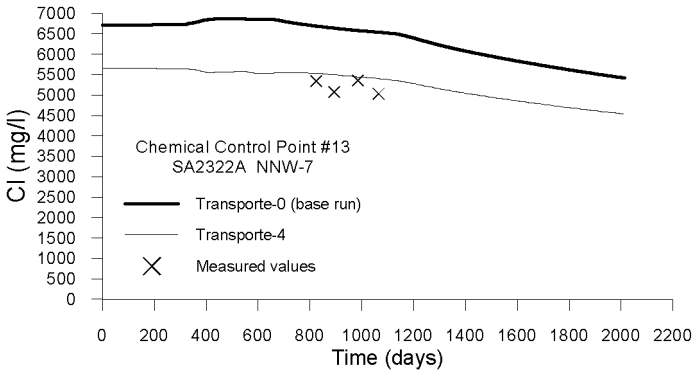

Figure 7.37 Chloride concentrations at control point 13: Measured values and computed results with run Transporte-0 (base run) and run Transporte-4 (new initial conditions generated by kriging).

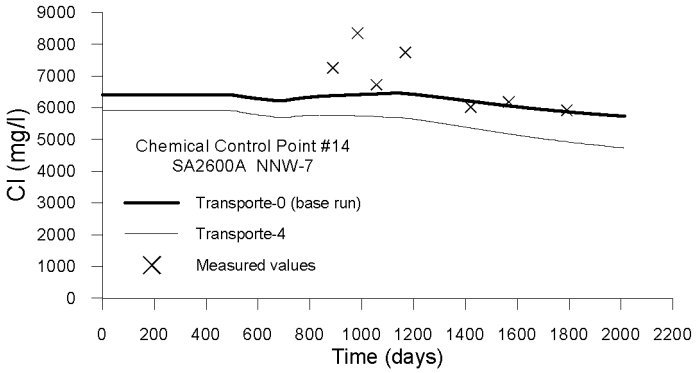

Figure 7.38 Chloride concentrations at control point 14: Measured values and computed results with run Transporte-0 (base run) and run Transporte-4 (new initial conditions generated by kriging).

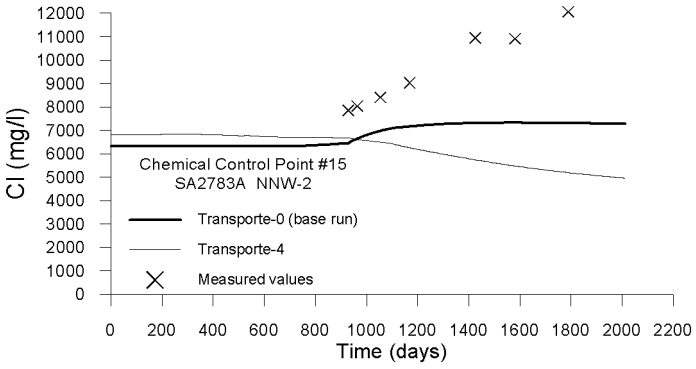

Figure 7.39 Chloride concentrations at control point 15: Measured values and computed results with run Transporte-0 (base run) and run Transporte-4 (new initial conditions generated by kriging).

8 MODEL VALIDATION

8.1 GROUNDWATER FLOW: ADDITIONAL DATA

Figures 8.1 through 8.15 show the comparison between computed and measured groundwater heads at the 15 selected control points (Appendix 2). These figures show the same computed results already shown at Chapter 5, but measured data have been updated with additional data not used in the calibration of the groundwater flow model (validation data). Data used for calibration include all available database between July, 1st of 1990 and January, 24th of 1994, for the 15 selected control points. Validation data include all available data until December, 31st of 1996.

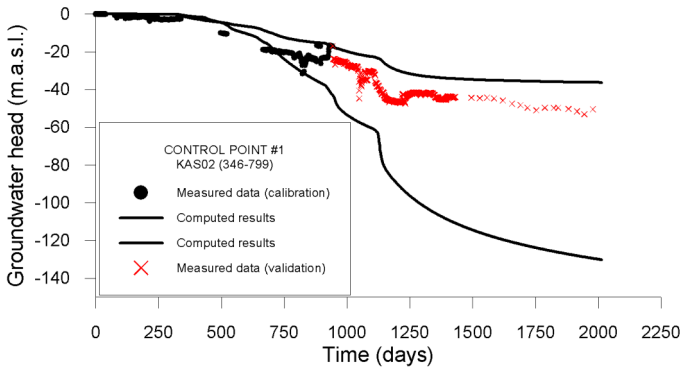

Figure 8.1 Computed and measured groundwater head at KAS02 (346-799) borehole. Measured values have been updated with additional data not used in the calibration stage.

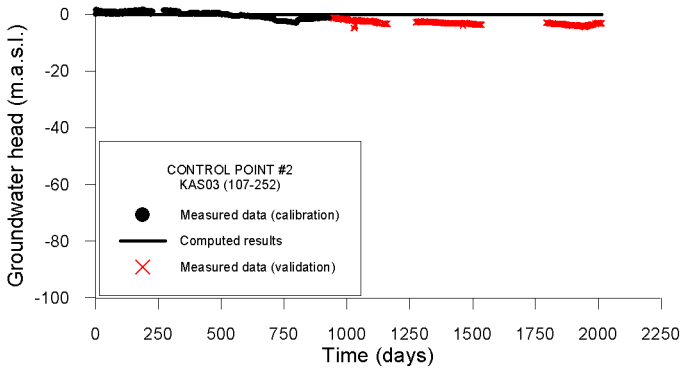

Figure 8.2 Computed and measured groundwater head at KAS03 (107-252) borehole. Measured values have been updated with additional data not used in the calibration stage.

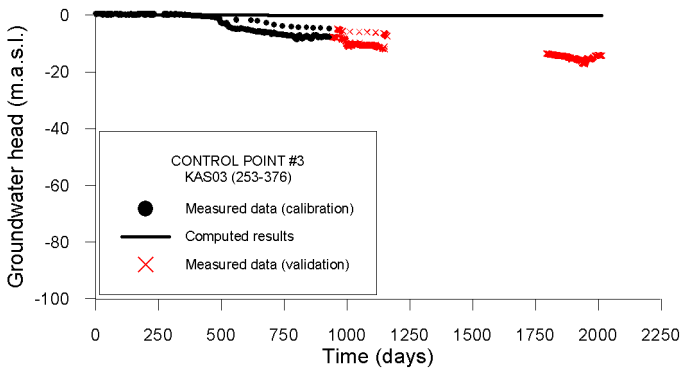

Figure 8.3 Computed and measured groundwater head at KAS03 (252-373) borehole. Measured values have been updated with additional data not used in the calibration stage.

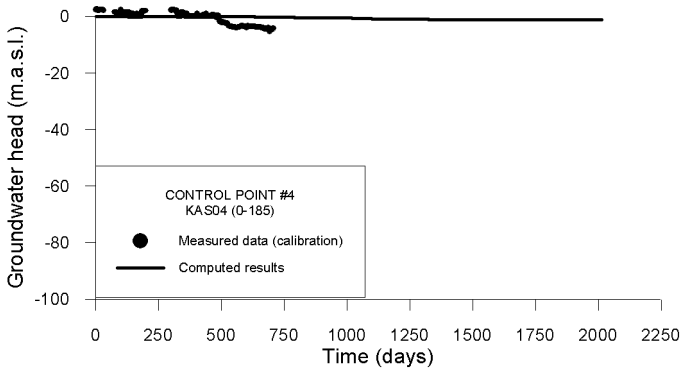

Figure 8.4 Computed and measured groundwater head at KAS04 (0-185) borehole. There are no additional (validation) data for this control point.

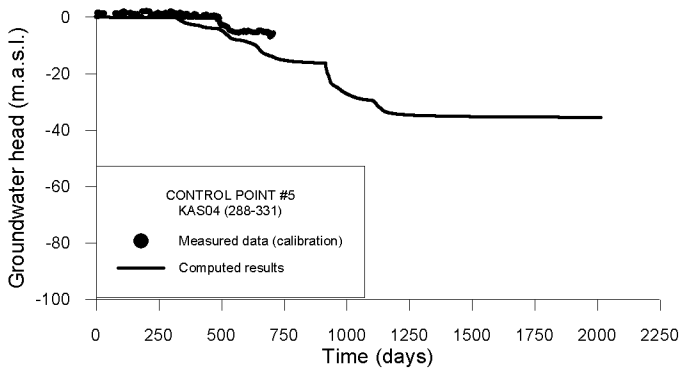

Figure 8.5 Computed and measured groundwater head at KAS04 (288-331) borehole. There are no additional (validation) data for this control point.

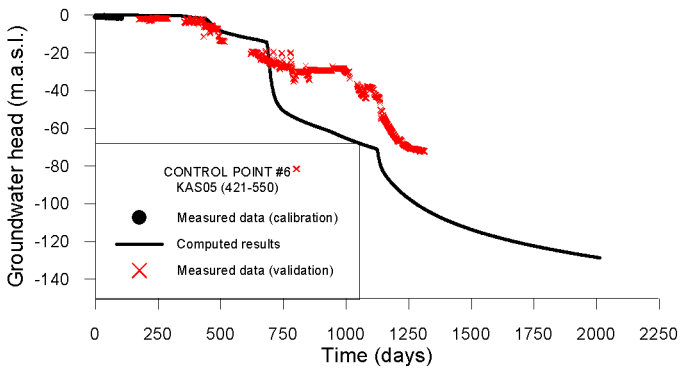

Figure 8.6 Computed and measured groundwater head at KAS05 (440-550) borehole. Measured values have been updated with additional data not used in the calibration stage.

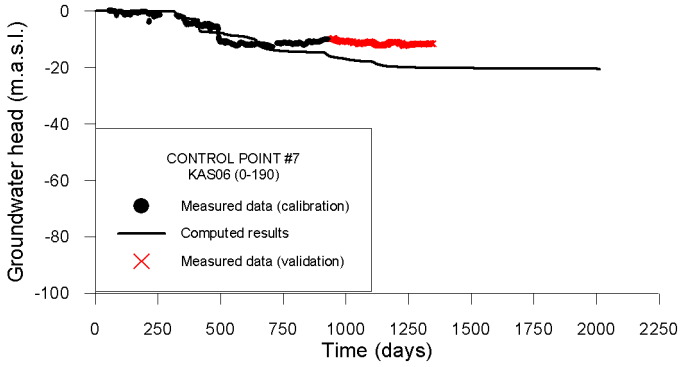

Figure 8.7 Computed and measured groundwater head at KAS06 (0-190) borehole. Measured values have been updated with additional data not used in the calibration stage.

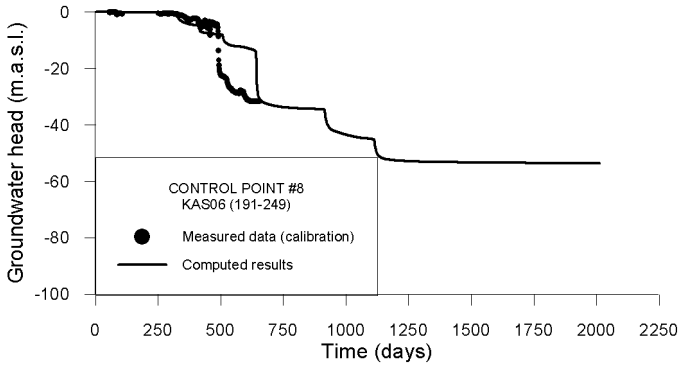

Figure 8.8 Computed and measured groundwater head at KAS06 (191-249) borehole. There are no additional (validation) data for this control point.

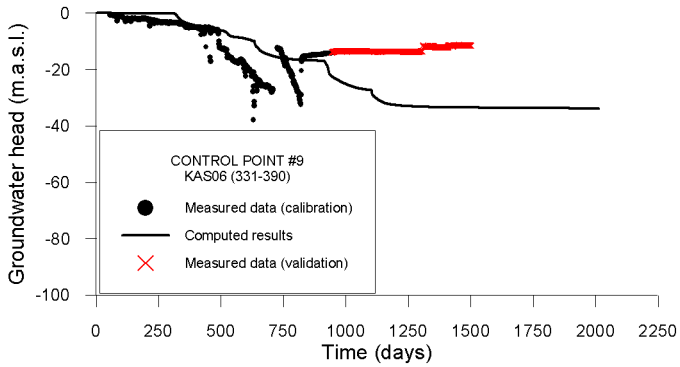

Figure 8.9 Computed and measured groundwater head at KAS06 (331-390) borehole. Measured values have been updated with additional data not used in the calibration stage.

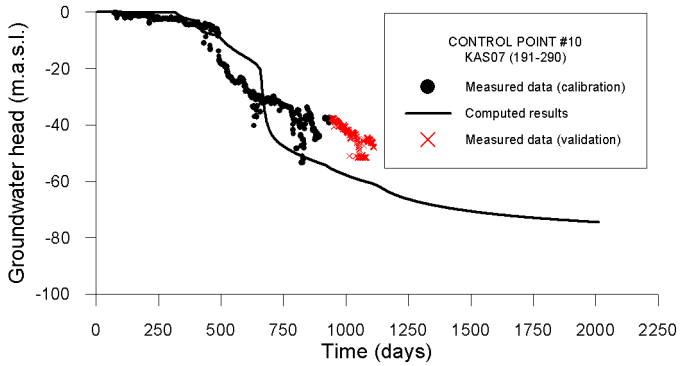

Figure 8.10 Computed and measured groundwater head at KAS07 (191-290) borehole. Measured values have been updated with additional data not used in the calibration stage.

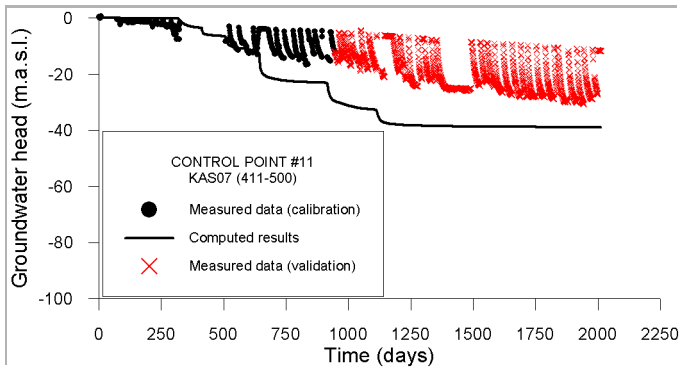

Figure 8.11 Computed and measured groundwater head at KAS07 (411-500) borehole. Measured values have been updated with additional data not used in the calibration stage.

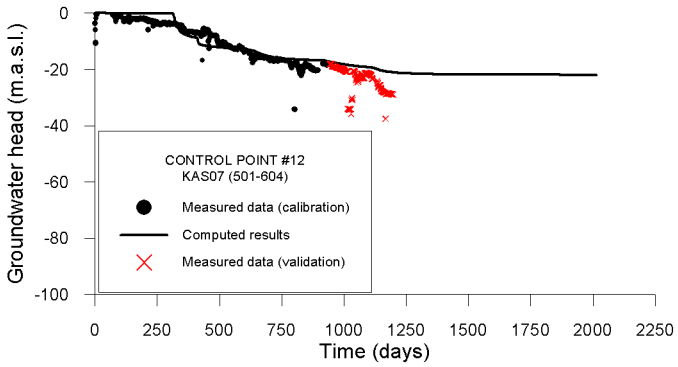

Figure 8.12 Computed and measured groundwater head at KAS07 (501-604) borehole. Measured values have been updated with additional data not used in the calibration stage.

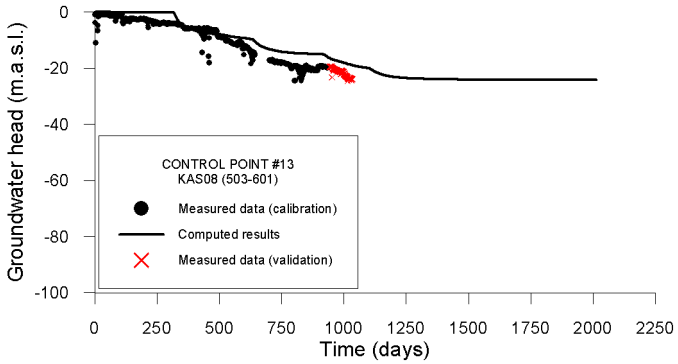

Figure 8.13 Computed and measured groundwater head at KAS08 (503-601) borehole. Measured values have been updated with additional data not used in the calibration stage.

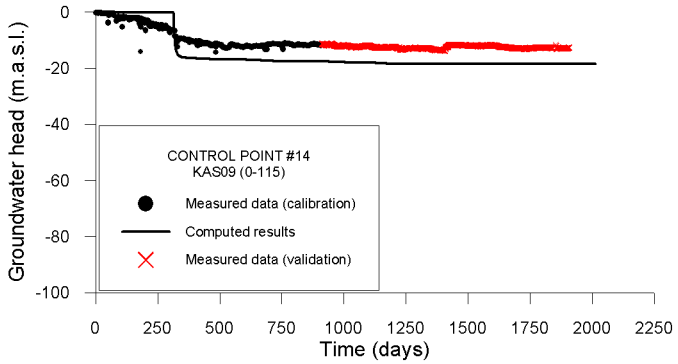

Figure 8.14 Computed and measured groundwater head at KAS09 (0-115) borehole. Measured values have been updated with additional data not used in the calibration stage.

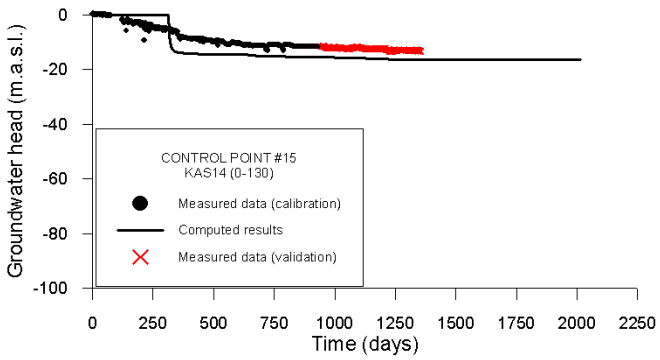

Figure 8.15 Computed and measured groundwater head at KAS14 (0-130) borehole. Measured values have been updated with additional data not used in the calibration stage.

The comparison between measured and computed groundwater heads at the 15 selected control points show that the performed numerical model is able to reproduce, for the most part, the impact of the tunnel construction on the groundwater system of the Äspö Island. Taking into consideration the scale and complex geometry of the model, we think that computed groundwater heads predict reasonably good measured field data for the validation period in most of the selected control points. One of the most relevant discrepancy is found in KAS03 (252-373) borehole (Figure 8.3), where the numerical model did not compute any drawdown but actually a steady drawdown of around 15 m was measured. Measured groundwater heads at boreholes KAS06 (331-390) and KAS07 (411-500) show clear anomalies which are not reproductible with the numerical model. The rest of the selected control points show a good agreement with respect to the additional data not used for calibration. A very remarkable control point is KAS05 (440-550) borehole section (Figure 8.6) where almost no calibration data were used.

It is worth refering back to Figure 5.9a (also Figure 8.1) which correspond to a packed borehole interval larger than 450 m. This interval is intersected by 2 HCD but there is a single measurement for the whole borehole interval. In the numerical model there is not hydraulic connection between both HCD and that is the reason why 2 different responses are computed. It can be noticed that there is a significant step drawdown (measured) at day 1100 which is clearly reproduced by the numerical model. In the case of Figure 8.8 there is a drastic measured drawdown that the model does not reproduce. This observation point (number 8) is located on the HCD NNW-1 which was crossed by the tunnel construction during day 509. Nevertheless, there are other control points located in the same HCD that show a good agreement with measured data, in addition to the good agreement also achieved in the computed flow rates into the tunnel sections connected with this HCD. A possible explanation for this main discrepancy can be found in the ocurrence of heterogeneity inside an individual fracture zone. Other possibility is related with the ocurrence of some conductive features not included in the geometrical model (like the 'mystery feature' proposed by the Golder-JNC Team).

8.2 TRANSPORT OF SOLUTES: PREDICTIONS

As a difference with respect to the groundwater flow model, the validation of the solute transport model was done by means of predicting the breaktrough curves at

some selected prediction points. Measured field database was avilable for the tunnel section 0-2900 m, while no information was available for the prediction section of the tunnel (2900-3600 m) during the calibration stage.

Predictions for 3 of the 4 proposed control points have been made. One of the proposed control points is located within a Rock Domain, and due to the fact that the selected approach of the numerical model accounts only for the Hydraulic Conductor Domains (see Chapter 4), predictions at Rock Domains were not possible.

As comented in Chapter 6, almost no calibration of the numerical model was made with respect to the transport parameters. The sensitivity analyses shown at Chapter 7 leads to the conclusion that the most important uncertainty with respect to the transport of solutes is associated with the establishment of the initial conditions. In fact, it has been shown that one of the performed sensitivity runs (with an alternative interpolation of the initial concentration field) was able to compute as good results as those computed by the base run and, in addition to that, measured data at many of the selected chemical control points were found to be within the range of the computed results by these two runs of the numerical model. Due to the important uncertainty detected in the initial conditions, predictions were performed as a range instead as a single breakthrough curve. The range of the prediction correspond to the band bounded by the results of two runs of the numerical model corresponding to two different realizations of initial conditions.

Figures 8.16, 8.17 and 8.18 show the comparison between computed predictions for chloride breakthrough curves and measured values at the 3 selected prediction points.

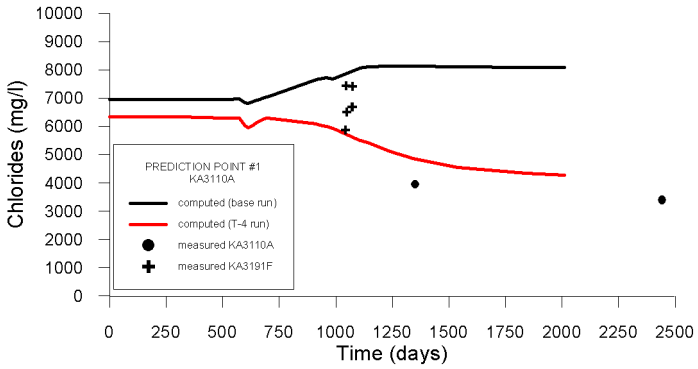

Figure 8.16 Computed and measured breakthrough curves at the prediction point KA3110A.

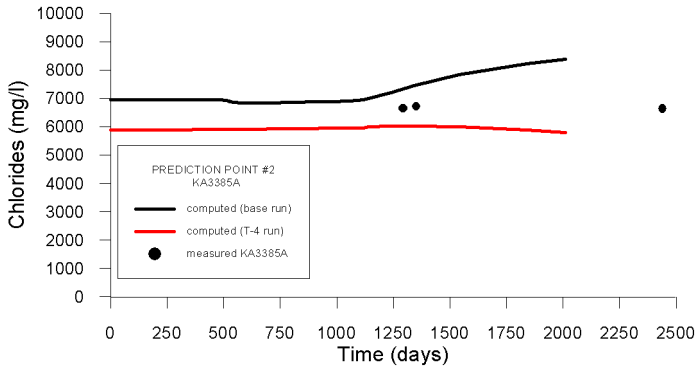

Figure 8.17 Computed and measured breakthrough curves at the prediction point KA3385A.

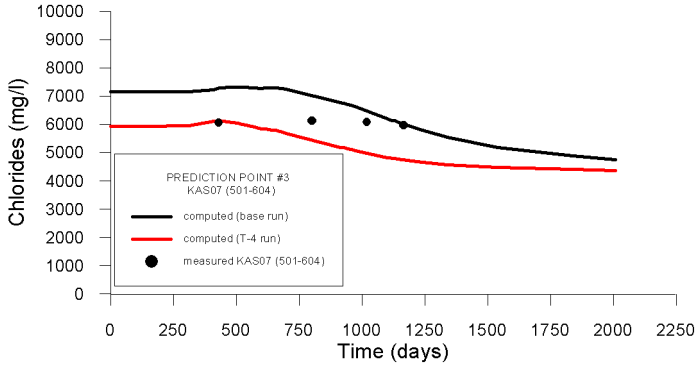

Figure 8.18 Computed and measured breakthrough curves at the prediction point KAS07(501-604).

In the same manner than was observed for many control points located at the calibration section of the tunnel, measured data are within the range of the computed results with both runs of the numerical model. This fact indicates that the available database for undisturbed conditions (prior to the tunnel construction) is not complete enough to generate robust initial conditions for the numerical model. The evaluation of the existent uncertainty associated to the generation of the initial conditions allows one to estimate the accuracy of the numerical model. Thus, predictions can be made as a confidence range better than as a single computed breakthrough curve.

Beacuse the computer requirements (mainly because CPU time) of the numerical model, the sensitivity analyses was performed just in terms of chloride concentrations. In fact, the numerical model does not account for chemical reactions and then, the achieved conclusions can be extrapolated for any other solute. Mixing proportions (of the 4 reference waters proposed by the M3 model) at the prediction points have been also computed, but only using the base run of the numerical model. These computed results for mixing fractions at the prediction points can be saw at Appendix 4.

9 ASSESSMENT OF THE CONSISTENCY BETWEEN HYDRODINAMIC AND HYDROCHEMICAL MIXING MODELS

9.1 MIXING MODELING BACKGROUND

A great effort of hydrochemical research has been done at the Äspö site during the last 12 years. Main achievements and conclusions concerning to the hydrochemistry research are summarized in Rhén et al. (1997 a,b) and Laaksoharju & Wallin (1997). During pre-investigation and construction stages, systematical sampling of groundwater was performed both in boreholes and tunnel walls. Chemical analyses of these samples in addition to mineralogical and bacteriological characterization constitute the background to establish a consistent hydrochemical model of the Äspo site.

One remarkable hydrochemical feature is the ocurrence of a clear salinity gradient in depth. With undisturbed conditions, there was a 100-200 m thick fresh water lens below Äspö island surface, follow by a progressive salinity increase, reaching values of 20 g/l at a depth of 800 m.

The complexity of the groundwater chemistry of the Äspö system is the result of the very complex geological and paleoclimatic framework of the last thousands of years at this place. It is well known that the Baltic Platform has been affected by a number of important quaternary glaciations. Ice load was the responsible of isostatic movements which undoubtly affect the groundwater system. During the last 13,000 years, the Äspö site has been covered by fresh water (deglaciation) as well as by several marine waters untill reaching nowadays geographycal setting. Paleogeographycal history of the Äspö site is rigorously explained by Smellie et al. (1995).

Laaksoharju et al. (1999 a,b) propose a hydrochemical model to explain the chemical groundwater evolution at Äspö due to the impact of the tunnel construction (M3 model). The main premise of this hydrochemical model assumes that a given groundwater composition is a result of mixing between different initial waters as well as chemical processes. M3 model consist of 3 steps where the first one is a standard multivariate analysis (Principal Component Analysis) to define extreme (or reference) waters, followed by a mixing calculation stage and by a mass balance computation final step, which allows to compute deviations of the ideal mixing behaviour. Eventually, deviations are used to quantify sink and sources of chemical species which can be related with active chemical processes. Laaksoharju et al. (1999 a) propose that, in general, groundwater composition of the Äspö site can be modelled as a mixture of 4 reference groundwater types: brine, glacial, Baltic Sea and meteoric waters. An important conclusion derived of M3 model is that mixing has a dominating impact on the present Äspö groundwater chemistry. Major deviations of the ideal mixing are shown by Na^+, Ca^{2+}, HCO_3^- and SO_4^{2-}, wich is consistent with the results of other hydrochemical studies made at the Äspö HRL. Banwart et al. (1995, 1999) explain the hydrochemistry evolution of the Redox Zone Experiment as a dilution of the saline native groundwater by fresh recharge water. Similarly to M3 model, the mixing model performed by Banwart et al (1995) for the Redox Zone found that the main deviations form the ideal mixing behaviour was shown by Na^+, Ca^{2+}, HCO_3^- and SO_4^{2-}.

9.2 COMPARISON OF HYDRODYNAMIC AND HYDROCHEMICAL MIXING MODEL RESULTS

Mixing models entail a subjective part due to the definition or selection of the extreme components and even more if some of these extreme waters correspond to a relict (fossil) water. On the other hand, mechanistic models, such as hydrodynamic groundwater flow and solute transport numerical models, require using a set of parameters and assumptions which could derive into great uncertainties when a model of a complex, natural system is attempted. In this chapter results of the proposed hydrodynamic numerical model are compared with the results of the hydrochemical mixing model (M3 model) proposed by Laaksoharju et al. (1999a).

Once calibrated the hydrodynamic groundwater flow and transport numerical model, it has been shown that the numerical model is able to reproduce the impact of the tunnel construction on the groundwater system of the Äspö Island. Comparison between measured data and computed results shown a very good agreement in terms of inflows into the tunnel, groundwater head at packed borehole sections and break-through curves of conservative species at boreholes located in the tunnel surroundings.

A initial distribution of the mixing fractions of the 4 main reference waters proposed by M3 model (Brine, Baltic Sea, Glacial and Meteoric) were included into the hydrodynamic model and considered as conservative species. Thus, consistency between hydrodynamic numerical and M3 models can be checked by comparison of the results computed by both type of models.

If the hydrodynamic numerical model is consistent and well constructed (which means that is really able to reproduce the natural system) and, if the hydrochemical evolution of the system can be explained mainly as the mixing of 4 reference waters (as proposed by M3 model), then “transported” mixing fractions evolution must be in agreement with M3 results.

In general, a very good agreement was observed between the results computed by the hydrodynamic groundwater flow and solute transport numerical model and those proposed by the hydrochemical mixing model. Looking at the computed results for chlorides and ^{18}O (see Chapter 6) it was noticed that the better the agreement with conservative species the better the agreement with M3 model results. In fact, a better agreement for mixing fractions than for a conservative species would make no sense within the actual approach used to assess the consistency between both kind of models.

Figures 9.1 through 9.5 show the comparison between the mixing fractions computed by both types of models at 5 of the 15 control points. The selected control points to make the comparison correspond to some of those control points showing a better agreement for conservative species (see Chapter 6). Computed results for the rest of the selected control points are reported in the Appendix 4.

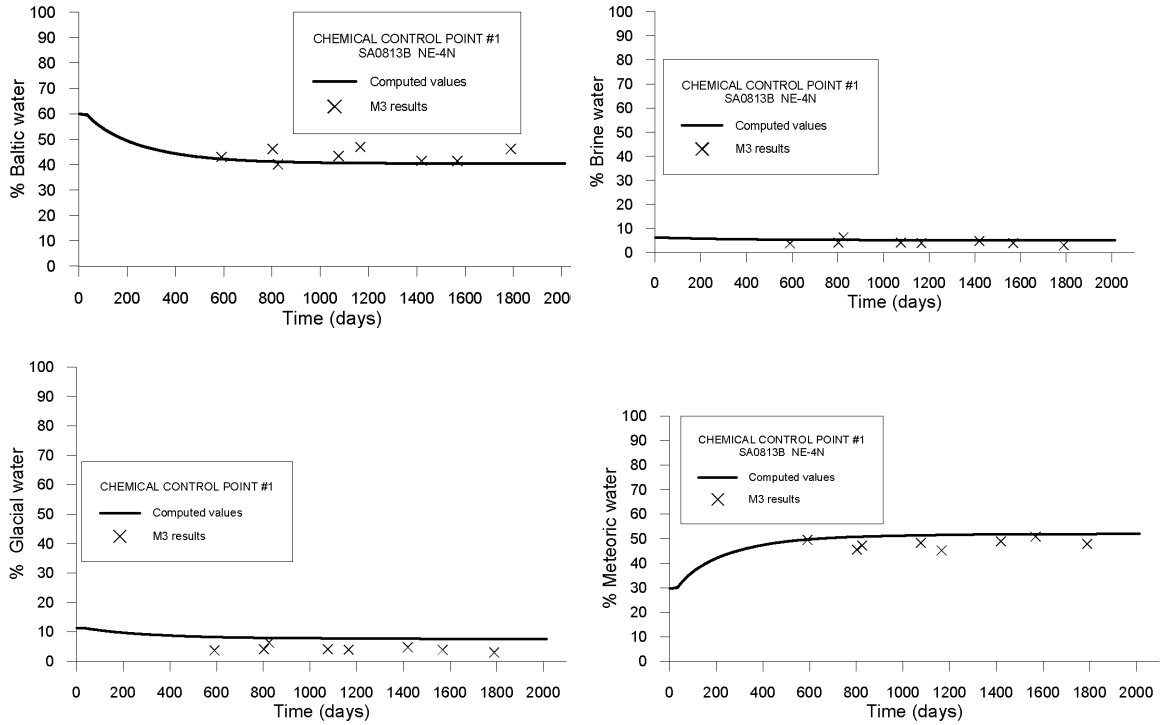

Figure 9.1 Mixing fractions evolution at SA0813B borehole. Solid line: Hydrodynamic numerical model results. Simbols: M3 results.

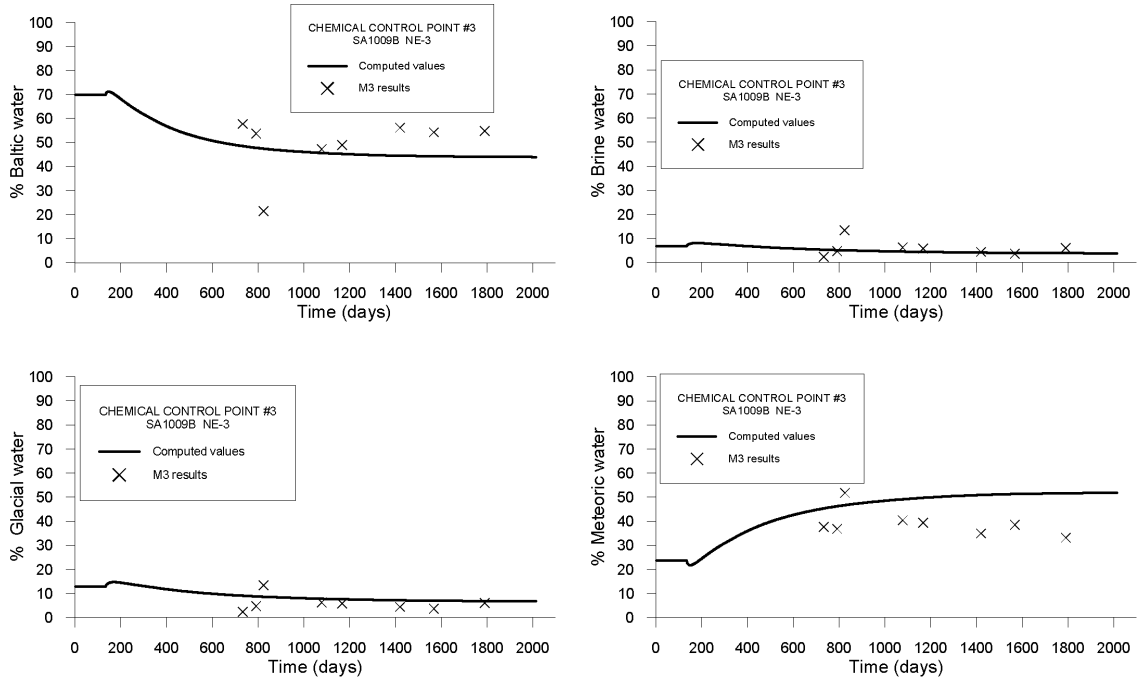

Figure 9.2 Mixing fractions evolution at SA1009B borehole. Solid line: Hydrodynamic numerical model results. Simbols: M3 results.

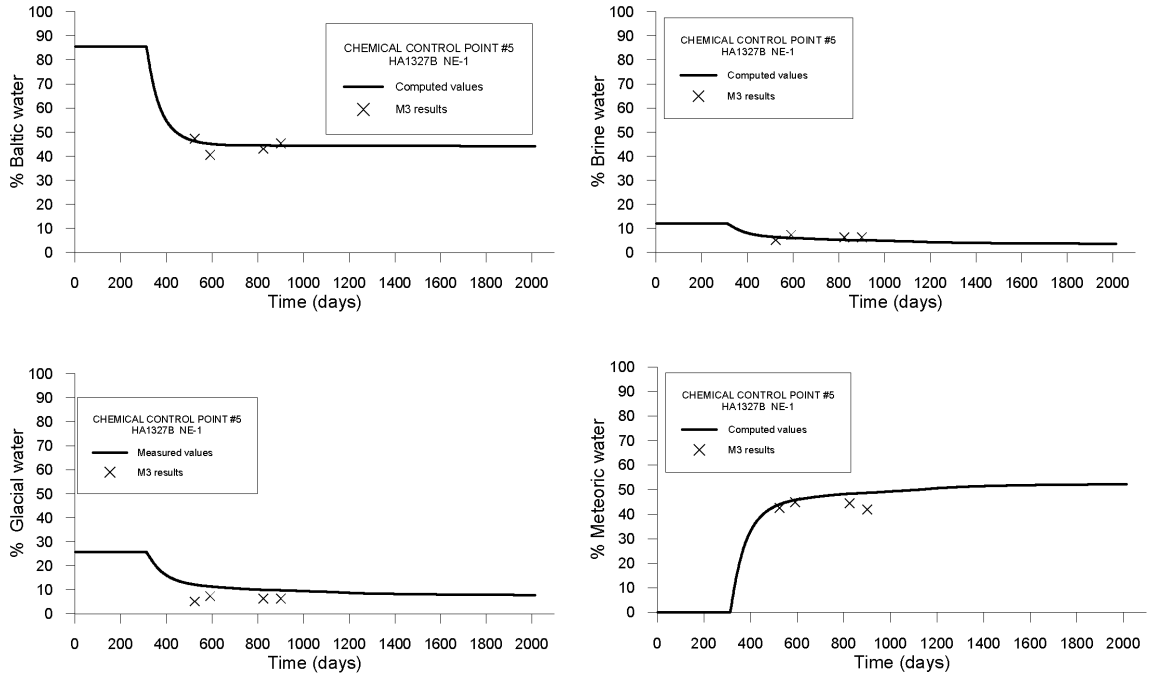

Figure 9.3 Mixing fractions evolution at HA1327B borehole. Solid line: Hydrodynamic numerical model results. Simbols: M3 results.

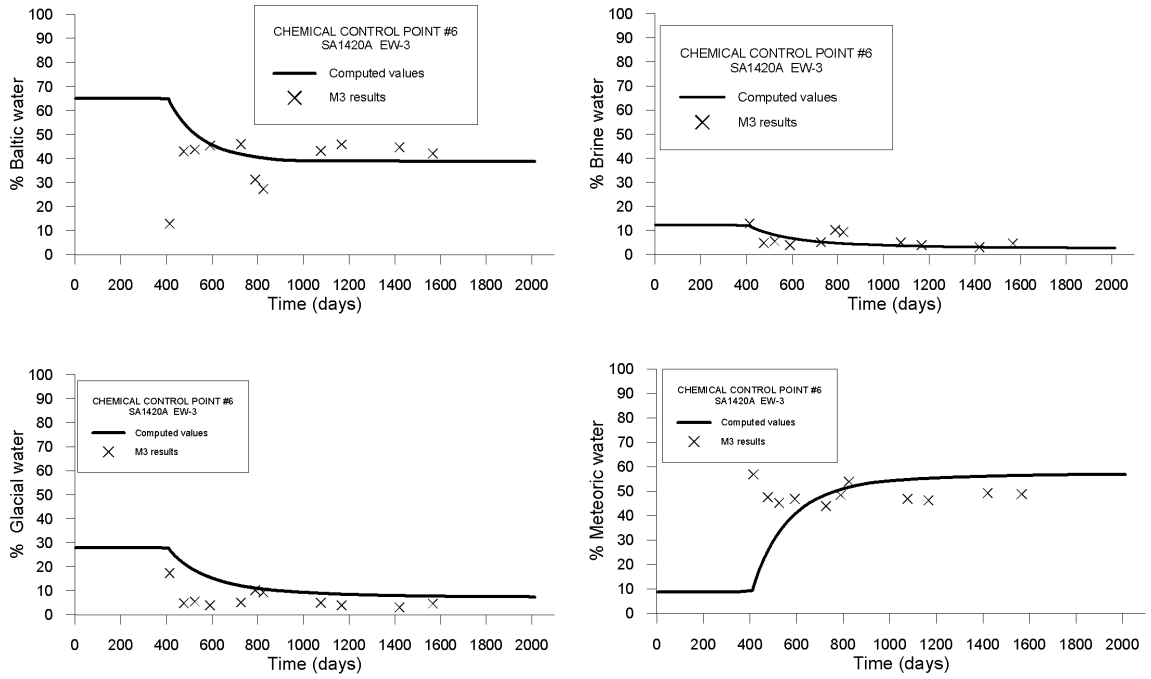

Figure 9.4 Mixing fractions evolution at SA1420A borehole. Solid line: Hydrodynamic numerical model results. Simbols: M3 results.

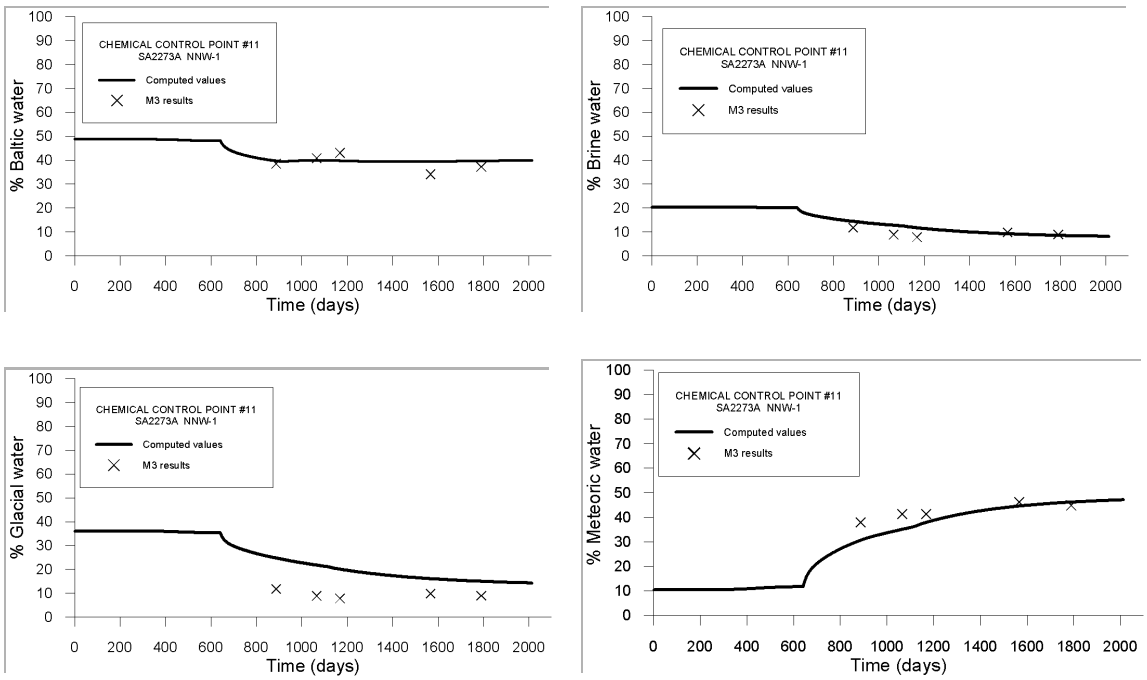

Figure 9.5 Mixing fractions evolution at SA2273A borehole. Solid line: Hydrodynamic numerical model results. Simbols: M3 results.

Looking at figures 9.1 through 9.5 it can be stated that there is an excellent agreement between the hydrodynamically computed mixing fractions and the hydrochemical mixing model (M3 model) results. In fact, the agrement is even better if the accuracy of the M3 model is taken into account. Laaksoharju (2000) states that the uncertainty of the M3 model is < 10% of a mixing fraction. On the other hand, there are also uncertainties related with the hydrodynamic solute transport numerical model. Figure 9.6 show the total sum of the computed mixing proportions at each node of the finite element mesh used in the hydrodynamic model. It can be noticed that there are several nodes where the hydrodynamic model computes a total sum which is greater than 100%. This fact does not reflect the existency of any kind of numerical instability (which was strongly verified when setting up the numerical model), but is reflecting the effect of the interpolation to generate the initial conditions of the numerical model. The possibility of numerical instabilities can be rejected by looking at Figure 9.7, where the initial values of the mixing fractions used by the numerical model show even greater values of the total sum than those computed at the final time of the numerical model. In fact, the total sum of the mixing proportions is also unconsistent in the initial grid provided by the M3 model (Gurban et al, 1998), because this grid is also the result of the interpolation of the computed values (at the sampling points) to a regular 3-D grid (Figure 9.8).

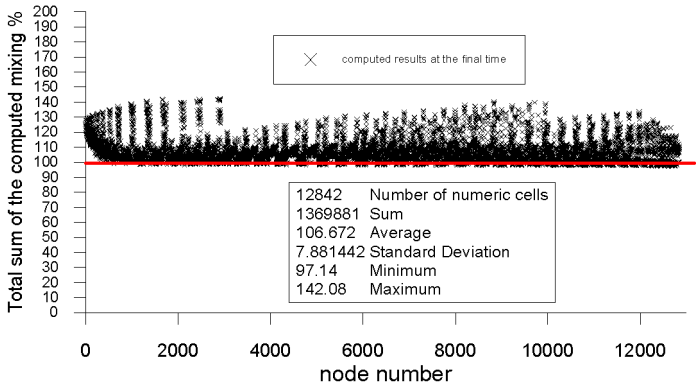

Figure 9.6 Total sum of the computed mixing fractions at each node of the hydrodynamic numerical model for the last computed time.

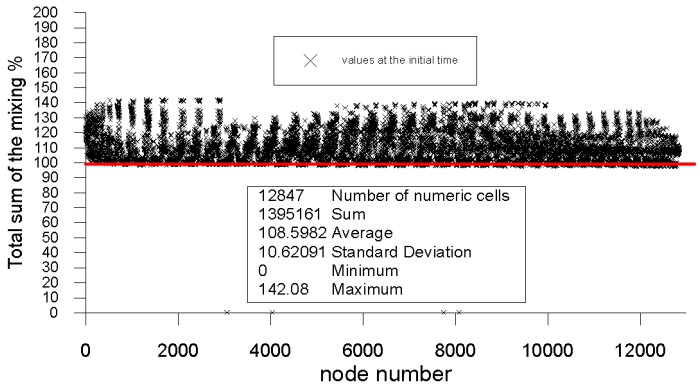

Figure 9.7 Total sum of the computed mixing fractions at each node of the hydrodynamic numerical model for the initial time.

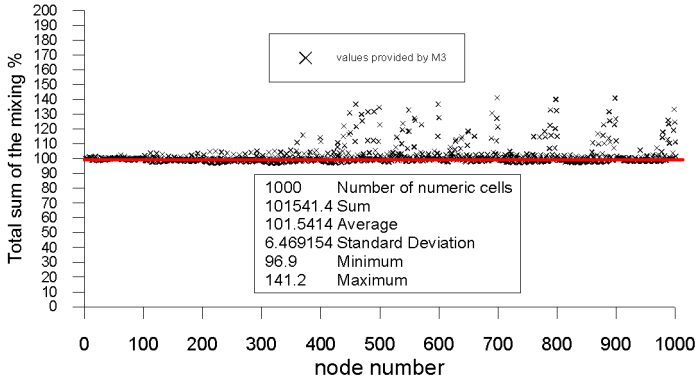

Figure 9.8 Total sum of the mixing fractions computed by the M3 model for undisturbed conditions, as provided by Gurban et al. (1998).

Regarding to all the actual uncertainties related both with hydrodynamic and hydrochemical mixing models, it can be stated that an absolute consistency between both kind of models has been found in this exercise. This absolute consistency must be understood as meaning that computed results by both models are always within the

range of the associated uncertainties of each model. The best agreements have been achieved for those control points which shown also the best agreement for the conservative species. At these control points (figures 9.1 through 9.5) we have the minimum uncertainties related with the hydrodynamic model. At the rest of the control points (Appendix 4) the differences between the results of both models are due to the occurrence of uncertainties related with the hydrodynamic model (mainly with respect to the initial conditions) and additional uncertainties, such as the associated with the M3 model and the interpolation of the mixing fractions further on the sampling points.

It would be useful to carry out an exercise that examines how analytical uncertainties in the chemical parameters that go into the M3 analysis are propagated into the outcome in terms of the of the proportions of refernce waters.

9.3 EVALUATING THE ROLE OF CHEMICAL REACTIONS FROM A HYDROGEOLOGICAL POINT OF VIEW

As mentioned above, by using the M3 method, Laaksoharju et al (1999 b) modelled the groundwater composition of the Äspö site as a mixture of four major groundwater types: Brine, Glacial, Baltic Sea and Meteoric waters. M3 modelling of the Äspö site indicates that the most reactive dissolved species (for which the higher deviations with respect to the ideal mixing are found) are Na^+, Ca^{2+}, HCO_3^- and SO_4^{2-}. Laaksoharju et al (1999 b) consider that the chemical processes having a dominant impact on the present Äspö groundwater chemistry are calcite dissolution and precipitation, redox reactions and biological processes.

Other mixing models have been also used to explain groundwater evolution at the Äspö site. Banwart et al (1995) explain the hydrochemistry evolution of the Redox Zone Experiment as a dilution of the saline native groundwater by fresh recharge water. Similarly to M3 model, the mixing model performed by Banwart et al (1995) for the Redox Zone found that the main deviations from the ideal mixing behaviour was shown by Na^+, Ca^{2+}, HCO_3^- and SO_4^{2-}. In the redox Zone Experiment the behaviour of Na^+ and Ca^{2+} is apparently consistent with cation exchange, with preferential exchange of dissolved Ca^{2+} and displacement of exchanged Na^+ during the dilution process of the saline groundwater. Isotopic and microbiological studies conclusively ruled out SO_4^{2-} reduction, and provide evidence supporting Fe(III) reduction as respiration pathway for oxidation of organic C in the fracture zone (Banwart et al., 1995; Banwart et al., 1999; Banwart 1999). A large increase in ^{14}C activity was measured in both dissolved organic and inorganic C during the experiment, which provide evidence for young organic C being oxidized. Significant amounts of dissolved CH_4 were also found in the fracture zone, suggesting that active methanogenesis occurs.

A relevant hydrochemical fact observed at the Redox Zone Experiment was a drastic increase in dissolved suphates when the groundwater system was altered by the tunnel construction. A conclusive explanation for this increase in dissolved SO_4^{2-} remains still to be found. SO_4^{2-}originating from either the sea water, deeper groundwater, atmospheric deposition or Fe-monosulphide minerals (found in the marine sediments surrounding the site) semms unconsistent with sulfur isotope signatures

(Banwart et al., 1999). Banwart et al. (1999) propose adsorption competition between HCO_3^- and SO_4^{2-} as a possible process to explain the recorded sulphate increasing during the Redox Experiment, mainly because this hypothesis could be consistent with sulphur isotopes. Although the hypothesis of anion exchange is attractive it remains to be quantitatively tested. Viani & Bruton (1997) demonstrate that anion exchange due to adsorption competition between HCO_3^- and SO_4^{2-} may occur, with HCO_3^- dominating the surfaces almost completely at the near neutral pH. However, they also conclude that the total adsorption capacity expected for the fracture zone is likely to be too small for anion exchange to explaining such a dramatic increase in sulphate concentrations during the experiment.

In spite of the fact that isotopical studies ruled out the dissolution of calcite as being the main process responsible for the increase in HCO_3^- concentrations, thermodynamic calculations show that shallow groundwater at the Äspö site is unsaturated with respect to calcite. Then dissolution of this mineral could be expected to take place during the experiment.

An alternative possibility to check the consistency between the hydrodynamic groundwater flow and solute transport model and the hydrochemical mixing models is to evaluate the role of the chemical reactions by looking at the deviations of the measured field data with respect to the computed concentrations by the hydrodynamic model. Similarly to the mixing models, if the numerical model is able to reproduce the behaviour of conservative species (such as chlorides and 18-0), then the observed deviations for other elements can be understood as a loss or gain in the groundwater samples which can be associated with a given reaction or a set of coupled chemical processes.

To evaluate the role of chemical reactions from a “hydrogeological point of view” a new multicomponent run of the numerical model was carried out. This run was performed by using exactly the same model (geometry, parameter, conditions, etc) than the previous run of conservative species and mixing fractions, but using those chemical species identified with the mixing models as being the most reactive species. Considered species in the new run of the numerical model were Na^+, Ca^{2+}, HCO_3^- and SO_4^{2-} . Similarly that for the mixing fractions, the 5 control points showing a better agreement between measured and computed concentations for the conservative species were selected to evaluate the computed results for the reactive species. Figures 9.9 through 9.13 show the comparison between computed results and measured breakthrough curves at the 5 selected control points. We think that this exercise is an illustrative approach to demonstrate that there are not conservative species in the system that can be associated with chemical processes. However this is just a visual estimate and then, it is useful for establishing a qualitative evaluation of the role of the chemical processes. The proper way to follow with a quantitative treatment of that problem is coupling hydrochemistry to hydrodynamics by menas of reactive transport modeling.

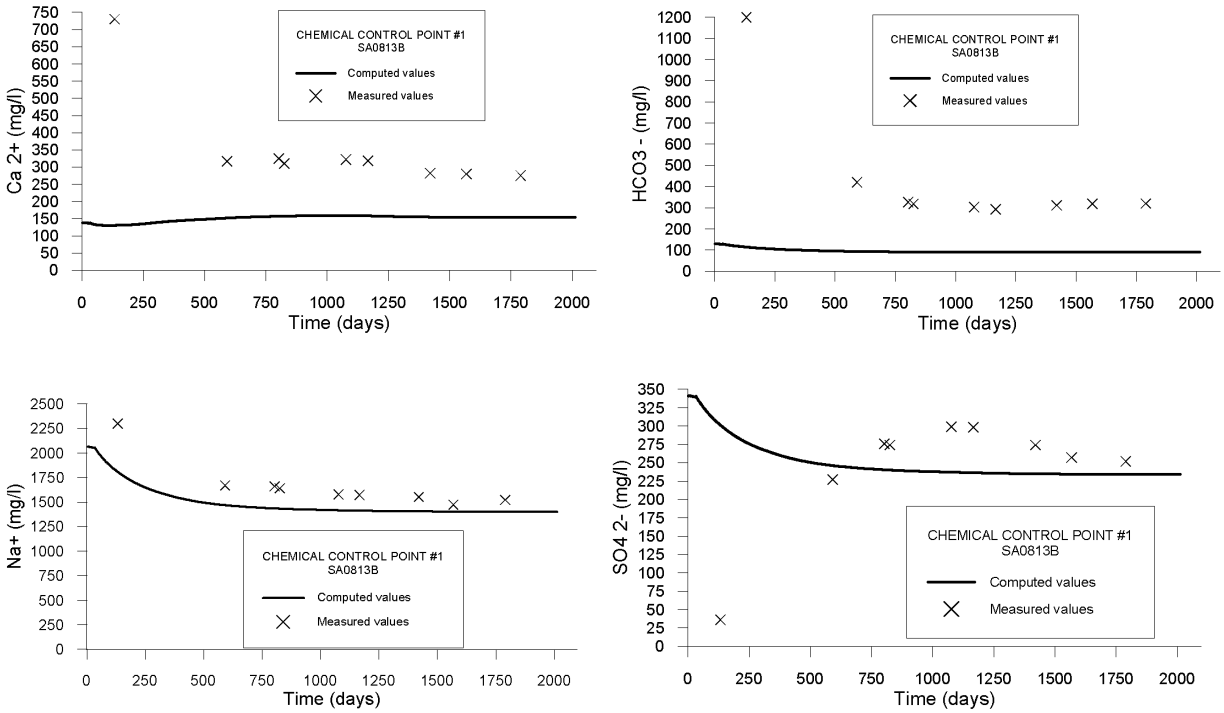

Figure 9.9 Comparison between computed and measured concentrations of Ca^{2+}, HCO_3^-, Na^+ and SO_4^{2-} at SA0813B borehole.

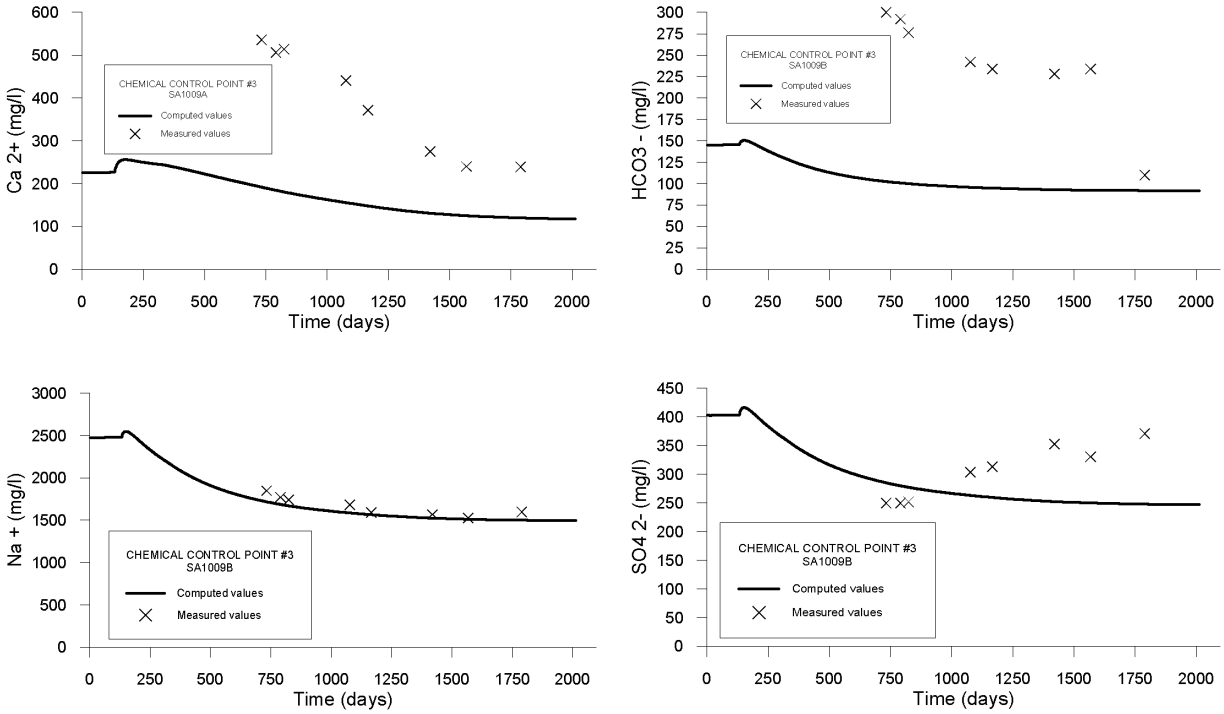

Figure 9.10 Comparison between computed and measured concentrations of Ca^{2+}, HCO_3^-, Na^+ and SO_4^{2-} at SA1009B borehole.

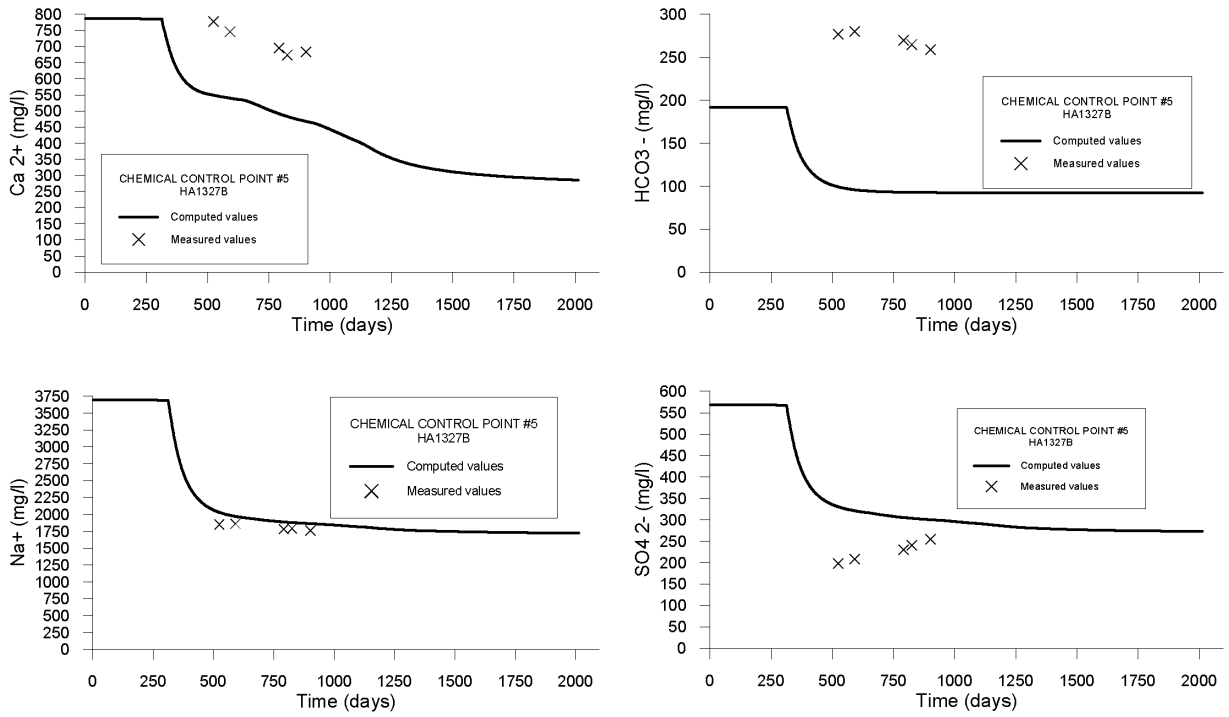

Figure 9.11 Comparison between computed and measured concentrations of Ca^{2+}, HCO_3^-, Na^+ and SO_4^{2-} at HA1327B borehole.

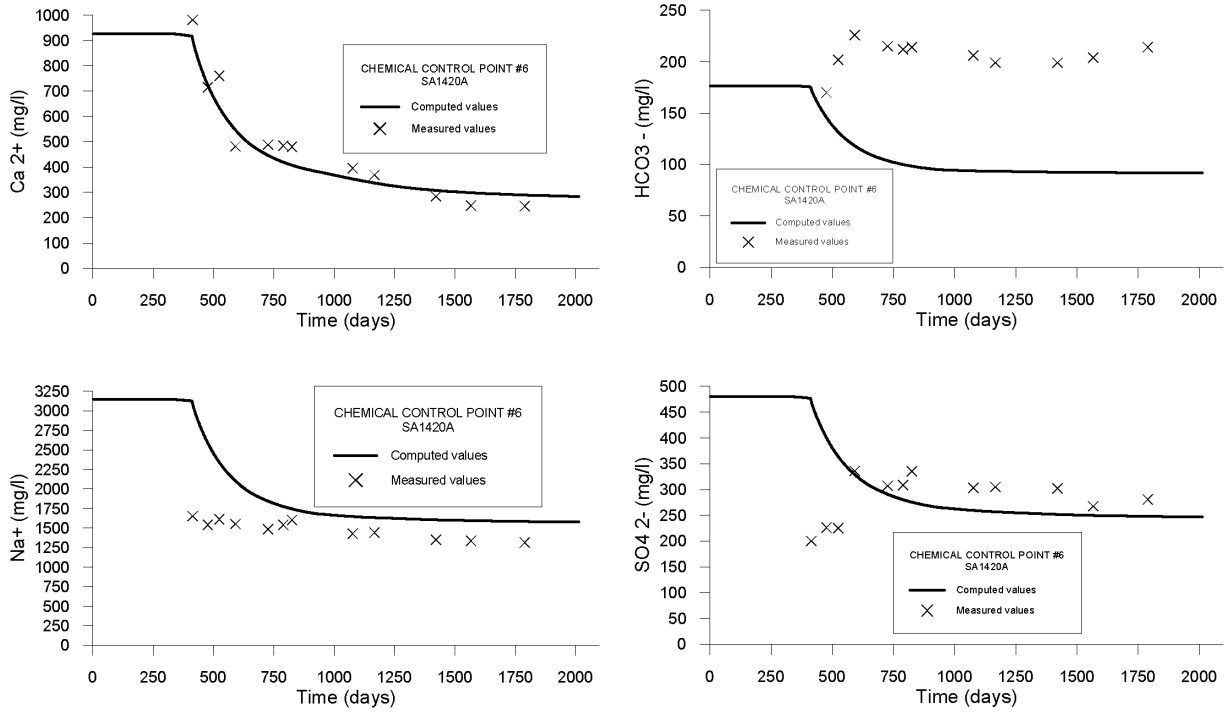

Figure 9.12 Comparison between computed and measured concentrations of Ca^{2+}, HCO_3^-, Na^+ and SO_4^{2-} at SA1420A borehole.

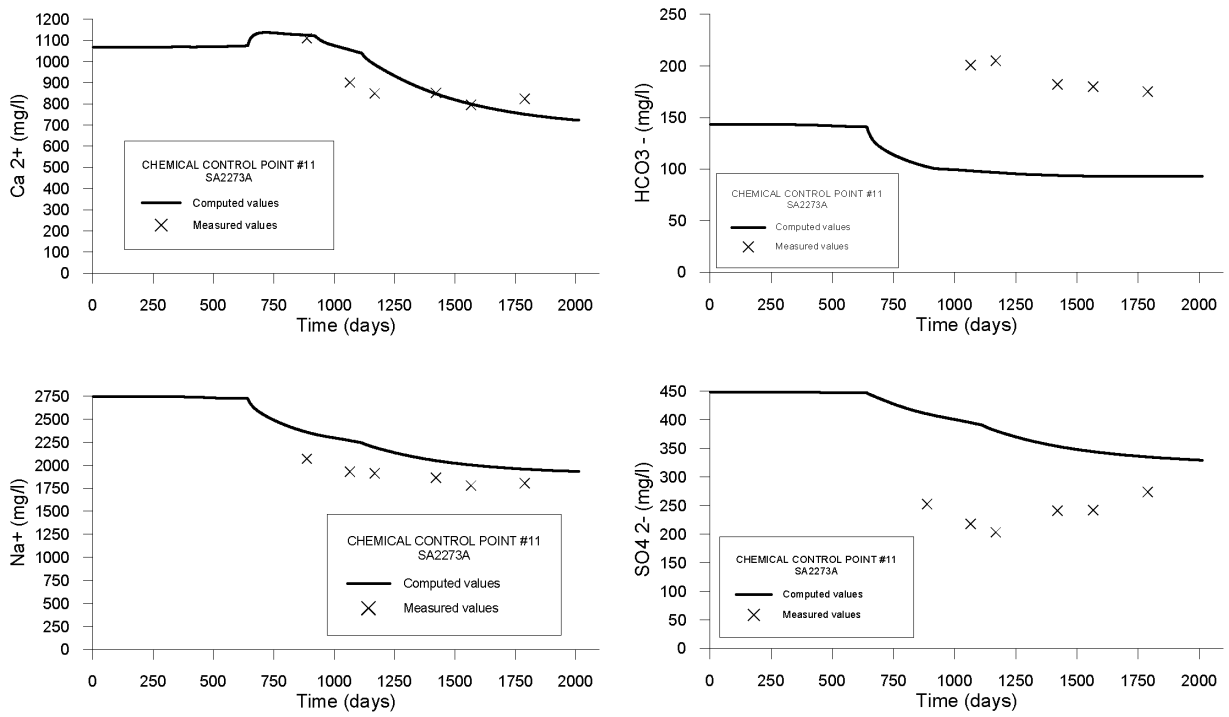

Figure 9.13 Comparison between computed and measured concentrations of Ca^{2+}, HCO_3^-, Na^+ and SO_4^{2-} at SA2273A borehole.

As expected, it can be noticed at figures 9.9-9.13 that a worse fit between measured and computed values exists for reactive species than that for the typically conservative species.

For bicarbonates, the numerical model always computes lower values than those measured at the control points. This kind of deviation from the conservative behaviour constitute an evidence of chemical sources for dissolved HCO_3^- . In the Äspö site framework, and considering the available previous hydrochemical knowledge of the area, two main processes can be invoked: 1) organic carbon oxidation (through oxygen or Fe(III) reduction) and, 2) calcite dissolution. In spite of field data at all the selected control points show a positive deviation of HCO_3^- (with respect to the conservative ideal behaviour), the evolution of this component is not exactly equal at all the control points. Looking at the measured brekthrough curves, it is possible to notice that at SA0813B, SA1009B and HA1327B boreholes (Figures 9.9, 9.10 and 9.11, respectively), measured concentrations of bicarbonate show a clear dilution behaviour, while at the other two control points (SA1420A and SA2273A) the behaviour is just the opposite, it is to say a concentration pattern can be observed (Figures 9.12 and 9.13). This kind of contrary behaviour can be noticed very clear by comparison of figures 9.9 and 9.12. The computed ideal behaviour for all the control points was always a dilution, so, at two of the selected control points, in addition to a source of HCO_3^- , there must be a process (probably chemical) more important than water mixing. This additional process (not observed at other control points) is able to mask the effect of the mixing.

In addition to the HCO_3^- pattern, other clear difference exists between the first three control points with respect to the other two. At the first three control points (figures 9.9 through 9.11) comparison between measured and computed calcium concentrations indicates a clear source for this species (measured values are always higher than the computed results), while at the other two control points (figures 9.12 and 9.13) measured calcium concentrations fit perfectly (lets say surprisingly) with the computed conservative behaviour.

Analyzing HCO_3^- and Ca^{+2} behaviour at the same time allows to conclude that there are zones in which both species show a related pattern of dilution but with higher concentrations than those predicted by conservative transport, while, on the other hand, there are other zones in which calcium behaves mainly as a conservative species and HCO_3^- shows an opposite pattern (concentration pattern) than that predicted by the conservative model. An important difference found for the two groups of observation points having different behaviour of calcium and bicarbonates, was that the first three points (SA0813A, SA1009B and HA1327B) are located on the fracture zones NE-4N, NE-3 and NE-1, respectively. These three fracture zones are intersected by the tunnel under the Baltic Sea, while the other two remaining control points (SA1420A and SA2273A) are located on the fracture zones EW-3 and NNW-1, respectively, which are intersected by the tunnel under the Äspö island.

Banwart (1999) propose the oxidation of dissolved organic matter through Fe(III) reduction as an explanation for the HCO_3^- increase recorded at the redox zone. The availability of oxidized iron will probably be higher at the shallow fresh water system under Äspö Island (where oxidant conditions can be expected, or at least less reducing) than at the bottom of the Baltic sea. This fact could be an explanation for the observed differences at the control points. Reactive transport modelling of the Redox Zone Experiment (Molinero et al., 1999) predicts dissolution of calcite in the tunnel surroundings, after the tunnel intersection, so bicarbonate behaviour will probably be controlled by the result of coupling both chemical processes.

Contrary to the proposed by mixing models (Laaksoharju et al. 1999b; Banwart et al., 1999) no source of Na^+ has been detected with the hydrodynamic model. Measured and computed Na^+ concentrations show an excellent agreement, apparently as good as for chlorides (see figures 9.9 through 9.13). This apparent conservative behaviour of Na^+ is due to the fact that huge differences in concentration exists between fresh recharge water, baltic water, and saline native waters, so the possible ocurrence of exchange processes affecting Na^+ are masked by solute transport processes (or mixing).

Finally, for the sulphates behaviour, the numerical model predicts dilution patterns at the 5 selected control points, while measured data indicates a concentration pattern at all the control points (figures 9.9 through 9.13). As in the case of HCO_3^-, SO_4^{2-} evolution can not be explained with conservative transport or mixing models. The observed behaviour of SO_4^{2-} is very similar to the behaviour described by Banwart et al. (1999) for the Redox Zone Experiment. As was comented above, there is not a con-

clusive explanation for the observed increase in SO_4^{2-} . Possible hypothesis include pyrite dissolution, anion exchange, or other sources not considered in both hydrodynamic and mixing models. Anion exchange seems consistent with isotopical signature but unconsistent with the exchange capacity of the fracture zones at Äspö (is directely proportional to the amount of oxydes and hydroxydes in the fracture zones). On the other hand, reactive transport numerical model of the Redox Zone Experiment (Molinero et al., 1999) predicts dissolution of pyrite in the tunnel surroundings, due to the arrival of shallow fresh water unsaturated with respect to this mineral phase. However the numerical model computes a much lower increase in dissolved sulphates, so additional sources must occur to explain measured values. Other sources of sulphates can be located at the Baltic Sea sediments. Sundblad et al. (1991) report SO_4^{2-} concentrations of arround 2,000 mg/L measured at Baltic sediments near Äspö. Quantitative testing of the different hypothesis, by means of reactive transport numerical modelling, is actually being performed by the University of La Coruña - ENRESA Team.

Concerning to the sulfates behaviour, Laaksoharju (1999) propose sulphate reduction as a chemical reaction to consider in the Äspö modelling exercises. As shown at figures 9.9 through 9.13 measured data always indicate (at least form surface to 306 m depth) a sulphate increasing, the same than observed at the Redox Zone. These measured patterns are not consistent with the ocurrence of sulphate reduction, but with the opposite (oxidation), as was supported by reactive transport model results of the Redox Zone (Molinero et al. 1999).

10 CONCLUSIONS

The numerical modelling of the groundwater flow and solute transport of the Äspö site has been successfully performed.

The tunnel construction process has been simulated by means of 29 stages for the transient groundwater flow model. Flow rates into the tunnel are computed by the model and not prescribed as a boundary condition.

Computed flow rates show an excellent agreement with measured data in most of the tunnel sections. The comparison of the computed pressure heads and the measured values indicates that in general the numerical model is able to reproduce the measured drawdowns. Calibrated transmissivities are within the range of field measured values except for two of the 19 considered hydraulic domains, were a little lower transmmissivity value was calibrated. Finally, the groundwater flow numerical model has been succesfully validated against field data not used in the calibration stage.

Numerical results in terms of concentrations show an excellent agreement with measured data of chlorides and 18-oxygen. It is important to remark that solute transport results were achieved without calibration. With a strongly consistent (and calibrated) flow model, the numerical model reproduces conservative chemical concentrations using available transport parameters.

In order to assess uncertainty in initial and boundary conditions and parameters, a sensitivity analyses of the numerical model was done for groundwater flow and solute transport. Groundwater flow model is strongly sensitive to the initial conditions and transsmissivities of the Hydraulic Domains. On the contrary, the model is not sensitive to the parameters of the intersections among domains and with respect to the boundary conditions. Solute transport model is strongly dependent on initial conditions of concentrations. Initial concentration field was found as the most important source of uncertainty.

A good agreement was found between M3 model results and hydrodynamic numerical model of groundwater flow and solute transport. In general, it can be stated that a there is a consistency between both types of models. This consistency supports the hypothesis of the mixing of 4 extreme reference waters at the Äspö groundwater system, as proposed by M3 model. M3 results has been useful to shape some aspects of the Äspö site hydrogeology. However, the comparison of hydrodynamic and mixing models results must be taken carefuly, due to the combination of uncertainties on the mixing model (+/- 10%) together with the detected uncertainties in the interpolation of the mixing fractions further on the sampling points (+/- 10%).

Predictions at 3 of the 4 proposed prediction points have been made. They include a base run (best prediction) and a second run using an alternative initial concentrations field. The results of both runs provided a reliable prediction range which was in agreement with field measurements.

The role of the chemical reaction have been evaluated by means of comparison of computed results and measured concentrations of the typically non-conservative species. Sources of bicarbonate, calcium and sulphate have been clearly detected, which are assumed to be caused by chemical processes. A different behaviour of calcium and bicarbonates have been found depending on the location of the fracture zones. As a cualitative hypothesis, the carbonate system could be affected by the higher availability of Fe(III) expected under the islands. As proposed by Banwart (1999) for the Redox Zone, carbon oxidation through Fe(III) reduction could constitute a source of bicarbonates. This hypothesis (and other chemical behaviours which remains still unclear) can be quantitatively validated or rejected by means of coupled groundwater flow and reactive transport modelling.

11 REFERENCES

Ahlbom, K.; Olsson, O. & Sehlstedt, S. (1995): Temperature conditions in the SKB study sites. SKB TR 95-16.

Banwart, S.; Laaksoharju, M.; Pitkänen, P.; Snellman, M & Wallin, B (1995): "Development of a site scale model for reactive element dynamics". In: The Redox Experiment in Block Scale. Final Reporting of Results from the Three year Project. Chapter 6. Steven Banwart (Ed). SKB Progress Report 25-95-06.

Banwart, S. (1999): Reduction of iron(III) minerals by natural organic matter in groundwater. Geochimica et Cosmochimica Acta. Vol 63, nº 19/20, 2919-2928.

Banwart, S.; Gustafsson, E. & Laaksoharju, M. (1999): Hydrological and reactive processes during rapid recharge to fracture zones. The Äspö large scale redox experiment. App. Geoch. 14, 873-892.

Berkowitz, B. (1994): Modelling flow and contaminant transport in fractured media. Advances in Porous Media. Chapter 6. M.Y. Corapcioglu (Ed). Elsevier

Gurban, I.; Laaksoharju, M. & Andersson, C. (1998): Influences of the tunnel construction on the groundwater chemistry at Äspö. Task 5 Data Delivery. Äspö Hard Rock Laboratory IPR-02-58 (in press)

Juanes, R. (1997): Un código para la modelización tridimensional de flujo y transporte. Proyecto Técnico. ETS Ingenieros de Caminos, Canales y Puertos. Universidad de La Coruña. Unpublished.

Knutson, G., Morfelt, C.-O. (1993): Grundvatten-teori and tillämpning, AB Svensk Buggtjänst, Solna (Sweden).

Kornfalt, K.A. & Wikman, H. (1988): The rocks of the Äspö island. Description of the detailed maps of solid rocks including maps of 3 uncovered tranches. SKB PR 25-88-12.

Laaksoharju, M. & Wallin, B. (1997): Evolution of the groundwater chemistry at the Äspö Hard Rock Laboratory. Proceedings of the second Äspö International Geochemistry Workshop, June 6-7, 1995. SKB, International Cooperation Report 97-04.

Laaksoharju, M.; Tullborg, E.-L.; Wikberg, P.; Wallin, B & Smellie, J. (1999 a): Hydrogeochemical conditions and evolution at the Äspö HRL, Sweeden. App. Geoch. 14, 835-860.

Laaksoharju, M.; Skarman, C. & Skarman, E. (1999 b): Multivariate mixing and mass balance (M3) calculations, a new tool for decoding hydrogeochemical information. App. Geoch. 14, 861-872.

Laaksoharju, M. (2000): M3 calculations and their interpretation within Task 5. Task 5 domestic report. The Äspö Hard Rock Laboratory Figeholm, Sweden. Data del.14a.

Larson, S.A. & Berglund, J. (1992) : A Geochronological subdivision of the Transscandinavian Igneous Belt - three magmatic episodes. Geologiska Foreningens i Stockholm Forhandlingar, 114, 459-461.

Moreno, L.; Tsang, Y.W.; Tsang, C.F.; Hale, F.V. & Neretnieks, I. (1988): Flow and tracer transport in a single fracture: A stochastic model and its relation to some field observations. Water Resources Research, 24 (12): 2033-2048.

Rhén, I.; Bäckbom, G.; Gustafson, G.; Stanfors, R. & Wikberg, P. (1997b): Results from pre-investigations and detailed site characterization. Summary report. SKB TR 97-03.

Rhén, I.; Gustafson, G.; Stanfors, R. & Wikberg, P. (1997 b): Models based on site characterization 1986-1995. SKB TR 97-06.

Samper, F.J. (1990): Users Manual of GEOS: A general 3-D gesotatistical package for subsurface applications, Barcelona, 1990.

Smellie, J.A.T. & Laaksoharju, M. (1992): " The Äspö Hard Rock Laboratory: Final evaluation of the hydrogeochemical pre-investigations in relation to existing geologic and hydraulic conditions". SKB Technical Report 92-31.

Stanfors, R.; Rhén, I.; Tullborg, E-L & Wikberg, P. (1999): Overview of geological and hydrogeological conditions of the Äspö Hard Rock Laboratory site. Reference Unknown. Task #5 4th Workgroup Meeting Attachments.

Svensson, U. (1997): A regional analysis of groundwater flow and salinity distribution in the Äspö area. SKB TR 97-09.

APPENDIX 1: MODEL PARAMETERS

HYDRAULIC CONDUCTIVITIES

Hydraulic Conductor Domain	*Width (m)*	*Geometric mean of the measured hydraulic conductivity* (m/day)*	*Calibrated hydraulic conductivity (m/day)*	*Confidence limit* (2.5 %) (m/day)*	*Confidence limit* (97.5 %) (m/day)*	*Sample size* (-)*
EW-1N	30.00	4.32E-03	4.32E-03	4.32E-06	5.18E-01	4
EW-1S	30.00	6.34E-02	9.51E-02	4.90E-04	2.53E+00	4
EW-3	15.00	1.38E-01	1.38E-01	1.38E-02	6.91E-01	4
EW-7	10.00	5.88E-01	1.96E-01	8.64E-05	1.81E+02	3
NE-1	30.00	8.64E-01	1.50E-01	3.46E-01	1.21E+00	16
NE-2	5.00	7.08E-03	7.08E-03	9.46E-05	4.84E-02	12
NE-3	50.00	5.01E-01	2.72E-01	2.42E-01	1.24E+00	9
NE-4N	40.00	6.48E-02	6.48E-02	1.47E-02	3.02E-01	8
NE-4S	40.00	6.48E-02	6.48E-02	1.47E-02	3.02E-01	8
NNW-1	20.00	4.75E-02	3.00E-02	3.24E-03	1.06E-01	7
NNW-2	20.00	2.42E-01	2.42E-01	5.62E-04	1.90E+01	4
NNW-4	10.00	1.30E+00	2.25E-02	1.56E-02	5.18E+00	8
SFZ-11	20.00		1.56E-02			
NW-1	10.00	1.47E-03	1.47E-03	2.85E-04	4.23E+00	3
NNW-5	20.00	8.64E-03	2.00E-01	2.72E-03	3.84E-01	3
NNW-6	20.00		6.05E-02			
NNW-7	20.00	2.07E-02	5.00E-03	1.77E-02	7.78E-02	5
NNW-8	20.00	4.32E-02	8.64E-02	3.63E-06	8.64E-01	3
NNW-3	20.00		8.64E-02			

* Rhen et al. (1997 b)

SPECIFIC STORAGE COEFFICIENTS

Hydraulic Conductor Domain	*Width (m)*	*Measured specific storage coefficient* (m^{-1})*	*Calibrated specific storage coefficient (m^{-1})*
EW-1N	30.00		3.33E-06
EW-1S	30.00		4.80E-06
EW-3	15.00		1.03E-05
EW-7	10.00		3.5E-05
NE-1	30.00	8.66E-07	8.67E-05
NE-2	5.00		2.00E-05
NE-3	50.00		2.18E-05
NE-4N	40.00		4.6E-05
NE-4S	40.00		4.60E-06
NNW-1	20.00	2.50E-07	2.50E-06
NNW-2	20.00	1.00E-07	1.00E-05
NNW-4	10.00		6.52E-05
SFZ-11	20.00		5.00E-06
NW-1	10.00		1.00E-05
NNW-5	20.00		5.00E-06
NNW-6	20.00		5.05E-06
NNW-7	20.00		5.00E-06
NNW-8	20.00		5.00E-06
NNW-3	20.00		6.70E-06

* Rhen et al. (1997 b)

TRANSPORT PARAMETERS

Hydraulic Conductor Domain	*Width (m)*	*Estimated porosity** (-)*	*Estimated dispersivity*** (m)*	*Model porosity (-)*	*Model dispersivity (m)*
EW-1N	30.00		200	1.1E-04	200
EW-1S	30.00		200	8.4E-04	200
EW-3	15.00		200	1.0E-02	200
EW-7	10.00		200	2.0E-03	200
NE-1	30.00	6.2E-04 – 2.2E-02	200	7.0E-03	200
NE-2	5.00		200	1.6E-04	200
NE-3	50.00		200	2.5E-03	200
NE-4N	40.00		200	8.5E-04	200
NE-4S	40.00		200	8.5E-04	200
NNW-1	20.00	3.1E-04 – 1.3E-02	200	8.0E-04	200
NNW-2	20.00	2.6E-03 – 1.1E-02	200	5.0E-03	200
NNW-4	10.00		200	1.0E-03	200
SFZ-11	20.00		200	3.0E-04	200
NW-1	10.00		200	5.0E-04	200
NNW-5	20.00		200	2.0E-03	200
NNW-6	20.00		200	8.0E-04	200
NNW-7	20.00		200	1.0E-03	200
NNW-8	20.00		200	1.0E-03	200
NNW-3	20.00		200	1.0E-03	200

** Holmqvist & Andersson (1999). For the fracture zones without estimations, equation 8-8 of * Rhen et al. (1997 b) was taken as a first approximation.

*** Rhen et al. (1997 b), equation 8-15 assuming a spatial scale of 1 km.

APPENDIX 2: OBSERVATION POINTS

CONTROL POINTS					
TUNNEL INFLOWS		***GROUNDWATER HEADS***		***CHEMICAL CONCENTRATIONS***	
Number	*Tunnel section*	*Number*	*Borehole section*	*Number*	*Borehole section*
1	MA1030G	1	KAS02 (346.799)	1	SA0813B
2	MA1372G	2	KAS03 (107-252)	2	SA0958B
3	MA1584G	3	KAS03 (253-376)	3	SA1009B
4	MA1745G	4	KAS04 (0-185)	4	SA1210A
5	MA1883G	5	KAS04 (288-331)	5	HA1327B
6	MA2028G	6	KAS05 (440-550)	6	SA1420A
7	MA2178G	7	KAS06 (0-190)	7	SA1614B
8	MA2357G	8	KAS06 (191-249)	8	SA1696B
9	MA2496G	9	KAS06 (331-390)	9	SA1828B
10	MA2699G	10	KAS07 (191-290)	10	SA2074A
11	MA2840G	11	KAS07 (411-500)	11	SA2273A
12	MA2994G	12	KAS07 (501-604)	12	SA2273B
13	MA3179G	13	KAS08 (503-601)	13	SA2322A
14	MA3411G + MA3426G + MF0061G	14	KAS09 (0-115)	14	SA2600A
		15	KAS14 (0-130)	15	SA2783A

PREDICTION POINTS	
1	KA3110A
2	KA3385A
3	KAS07 (501-604)

APPENDIX 3: MODELING QUESTIONAIRE FOR TASK 5

1. SCOPE AND ISSUES

a) What was the purpose for your participation in Task 5?

*The main motivation of ENRESA participation in TF5 through UDC group was the "validation" of current numerical models for coupled groundwater flow and reactive transport. Though not entirely coincident with the objectives of TF5, UDC aims were closely related to the issue of consistency of hydrodynamic and hydrogeochemical models. A strong way to check the consistency of hydrodynamic and hydrogeochemical models consists on constructing coupled flow and reactive transport models.

b) What issues did you wish to address through partici-pation in Task 5?

2. CONCEPTUAL MODEL AND DATA BASE

Please describe your models using the tables 1-3 in the appendix.

a) To what extent have you used the data sets delivered? Please fill in Table 4 in the appendix.

b) Specify more exactly what data in the data sets you actual-ly used? Please fill in "Comments" in Table 4.

c) What additional data did you use if any and what assumptions were made to fill in data not provided in the Data Distributions but required by your model? ? Please add in the last part of Table 4.

d) Which processes are the most significant for the situation at the Äspö site during the simulation period?

*Groundwater flow induced by the tunnel construction, mass transfer due to advection and dispersion. These processes induce mixing of the different initial and boundary water types.

3. MODEL GEOMETRY/STRUCTURAL MODEL

a) How did you geometrically represent the ÄSPÖ site and its fea-tures/zones?

*The modelled domain was represented as a volume of 2 x 2 x 1 km. The selected modelling approach was a deterministic discrete fracture network including the main Hydraulic Conductor Domains. Our numerical models assume that the Rock Mass Domains play a much less relevant role than hydraulic-conducting domains. Therefore, they could be ignored. The comparison of measurements and model results confirm for the most part the plausibility of this assumption.

b) Which features were considered the most significant for the under-standing of flow and transport in the ÄSPÖ site, and why?

*Almost all the Hydraulic Conductor Domains are important for adequately representing groundwater flow and solute transport of solutes. Only Hydraulic Conductor Domain SFZ14 is considered to have much less importance, because it is intersected neither by the tunnel nor by other Conductor Domains.

*Definition of proper initial and boundary conditions (especially for solute transport) was found to be also a key issue in understanding flow and transport.

c) Motivate selected numerical discretization in relation to used values of correlation length and/or dispersion length.

*The main constrain for numerical spatial discretization was motivated by Peclet and Courant numbers, the latter depending also on time discretization. The average size of the elements was between 20 and 40 m. Therefore, flow parameters obtained by from 30 m length packer tests were considered the most appropriate for assigning model parameters.

4a. MATERIAL PROPERTIES - HYDROGEOLOGY

a) How did you represent the material properties in the hydraulic units used to represent the ÄSPÖ SITE?

*Properties of Hydraulic Conductor Domains are assumed to be deterministic and constant throughout each domain. Each domain may have different properties (T, S, posorosity, dispersivity).

*Rock Mass Domains were disregarded.

b) What is the basis for your assumptions regarding material prop-erties?

*Flow rates into tunnel sections not intersected by Hydraulic Conductor Domains are generally small.

*The width of the Hydraulic Conductor Domains, as well as the short time-scale of the model allow us to assume that the role of the rock domains in terms of flow and matrix diffusion is not relevant.

c) Which assumptions were the most significant, and why?

*Neglecting Rock Domains resulted in substantial savings of CPU time and hardware (memory) requirements what allowed us to simulate both transient flow and transport. The calibrated flow model reproduces accurately the natural responses of the system in terms of flow rates and groundwater heads.

*However, the numerical model has a tendency to slightly under-predict the flow rate and over-predict drawdowns (in almost all the control points). These discrepancies are attributed to the assumption of neglecting Rock Mass Domains.

4b. CHEMICAL REACTIONS - HYDROCHEMISTRY

a) What chemical reactions did you include?

*No chemical processes are included in the site-scale Äspö model.

*The coupling among hydrogeology and hydrochemistry is been attempted at the Redox Zone. Preliminary results of a groundwater flow and reactive transport numerical model for the Redox Zone have been achieved. The numerical model accounts for aqueous complexation, acid-base, redox, mineral dissolution-precipitation and cation exchange reactions.

b) What is the basis for your assumptions regarding the chosen chemical reactions?

*Field measurements and conceptual models proposed by the Redox Zone Experiment Project (Banwart et al., 1995).

c) Which reactions were the most significant, and why?

*Cation Exchange between Na / Ca was quantitatively found out to explain the observed "excess" in Na. Exchange capacity proposed by Banwart et al (1995) must be increased in 2 orders of magnitude.
*Dissolution/precipitation of Redox sensitive mineral phases (pyrite, goetite). The presence of trace amounts of pyrite is enough to maintain reducing conditions (similar to those measured in the field) around the tunnel during the experiment.
*Calcite dissolution/precipitation.
*No suitable conceptual explanation exists for the dramatic increase in bicarbonate and sulphate concentrations during the Redox Experiment. Several hypothesis have been quantitatively tested by means of reactive transport numerical modelling.

5a. BOUNDARY CONDITIONS FOR HYDROGEOLOGICAL MODEL

a) What boundary conditions were used in the modelling of the ÄSPÖ site tests?

*Prescribed groundwater head equals to the initial value on the side boundaries and Baltic Sea.
*Prescribed recharge rate on top of the conductive features (5 mm/year at the island).
*Impervious boundary at the bottom.

b) What was the basis for your assumptions regarding boundary condi-tions?

*The lack of data about deep and lateral side boundaries.
*Previous estimations about deep recharge at the Äspö site.

c) Which assumptions were the most significant, and why?

*Sensitivity analyses indicate that the numerical model is almost not sensitive with respect to the boundary conditions.

5b. BOUNDARY/INITIAL CONDITIONS FOR HYDROCHEMICAL MODEL

a) What boundary conditions were used in the modelling of the ÄSPÖ site tests?

*Prescribed concentrations on the lateral and bottom sides, and Baltic and

meteoric concentrations on the top boundary.

b) What was the basis for your assumptions regarding boundary conditions?

*Most of the chemical components show a stratified pattern under undisturbed conditions, which was the reason to assume the initial concentration as the prescribed value on the sides. The lack of data at depths greater than 1000 m was a limiting factor to choose the appropriate bottom boundary condition.

c) Which assumptions were the most significant, and why?

*Sensitivity analyses results definitely indicate that the model is strongly sensitive to the initial distribution of concentrations.

6. MODEL CALIBRATION

a) To what extent did you calibrate your model on the provided hydraulic information? (Steady state and transient hydraulic head etc.)

*A great effort of calibration was made for the groundwater numerical model. Hand calibration with more than 30 runs of the transient model were performed and numerical results were compared against time series data of inflows into the tunnel and groundwater heads in the boreholes.

b) To what extent did you calibrate your model on the provided "trans-port data"? (Breakthrough curves etc.)

*No calibration of transport parameters was done. Sensitivity runs were performed in order to evaluate the uncertainty in the initial and boundary conditions.

c) To what extent did you calibrate your model on the provided hydrochemical data? (Mixing ratios; density/salinity etc.)

*No calibration with respect to hydrochemistry was done.

d) What parameters did you vary?

*Transmissivity and storativity of the conductive domains, leakage coefficients at the tunnel, transmissivity and storativity of the intersections between conductive domains and the value of groundwater recharge.

e) Which parameters were the most significant, and why?

*Calibrated parameters include transmissivity of the conductive domains and leakage coefficients of the tunnel. Sensitivity analyses indicate that the uncertainty in calibrated parameters is rather small.

f) Compare the calibrated model parameters with the initial data base - comments?

*Comparison among the initial parameters and those calibrated with the numerical model are shown in the Appendix 1 of the report. The bigger effort of calibration was done for transmissivities of conductive features. Initially the geometric mean value was adopted for each conductive domain. Calibrated values of transmissivities are within the range of field measurements for all the conductive features except for NE-1 and NNW-7, in which the calibrated value was 2 and 3.5 times lower than the minimum measured value, respectively.

7. SENSITIVITY ANALYSIS

Identify the sensitivity in your model output to:

a) the discretization used

*Not sensitive

b) the transmissivity/hydraulic conductivity (distribution) used

*Water heads and flow rates into the tunnel are very sensitive to changes in T and S.

c) transport parameters used

*Concentrations are not very sensitive to changes in transport parameters.

d) chemical mixing parameters used

*Computed mixing fractions are most sensitive to initial values.

e) chemical reaction parameters used

*Reactive transport modelling at the Redox Zone indicate that computed concentrations are sensitive to transport parameters (dispersivity, porosity) and chemical parameters such as exchange capacity for the clayely fracture fillings.

8. LESSONS LEARNED

a) Given your experience in implementing and modelling the ÄSPÖ site, what changes do you rec-om-mend with regards to:

- Experimental site characterisation?

*A more detailed characterization in terms of undisturbed distribution of groundwater concentrations.

- Presentation of characterisation data?

*OK

-
Performance measures and presentation formats?

*OK

b) What additional site-specific data would be required to make a more reliable prediction of the tracer experiments?

*Data about surface recharge reaching the deep aquifer.
*Skin factors or leakage coefficients at the tunnel surroundings.
*More complete time-series for groundwater concentrations at the boreholes.

c) What conclusions can be made regarding your conceptual model utilised for the exercise?

*The impact of the tunnel construction can be reproduced accurately by numerical modelling just accounting for the main hydraulic conductor domains.
*A good calibrated groundwater flow model is able to reproduce conservative concentration evolutions in most of the observation points.
*Evaluation of the main uncertainties of the model allows us to make reliable predictions of conservative solutes.

d) What additional generic research results are required to improve the ability to carry out predictive modelling of transport on the site scale?

*Exploring the connectivity among the main conductive features.
*Field experiments to evaluate the value of the recharge.
*A more detailed sampling program for chemical analyses.
*Finding out strongest hydrochemical conceptual models to explain the evolution of some groundwater components (sulfate increase induced by tunnel construction), for which there is not a satisfactory explanation.

9. RESOLUTION OF ISSUES AND UNCERTAINTIES

a) What inferences did you make regarding the descrip-tive structural-hydraulic model on the site scale for the ÄSPÖ site?

*Main fracture zones strongly control the hydrogeology of the Äspö site.
*The great effort in structural and hydraulic characterization of the Äspö site provides a good knowledge of the hydrogeology and allows setting up a sound conceptual model, which is necessary for constructing sound numerical models.
*Tunnel construction produces a hydrogeological disturbance, which is the responsible of the occurrence of large mass transfer into the groundwater. Groundwater flow and mass transfer processes produce a mixing of waters which is responsible for the hydrochemical evolution of the Äspö site. In spite of the fact that most of the primary components can be explained by conservative transport, there are some species influenced by chemical processes. The evolution of these reactive species could strongly modify important hydrochemical conditions of the system such as pH or redox conditions.

b) What inference did you make regarding the active hydochemical processes, hydrochemical data provided and the hydrochemical changes calculated?

*The main detected hydrochemical processes include pyrite dissolution, calcite dissolution/precipitation and cation exchange. There remain uncertainties about chemical processes affecting bicarbonate and sulphate evolution after the tunnel construction.

c) What issues did your model application resolve?

*The uncertainty related with the hydraulic behaviour of the intersection zones between hydraulic conductor domains is not very relevant for the hydrogeological response of the system.

*Mixing of water due to conservative mass transfer into the groundwater can explain the hydrochemical behaviour of the system for most of the species.

*Computed results based in a hydrodynamic approach are quite consistent with the results computed with a mixing model. The hydrodynamic model results support the conclusions of mixing hydrochemical models.

d) What additional issues were raised by the model application?

*A coupled numerical modelling of groundwater flow, transport of solutes and geochemical reactions has been performed. An alternative conceptual model for the hydrogeology of the Redox Zone has been formulated by means of the numerical model. The coupled numerical model is able to reproduce the patterns of many chemical species. However, some discrepancies are found for bicarbonate and sulfate.

10. INTEGRATION OF THE HYDOGEOLOGICAL AND HYDROCHEMICAL MODELLING

a) How did you integrate the hydrogeological and hydrochemical work?

*At the site scale model (Aspo), only the consistency between hydrogeological and hydrogeochemical (mixing) models was tested by means of mixing frations. Predictions of mixing fractions derived from the hydrogeological model compared favourably with M3 results at control points.

*The UDC group is the only team which has attempted a full integration of hydrogeological and hydrogeochemical models at the Redox Zone by means of a coupled flow and multicomponent reactive transport model. This approach is a much stronger (and therefore more complex) way to integrate hydrogeology and hydrogeochemistry.

b) How can the integration of the hydrogeological and hydrochemical work be improved?

*By means of a coupled flow and multicomponent reactive transport model in the way that the UDC group has done it in the Redox Zone.

c) Hydrogeologist: How has the hydrochemistry contributed to your understanding of the hydrogeology around the Äspö site?

*Mixing fractions computed with M3, which contain a significant uncertainty,

have been found useful to shape some aspects of the flow and transport model.

d) Hydrochemist: How has the hydrogeology contributed to your understanding of the hydrochemistry around the Äspö site?

*Hydrogeology has been found to be fundamental for understanding the hydrochemistry around the Äspö site

Table 1 Description of model for water flow calculations

TOPIC	Example	University of La Coruña - ENRESA model
Type of model	Stochastic continuum model	Deterministic discrete fracture network model.
Process description	Darcy´s flow including density driven flow. (Transport equation for salinity is used for calculation of the density)	Transient groundwater flow assuming Darcy's Law and neglecting density effects.
Geometric framework and parameters	Model size: 1.8x1.8x1 km^3 . Deterministic features: All deterministic features provided in the data set. Rock outside the deterministic features modelled as stochastic continuum.	2 x 2 x 1 km^3 Deterministic features: All deterministic features provided in the data set. Rock outside the deterministic features neglected.
Material properties and hydrological properties	Deterministic features: Transmissivity (T), Storativity(S) Rock outside deterministic features: Hydraulic conductivity(K), Specific storage (Ss)	Deterministic features: Transmissivity (T), Storativity(S) Rock outside deterministic features: neglected
Spatial assignment method	Deterministic features: Constant within each feature (T,S). No changes due to calibration. Rock outside deterministic features: (K,Ss) lognormal distribution with correlation length xx. Mean, standard deviation and correlation based on calibration of the model	Deterministic features: Transmissivity (T), Storativity(S) : Constant within each feature
Boundary conditions	Surface: Constant flux. Sea: Constant head Vertical-North: Fixed pressure based on vertical salinity distribution. Vertical-East: Fixed pressure based on vertical salinity distribution. Vertical-South: Fixed pressure based on vertical salinity distribution. Vertical-West: Fixed pressure based on vertical salinity distribution. Bottom: No flux. Linear change by time based regional simulations for undisturbed conditions and with Äspö tunnel present.	Surface: Constant flux. Sea: Constant head Vertical-North: Fixed pressure equals to the initial one Vertical-East: Fixed pressure equals to the initial one Vertical-South: Fixed pressure equals to the initial one Vertical-West: Fixed pressure equals to the initial one Bottom: No flux.
Numerical tool	PHOENICS	TRANMEF-3
Numerical method	Finite volume method	Finite Element Method
Output parameters	Head, flow and salinity field.	Head and Flow

Table 2 Description of model for tracer transport calculations

TOPIC	EXAMPLE	University of La Coruña - ENRESA model
Type of model	Stochastic continuum model	Deterministic discrete fracture network model.
Process description	Advection and diffusion, spreading due to spatially variable velocity and molecular diffusion.	Advection Dispersion Molecular diffusion
Geometric framework and parameters	Model size: 1.8x1.8x1 km^3 . Deterministic features: All deterministic features provided in the data set. Rock outside the deterministic features modelled as stochastic continuum.	Model size: 2 x 2x 1 km^3 . Deterministic features: All deterministic features provided in the data set. Rock outside the deterministic features: neglected
Material properties	Flow porosity (ne)	Flow porosity Dispersivity Molecular diffusion coefficients
Spatial assignment method	ne based on hydraulic conductivity value (TR 97-06) for each cell in model, including deterministic features and rock outside these features.	Deterministic based in the availble data set
Boundary conditions	Mixing ratios for endmembers as provided as initial conditions in data sets.	Prescribed concentrations for end memebers, chlorides and 18-O, as provided in the data set for the initial conditions
Numerical tool	PHOENICS	TRANMEF-3
Numerical method	Particle tracking method or tracking components by solving the advection/diffusion equation for each component	Finite Elements Method
Output parameters	Breakthrough curves	Concentrations and mass flows

Table 3 Description of model for chemical reactions calculations

TOPIC	EXAMPLE	University of La Coruña - ENRESA model
Type of model	xxx	Transient groundwater flow and reactive transport model in a single fracture zone.
Process description	Mixing. Reactions: Xx, Yy,Zz,Dd…..	Groundwater flow neglecting density effects Advection+dispersion+diffusion Homogeneous and heterogeneous chemical reactions assuming local equilibrium
Geometric framework and parameters	Modelling reactions within one fracture zone, NE-1.	Modelling groundwater flow and reactive solute transport in a single fracture zone: The Redox Zone
Reaction parameters	Xx: a=ff, b=gg,… Yy: c=. Zz: d=...	Standard thermodynamics database for equilibrium constants Available and published data for cation exchange reactions Available database of the Äspö HRL for groundwater flow and transport
Spatial distribution of reactions assumed	Xx: seafloor sediments Yz: Bedrock below sea, superficial Dd: Bedrock ground surface, superficial Yz: Bedrock below sea, at depth Zz: Bedrock ground surface, at depth Yy, Zz: near tunnel	All the assumed reactions could take place in the whole domain (hydrochemical system)
Boundary/initial conditions for the reactions	Xx: aaa… Yy: bbb…	Fresh water is assumed to be oxidant.
Numerical tool	Phreeque	VISUAL CORE^{2D}
Numerical method	xx	Finite Elements Method for groundwater flow and transport Finite Differences Method for geochemical reactions Sequential iteration approach for coupling solute transport and chemical reactions
Output parameters	xx	Heads, flow, concentrations in the liquid phase, concentrations in the solid phase, pH, eH and saturation index of the minerals.

Table 4a Summary of data usage

Data del. No	Data	Importance of data (see notes)	Comment
1	Hydrochemical data 1	P	
1a	Surface bore holes- undisturbed conditions, Äspö-Laxemar	P	
1b	Surface bore holes- disturbed conditions (by tunnel excavation), Äspö	P	
1c	Surface bore holes- undisturbed conditions, Ävrö	P	
1d	Surface bore holes- sampled during drilling, Äspö	P	
1e	Data related to the Redox experiment	P	
1f	Tunnel and tunnel bore holes- disturbed conditions		
2	Hydogeological data 1		
2a1	Annual mean air temperature	-	
2a2	Annual mean precipitation	-	
2a3	Annual mean evapotranspiration	-	
2b1	Tunnel front position by time	P	
2b2	Shaft position by time	P	
2c1	Geometry of main tunnel	P	
2c2	Geometry of shafts	P	
2d	Hydrochemistry at weirs (Cloride, pH, Electrical conductivity, period: July 1993- Aug 1993)	p	
2e	Geometry of the deterministic large hydraulic features (Most of them are fracture zones)	P	

Table 4b Summary of data usage

Data del. No	Data	Importance of data (see notes)	Comment
3	Hydrogeological data 2		
3a	Monthly mean flow rates measured at weirs. Tunnel section 0-2900m, period May 1991 – January 1994	P	
3b	Piezometric levels for period June 1st 1991 – May 21st 1993. Values with 30 days interval (Task 3 data set)	P	
3c	Salinity levels in bore hole sections for period -Sept 1993. (Task 3 data set)	-	
3d	Undisturbed piezometric levels	P	
3e	Co-ordinates for bore hole sections	P	
3f	Piezometric levels for period July 1st 1990 – January 24st 1994. Daily values.	P	
4	Hydochemical data 2		
4a	Chemical components, mixing proportions and deviations for all bore hole sections used in the M3 calculations	P	
4b	Bore holes with time series, > 3 samples (part of 4a)	P	
4c	Bore holes sections interpreted to intersect deterministic large hydraulic features (Most of them are fracture zones) (part of 4a)	M	
4d	Chemical components, mixing proportions and deviations. Grid data based on interpolation. Undisturbed conditions	P	
4e	Chemical components, mixing proportions and deviations. Grid data based on interpolation. Disturbed conditions (by tunnel excavation)	P	
4f	Boundary and initial conditions. Chemical components, mixing proportions and deviations (1989). Grid data for vertical boundaries based on interpolation. Undisturbed conditions	P	
4g	Boundary conditions after tunnel construction (1996) Chemical components, mixing proportions and deviations. Grid data for vertical boundaries based on interpolation. Disturbed conditions (by tunnel excavation)	P	

Table 4c Summary of data usage

Data del. No	Data	Importance of data (see notes)	Comment
5	Geographic data 1		
5a	Äspö coast line	M	
5b	Topography of Äspö and the nearby surroundings	M	
6	Hydro tests and tracer tests		
6a	Large scale interference tests (19 tests)	-	Time limitation
6b	Long time pump and tracer test, LPT2	-	Time limitation
7	Hydochemical data 3, update of data delivery 4 based on new endmembers. Recommended to be used instead of 4.		
7a	Chemical components, mixing proportions and deviations for all bore hole sections used in the M3 calculations	P	
7b	Bore holes with time series, > 3 samples (part of 7a)	P	
7c	Bore holes sections interpreted to intersect deterministic large hydraulic features (Most of them are fracture zones) (part of 7a)	P	
7d	Chemical components, mixing proportions and deviations. Grid data based on interpolation. Undisturbed conditions	P	
7e	Chemical components, mixing proportions and deviations. Grid data based on interpolation. Disturbed conditions (by tunnel excavation)	P	
7f	Boundary and initial conditions. Chemical components, mixing proportions and deviations (1989). Grid data for vertical boundaries based on interpolation. Undisturbed conditions	P	
7g	Boundary conditions after tunnel construction (1996) Chemical components, mixing proportions and deviations. Grid data for vertical boundaries based on interpolation. Disturbed conditions (by tunnel excavation)	P	

Table 4d Summary of data usage

Data del. No	Data	Importance of data (see notes)	Comment
8	Performance measures and reporting 1		
8a	Performance measures		
8b	Suggested control points. 6 points in tunnel section 0-2900m and 3 point in tunnel section 2900-3600m.	M	
8c	Suggested flowchart for illustration of modelling	X	
9	Hydrogeological data 3		
9a	Monthly mean flow rates measured at weirs. Tunnel section 0-3600m, period: May 1991- Dec 1996.	P	
10	Geographic data 2		
10a	Topography of Äspö and the nearby surroundings (larger area than 5b)	-	
10b	Co-ordinates for wetlands	-	
10c	Co-ordinates for lakes	-	
10d	Co-ordinates for catchments	-	
10e	Co-ordinates for streams	-	
10f	Co-ordinate transformation Äspö system- RAK	-	
11	Boundary and initial conditions		
11a	Pressure before tunnel construction, from the regional SKB model (TR 97-09)	M	
11b	Salinity before tunnel construction, from the regional SKB model (TR 97-09)	m	
11c	Pressure after tunnel construction, from the regional SKB model (TR 97-09)	M	
11d	Salinity after tunnel construction, from the regional SKB model (TR 97-09)	m	

Table 4e Summary of data usage

Data del. No	Data	Importance of data (see notes)	Comment
12	Performance measures and reporting 2		
12a	Suggested control points. 6 points in tunnel section 0-2900m and 3 point in tunnel section 2900-3600m (same as 8b) and 2 outside the tunnel.	M	
13	Transport parameters compiled		
13a	LPT2 tracer tests	P	
13b	Tracer test during passage of fracture zone NE-1	P	
13c	Redox tracer tests	P	
13d	TRUE-1 tracer tests	P	
14	Hydrochemical data 4		
14a	Groundwater reactions to consider within TASK5 modelling (Description of how M3 calculates the contribution of reactions and identifying dominating reactions based on the M3 calculations.	X	
15	Co-ordinates for the test sections defining the control points	P	
16	Co-ordinates for bore holes drilled from the tunnel	P	Data delivery very late

Table 4f Summary of data usage

Data del. No	Data	Importance of data (see notes)	Comment
17	Hydogeological data - prediction period		
17a	Hydrochemistry at weirs (Cloride, pH, Electrical conductivity, period: July 1993- Dec 1995)	P	
17b	Piezometric levels for period July 1st 1990 – Dec 1996. Daily values.	P	
18	Hydochemical data - prediction period.		
18a	Chemical components, mixing proportions and deviations for all bore hole sections used in the M3 calculations. Data for tunnel section 2900-3600m.	P	
18b	Bore holes with time series, > 3 samples (part of 18a)	P	
18c	Bore holes sections interpreted to intersect deterministic large hydraulic features (Most of them are fracture zones) (part of 18a)	P	
	Other data (part of data to Task 1, 3 and 4)	X	
	Fracture orientation, fracture spacing and trace length – tunnel data	-	
	Fracture orientation, fracture spacing– mapping of cores	-	
	Fracture orientation, fracture spacing and trace length – mapping of outcrops	-	
	The Redox Zone complete chemical database, including major, minor, trace and isotopes.		
	A surface recharge to the deeper aquifer of 5 mm/year. Inside the range proposed and published at several reports and scientific papers.		

P = data of great importance for quantitative estimation of model parameters
p = data of less importance for quantitative estimation of model parameters
M = data of great importance used qualitatively for setting up model
m = data of less importance used qualitatively for setting up model
X = data useful as general background information
- = data not used

APPENDIX 4: COMPUTED MIXING FRACTIONS AT CONTROL POINTS

CONTROL POINT 1

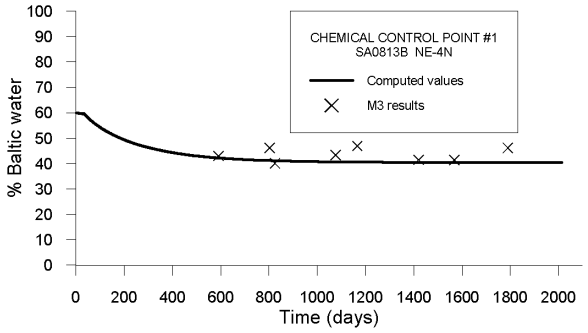

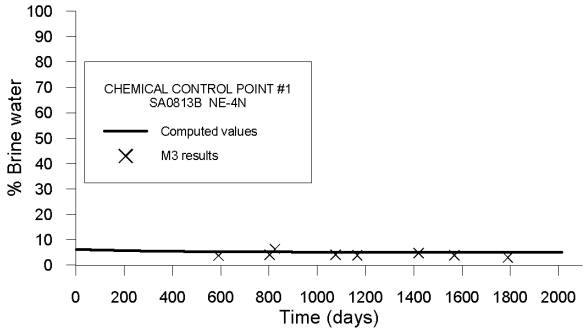

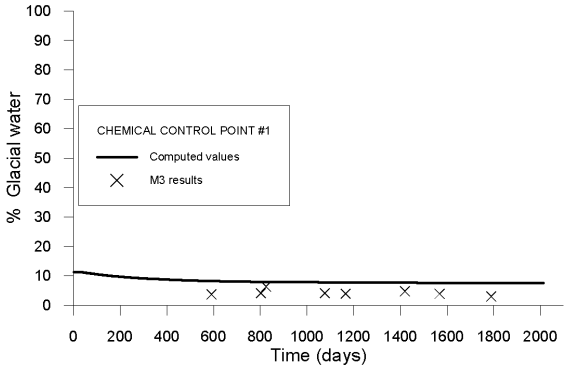

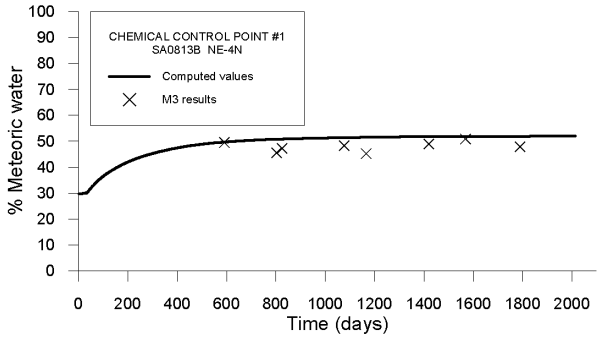

CONTROL POINT 2

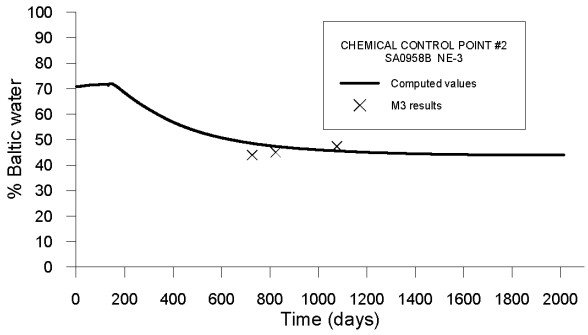

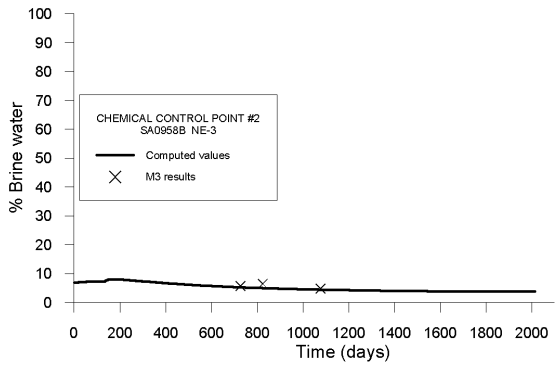

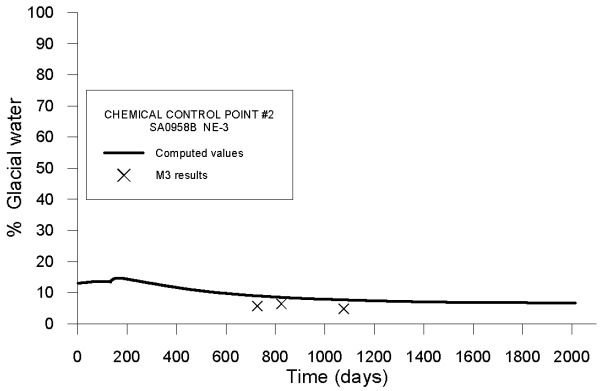

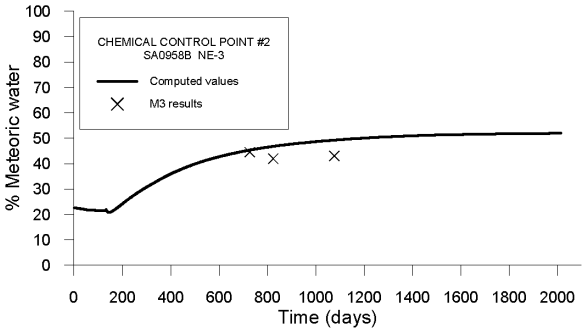

CONTROL POINT 3

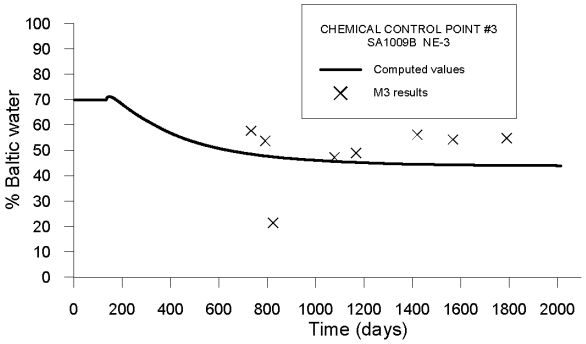

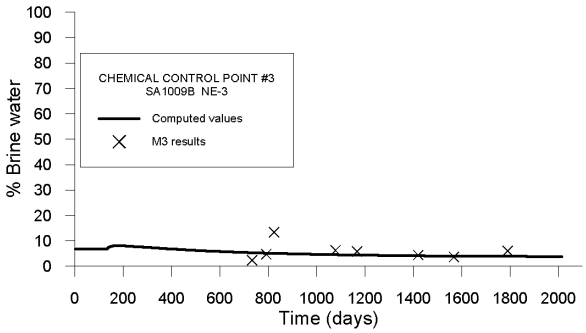

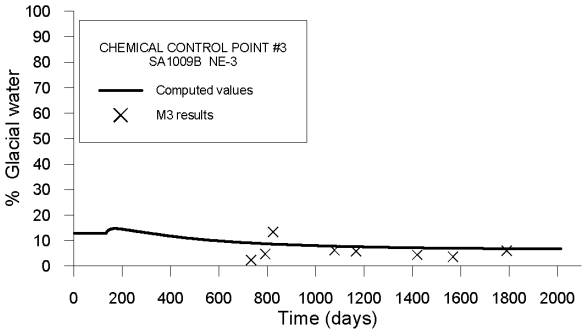

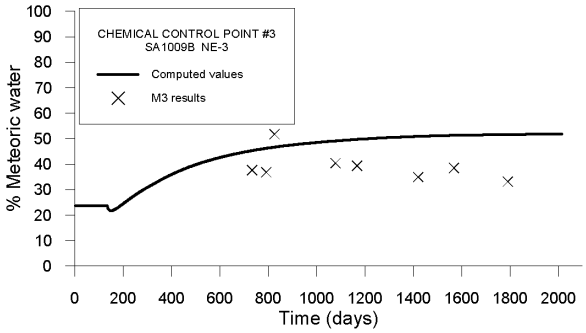

CONTROL POINT 4

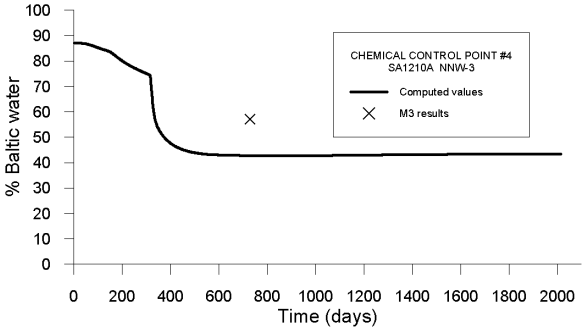

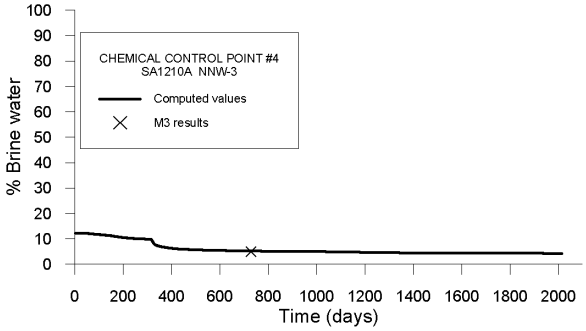

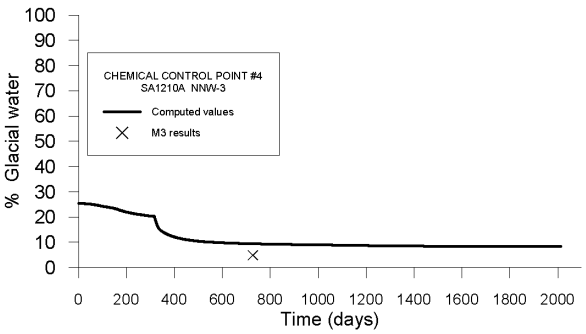

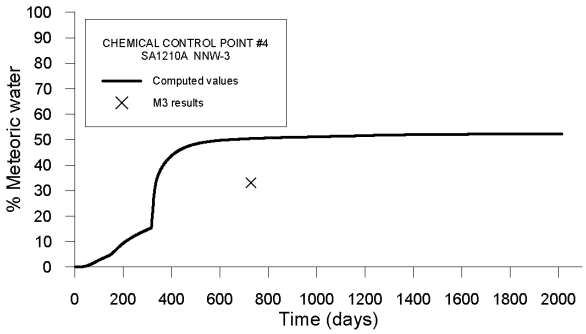

CONTROL POINT 5

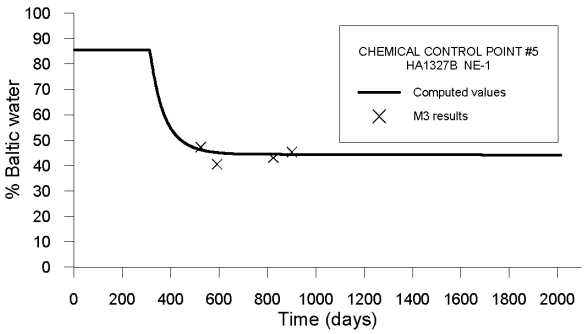

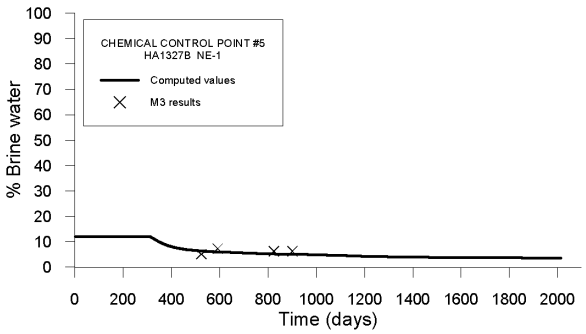

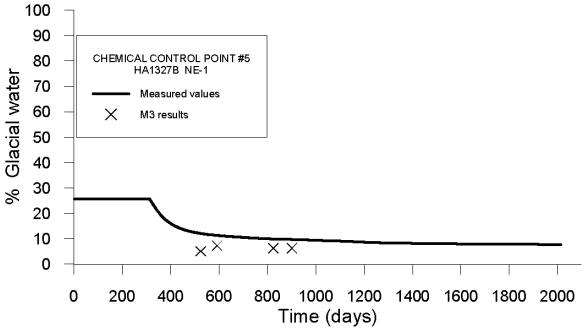

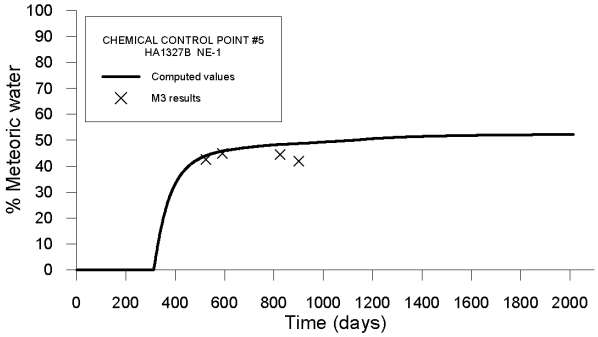

CONTROL POINT 6

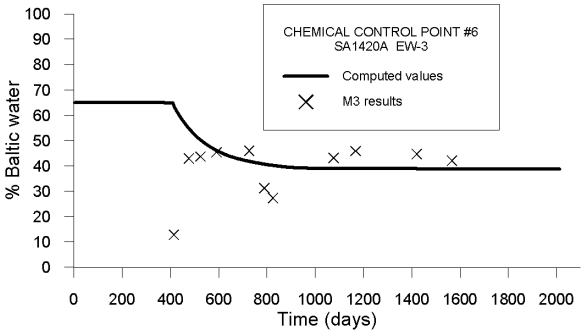

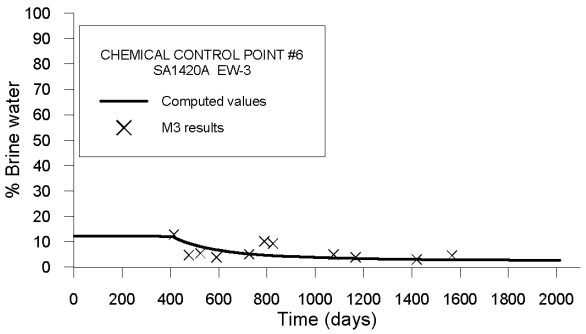

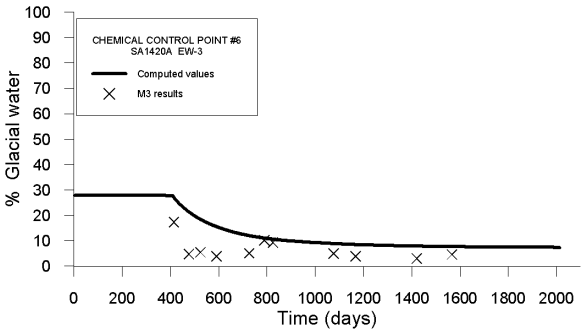

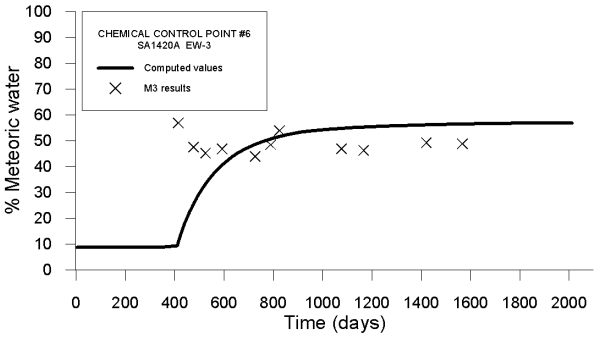

CONTROL POINT 7

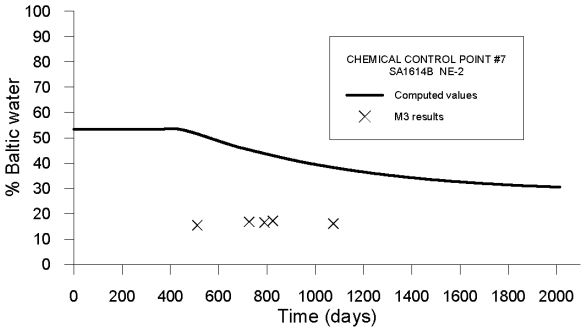

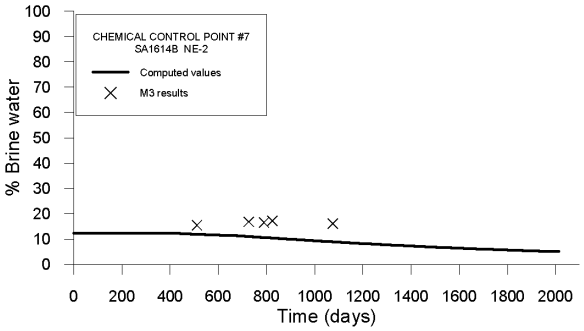

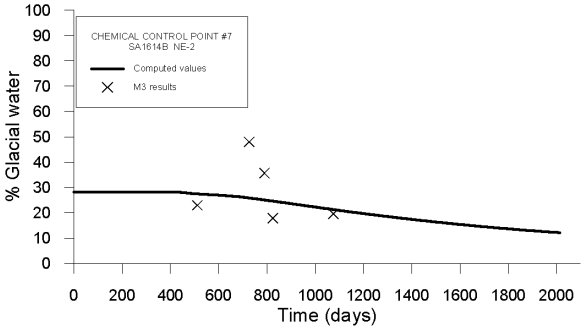

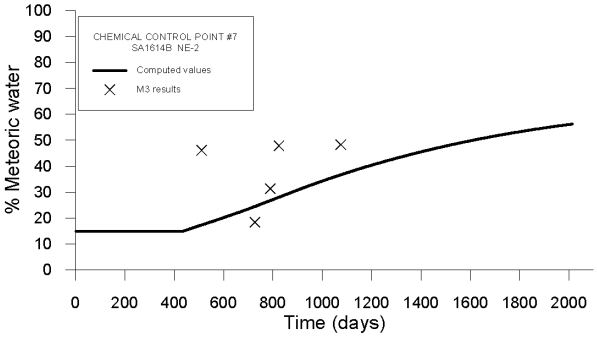

CONTROL POINT 8

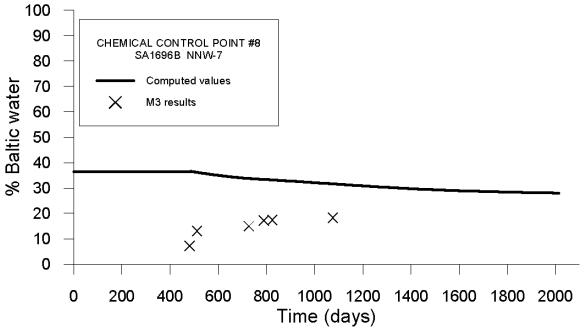

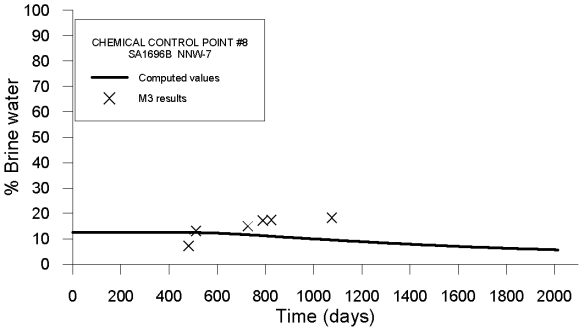

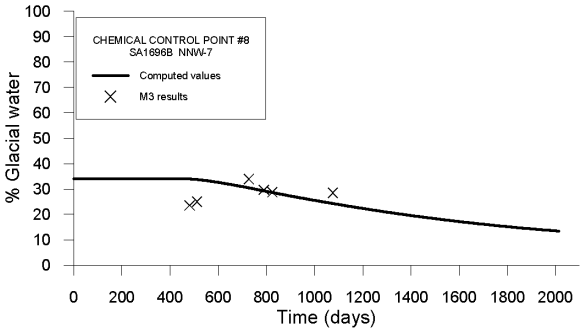

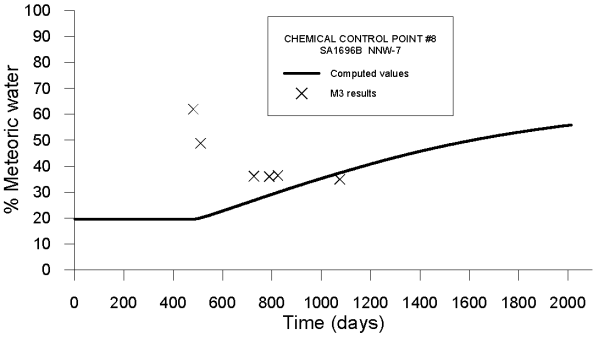

CONTROL POINT 9

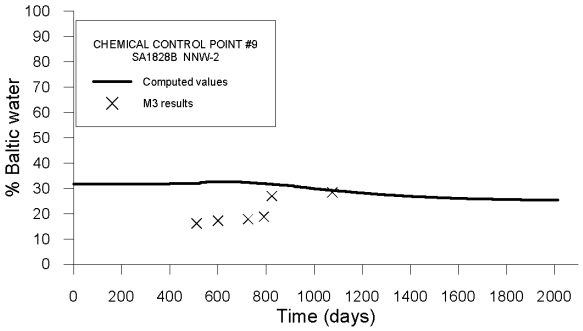

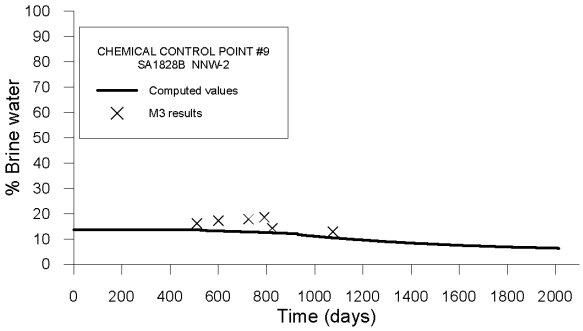

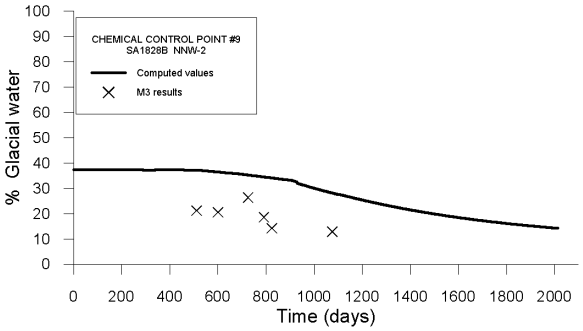

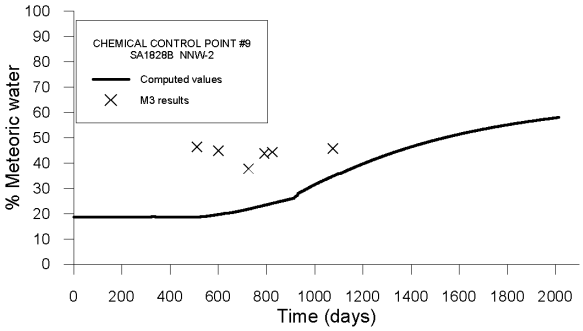

CONTROL POINT 10

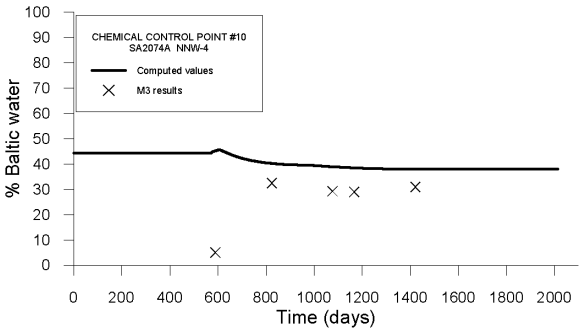

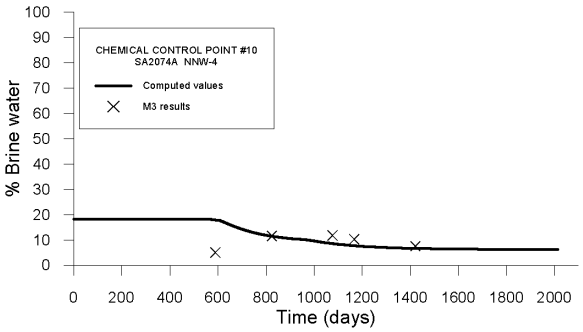

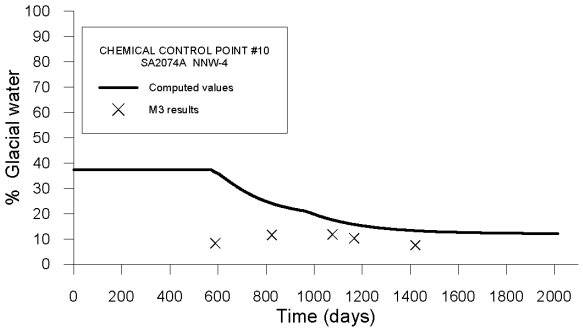

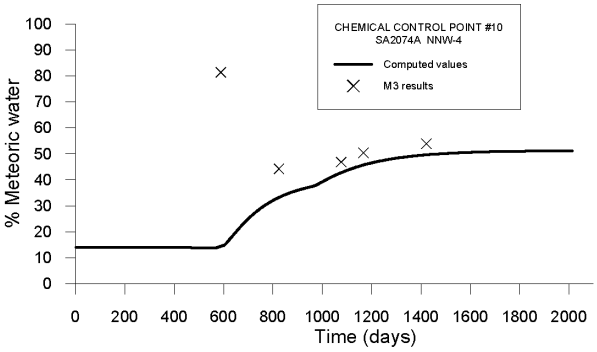

CONTROL POINT 11

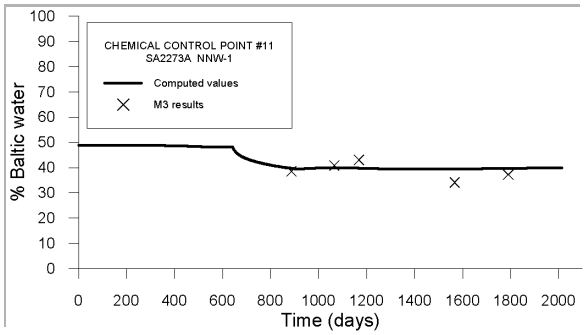

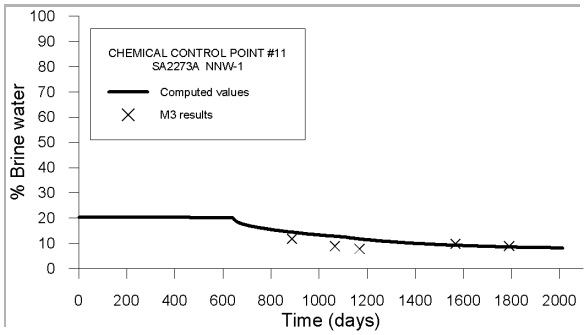

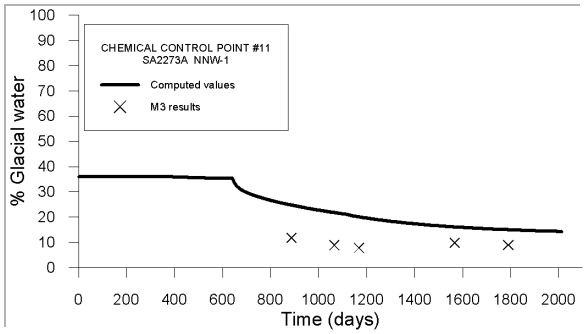

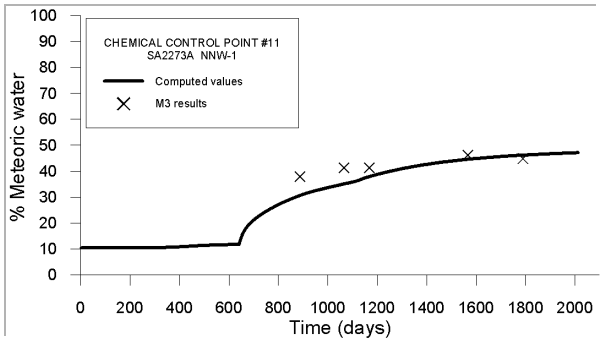

CONTROL POINT 12

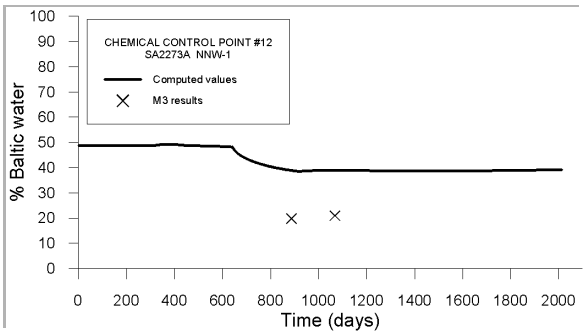

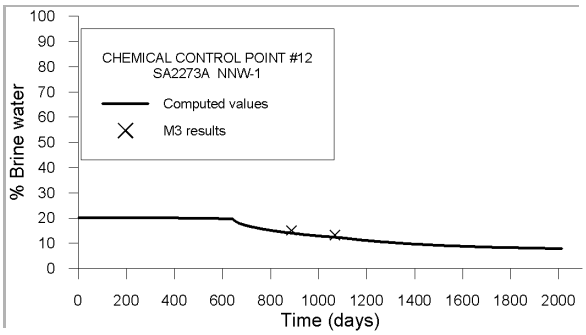

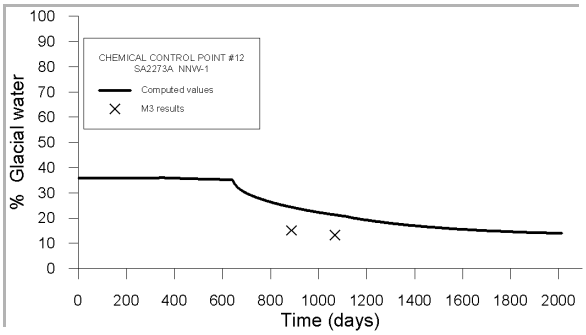

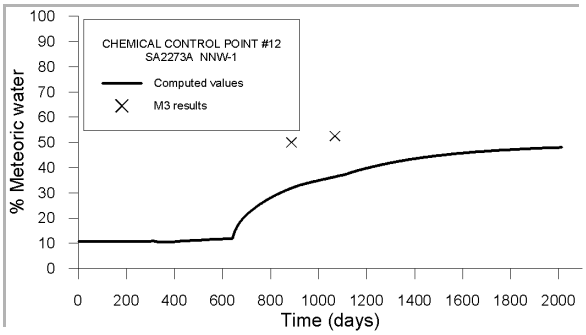

CONTROL POINT 13

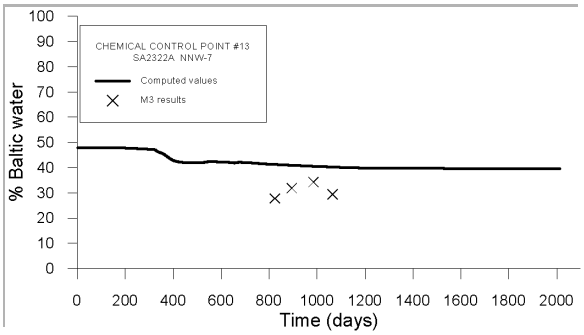

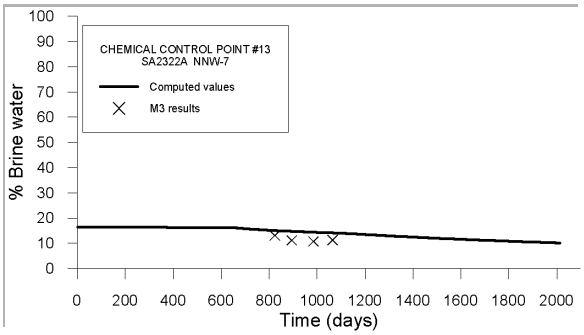

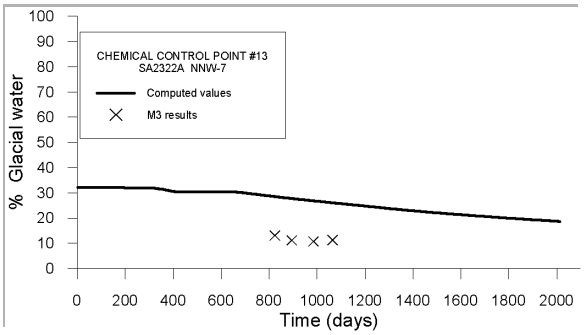

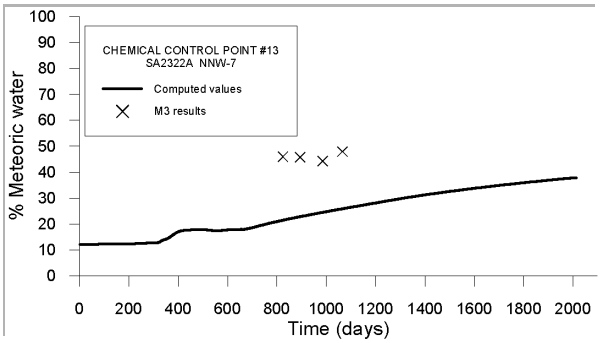

CONTROL POINT 14

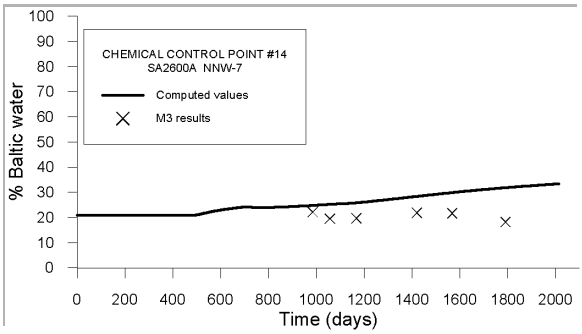

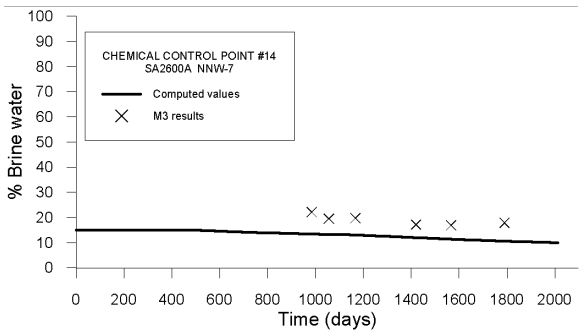

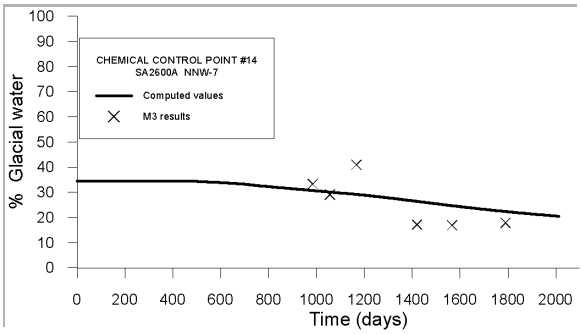

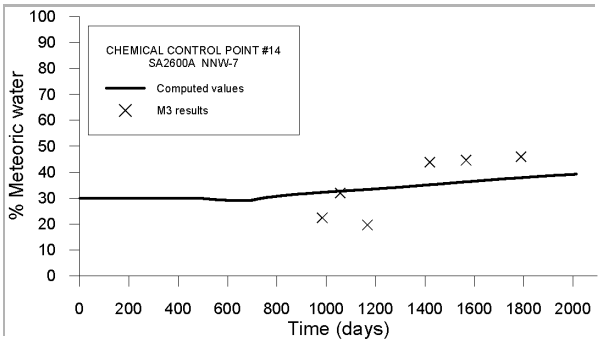

CONTROL POINT 15

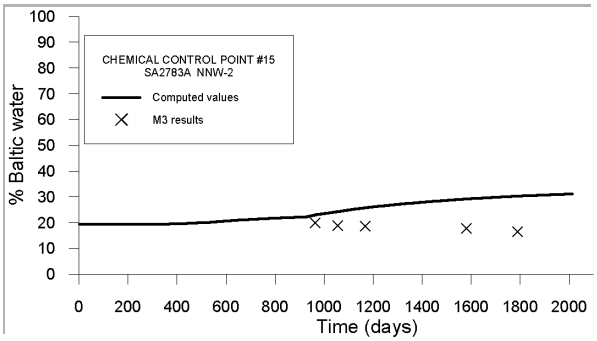

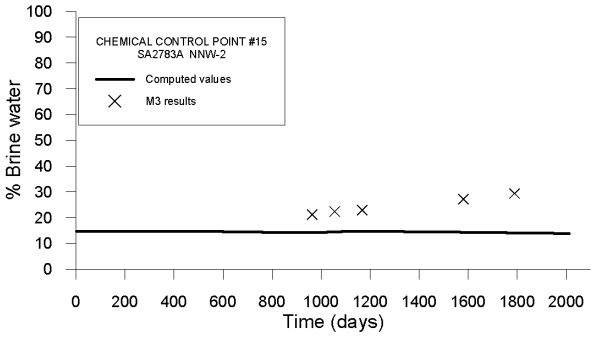

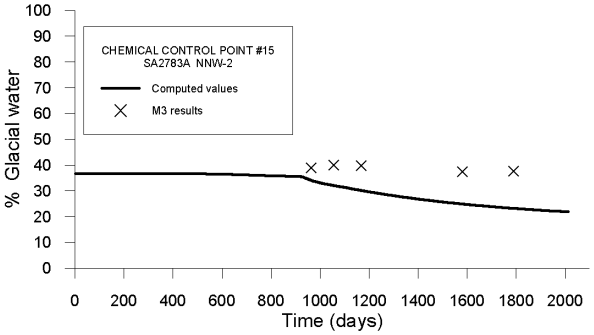

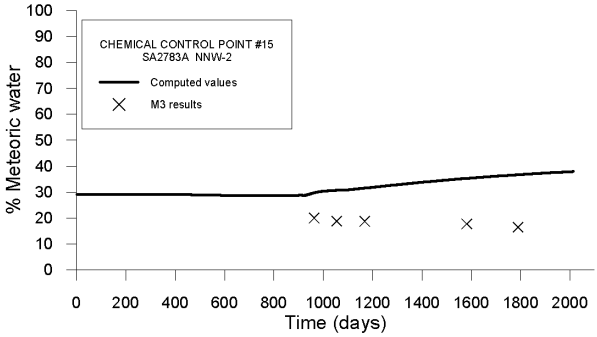

PREDICTION POINT 1

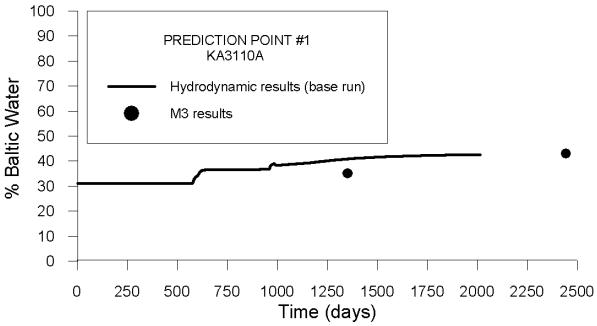

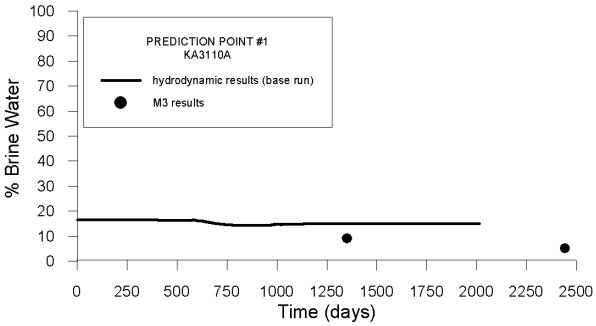

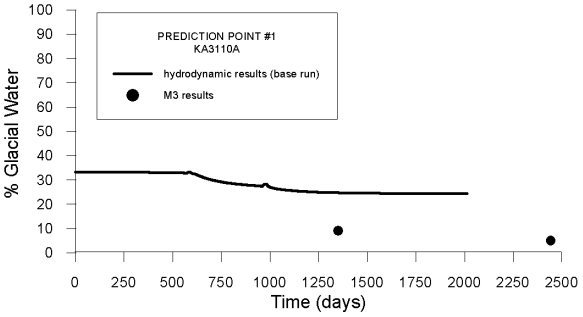

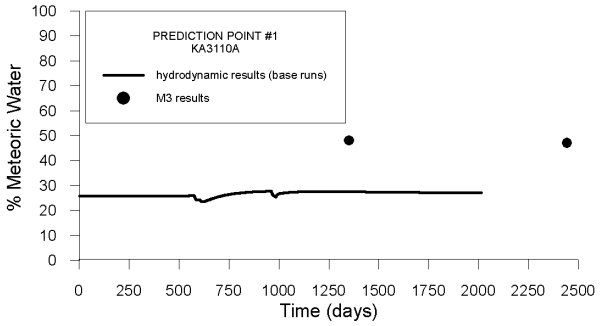

PREDICTION POINT 2

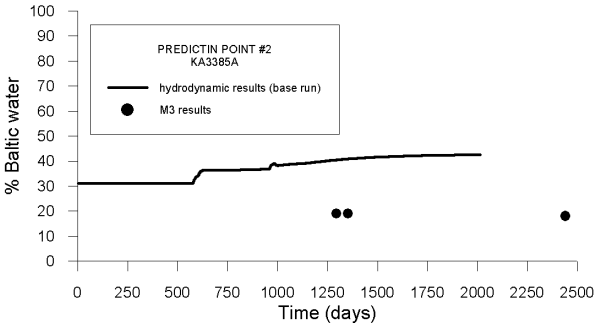

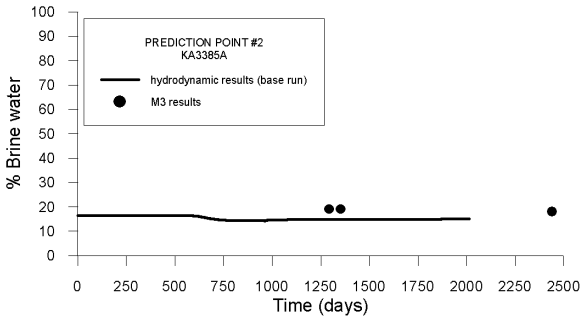

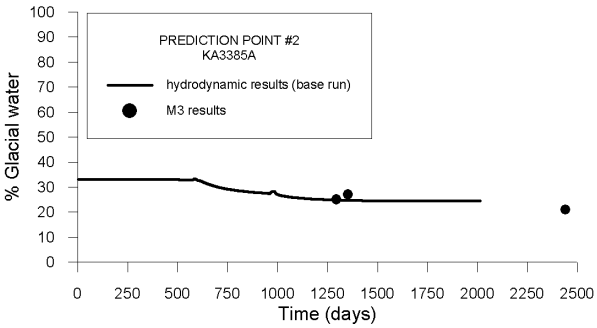

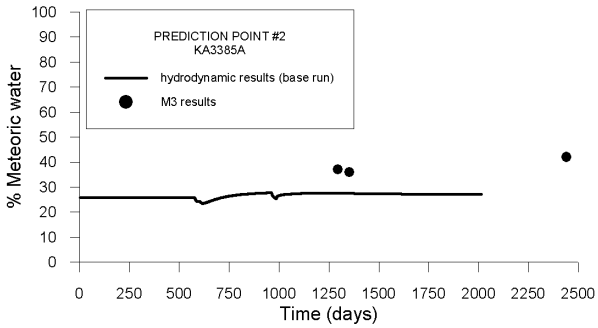

PREDICTION POINT 3

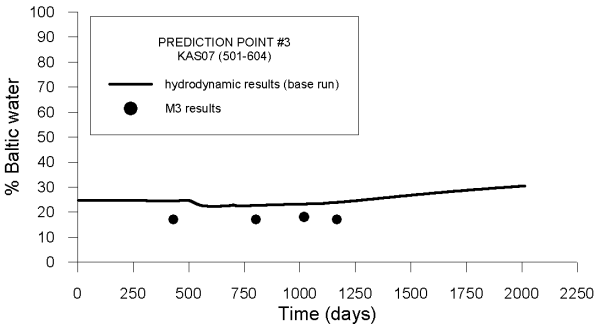

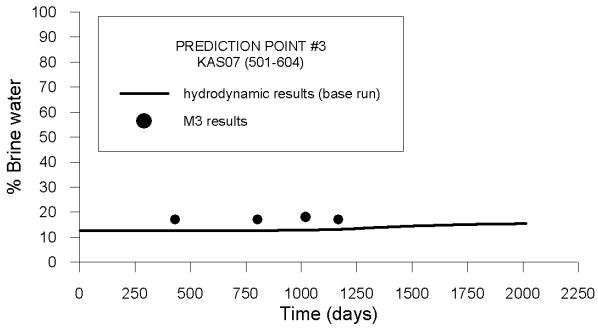

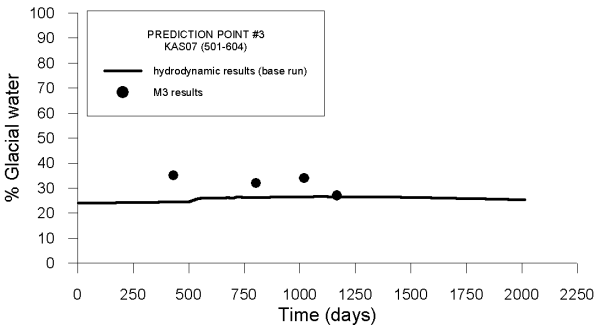

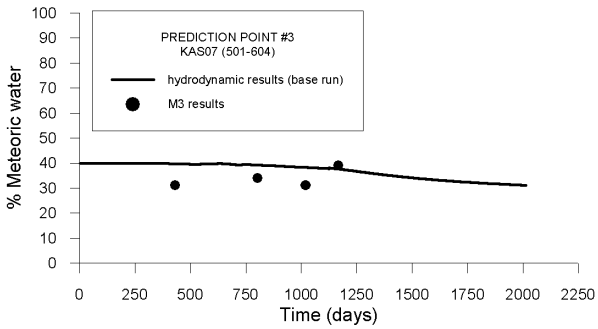

APPENDIX 5: MODELLING GROUNDWATER FLOW AND REACTIVE TRANSPORT INCLUDING MICROBIOLOGICAL PROCESSES: A LARGE-SCALE CASE STUDY AT THE REDOX ZONE.

Jorge Molinero, Gouxiang Zhang and Javier Samper. *

ABSTRACT: *The Äspö Hard Rock Laboratory (Äspö HRL) is a prototype full-scale underground repository for nuclear waste launched and operated by the Swedish Nuclear Fuel and Waste Management Company (SKB). The Redox Zone Experiment carried out at the Äspö HRL was performed in order to evaluate the effect of the construction of a tunnel on the hydrochemistry of a deep granitic formation. The availability of a large amount of hydrochemical information in this large-scale experiment provides a unique opportunity to test coupled groundwater flow and reactive solute transport modelling. Once calibrated, the flow and solute transport model is used to perform reactive transport simulations accounting for aqueous complexation, acid base reactions, redox processes, cation exchange and mineral dissolution/precipitation. This model is able to reproduce the observed behavoiur of most dissolved species. However, some discrepancies were found for dissolved bicarbonates and sulphates. A possible explanation for these discrepancies is the occurrence of microbially catalised processes. Based on groundwater microbiological studies, microbially-mediated processes have been incorporated into the reactive transport model. The final hydro-bio-geochemical model is able to reproduce the measured evolution of dissolved sulphate and bicarbonate, which constitutes a quantitative evidence of sulphur organic matter oxidation being the source of bicarbonate and sulphur.*

1. INTRODUCTION AND EXPERIMENTAL DESCRIPTION

The work presented here was not part of Task 5 but shows an example hydrochemical modeling of a part of the area that was included or close to the area modeled by different groups in Task 5.

The Äspö Hard Rock Laboratory (Äspö HRL) is a prototype, full-scale underground facility launched and operated by SKB (the Swedish Nuclear and Waste Management Company). The main aim of the Äspö HRL is to provide an opportunity for research, development and demonstration in a realistic rock environment down to the depth planned for a future deep repository. The Äspö HRL is located in the southeast part of Sweden, 400 km south of Stockholm. The underground facility consists of a 3,600 m long tunnel which starts with an access ramp and runs in two spirals down to a depth of 450 m under the Äspö island (Figure 1).

On March 13th, 1991 the access tunnel of the Äspö HRL intersected a vertical fracture zone ('Redox Zone') at a depth of 70 m below sea level (Figure 1). Prior to tunnel intersection, a borehole was drilled and sampled in order to document the undisturbed groundwater conditions at the projected tunnel position. These samples provided a reference point for comparing any subsequent evolution of groundwater conditions. The Redox Zone Experiment carried out at Äspö provides an excellent opportunity to test

* E.T.S. Ingenieros de Caminos, Canales y Puertos. Campus de Elviña s/n. 15192 A Coruña. Spain. Phone: (+34) 981-167000 / Fax: (+34) 981-167170 / E-mail: molinero@iccp.udc.es

the redox behaviour, and the hydrochemistry in general, when an isolated vertical fracture zone is disturbed by tunnel construction. The Redox Zone Experiment constitutes a long-erm *in situ* experiment with a large and detailed chemical database at several control points.

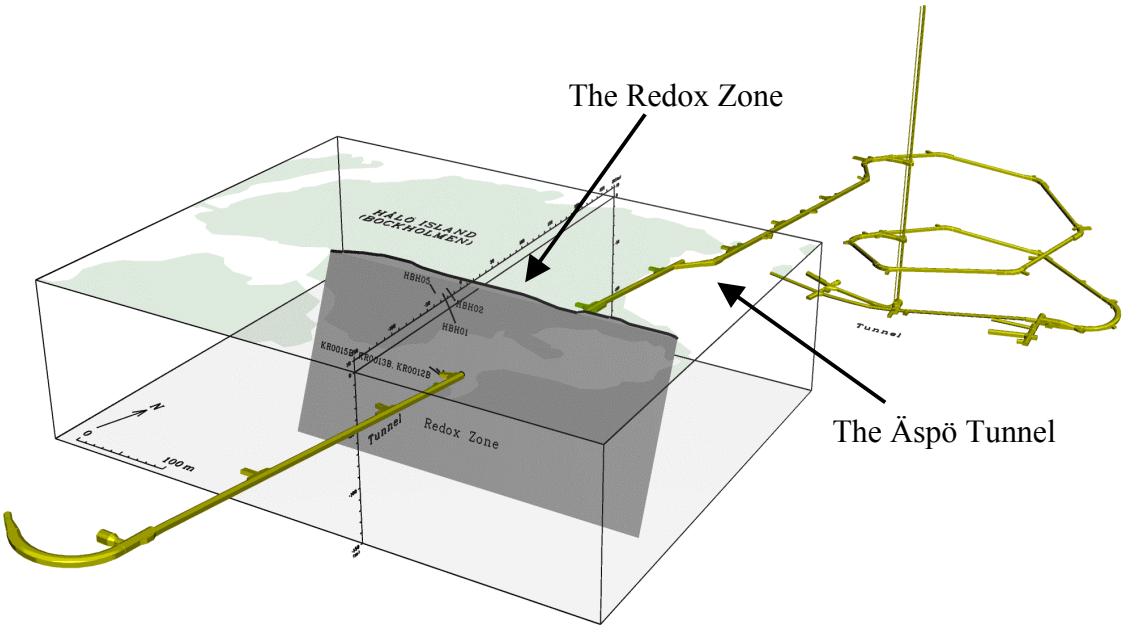

Figure 1. General layout of the Äspö HRL. The total length of the tunnel is 3,600 m. The spiral part of the underground excavation is connected to the Äspö Research Village by a hoist shaft. The first fracture zone intersected by the Äspö tunnel is known as the 'Redox Zone'.

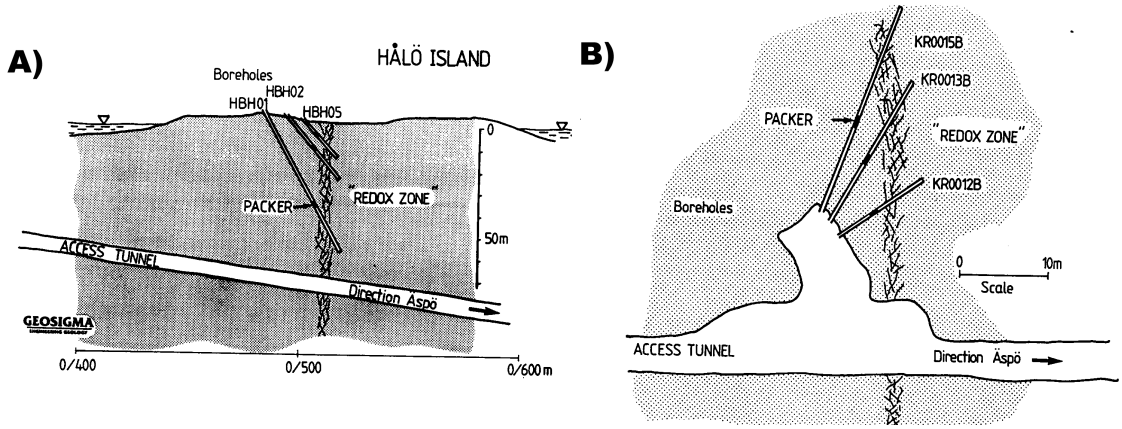

Figure 2. Section and planar views of the tunnel, fracture zone and sampling boreholes of the Redox Zone Experiment (Gustafsson et al., 1994). A) Section view with the location of boreholes drilled from the surface (HBH01, HBH02 and HBH05). B) Plan view with the location of boreholes drilled from the tunnel at a depth of 70 m.a.s.l. (KR0012B, KR0013B and KR0015B).

The intersection of the Redox Zone with the surface is observed as a small topographic depression (10 m wide and 2-3 m deep) on Hålö island. The geology of the area is characterised by a red to gray porphyritic granite-granodiorite known locally as

"Småland granite", which belongs to the vast Transcandinavian Granite-Porphyry Belt (Banwart et al., 1999). The fracture zone is approximately vertical and is clearly visible from the access tunnel as a band of water-bearing fractured rock, with a nominal width of 1 m. Figure 2 shows a section and a planar view of the fracture zone, and the location of the sampling points and boreholes.

2. FIELD DATA AND CONCEPTUAL MODEL

Immediately prior to the intersection of the tunnel, the water table above the tunnel position was approximately 0.5 m below the surface. Although there was some drawdown in the water table during the experiment, Banwart et al. (1994) reported that almost all the zone remained hydraulically saturated. Systematic sampling of groundwater was carried out in the boreholes and tunnel wall during the experiment. An excellent summary of the Redox Zone Experiment can be found in Banwart et al. (1999). Three weeks after the start of the experiment a sharp dilution front arrived to the access tunnel. This appeared as a dramatic decrease in Cl^- and cation concentrations in the groundwater flowing from the roof of the tunnel. A short time later, dissolved Fe concentrations in the tunnel inflows decreased to near zero for a period of a few weeks. This could be taken as an indication of the arrival of an oxidation front to the tunnel position (Banwart et al., 1999). After 50 days both the dissolved Fe concentrations at all sample locations and the stability of the continuously monitored redox potentials (within the range $-150 < Eh < -100$) indicated that anoxic conditions prevailed in the fracture zone. pH remained constant at a value around 8 throughout the experiment (Banwart ert al., 1999). Dilution of the formational saline groundwater by fresh recharge water is the dominant process controlling the hydrochemical evolution during the experiment. However, HCO_3^- and SO_4^{2-} concentrations increase significantly at the sampling points located at 70 m depth.

Isotopic (Banwart et al., 1996) and microbiological (Pedersen et al., 1995) studies conclusively ruled out SO_4^{2-} reduction during the experiment, and provide significant evidence supporting Fe(III) reduction as a respiration pathway for oxidation of organic carbon in the fracture zone. Results reported by Tullborg and Gustaffson (1999) illustrate the large increase in ^{14}C activity measured in both dissolved organic and inorganic carbon during the experiment, providing evidence for a source of young organic carbon oxidising into the groundwater. There is no conclusive explanation for the increase in dissolved SO_4^{2-} (Banwart et al., 1999). Sulphur isotope data (Wallin, 1995) show that SO_4^{2-} originating from either sea water, deeper groundwater or atmospheric precipitation, would not be consistent with the isotopic signature of dissolved SO_4^{2-} at the sampled boreholes. Banwart et al. (1999) state that the hypothesis of anion exchange between SO_4^{2-} and HCO_3^- is an attractive explanation, mainly because any change in the isotopic composition would be reflected identically for ions in solution or those adsorbed. However, Bruton and Viani (1997) conclude that the total adsorption capacity expected for the fracture zone, is likely to be too small for anion exchange to have a significant impact on the dissolved SO_4^{2}.

Molinero (2000) proposed a conceptual model for the hydrogeology of the Redox Zone Experiment which was based on the available information as well as on the results of previous numerical tests. The modelled domain is extended in order to reach natural groundwater boundaries. To the west, the central point of a rock landfill (Figure 3)

constitutes the highest topographic point. To the east, behind the Baltic estuary, the model was extended to the first maximum in topography at the Ävrö island. Two shallow fresh water lenses are expected under both the Bockholmen zone and Ävrö island (Figure 3). Under natural conditions both shallow hydrogeological systems are independent. Shallow groundwater flows from recharge zones to the Baltic estuary. A saline-fresh water interface must be present, reaching its maximum depth under the recharge zones and tending to zero at the Baltic estuary. After the tunnel intersection the hydraulic disturbance reaches the Baltic area, allowing the bypass of the Ävrö fresh water towards the tunnel location. This fresh water arrival is responsible for the dilution process observed at the tunnel position during the experiment. Figure 3 shows a scketch of the hydrogeological coneptual model.

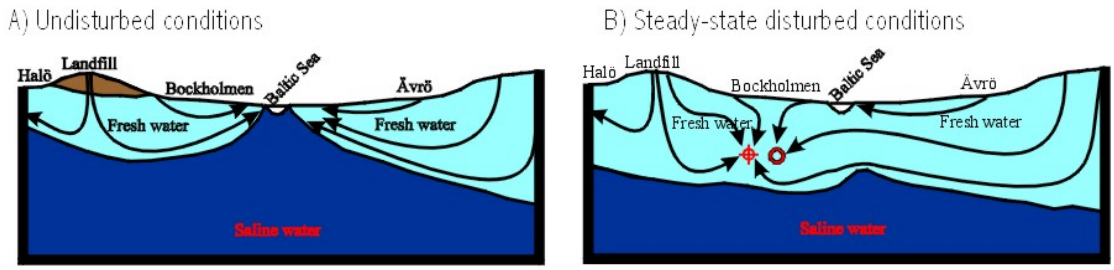

Figure 3. Hdrogeological conceptual model of the Redox Zone Experiment. A) Undisturbed conditions. B) Steady-state disturbed conditions after tunnel intersection and borehole opening.

3. NUMERICAL MODEL

Spatial discretisation of the model was performed by triangular finite elements (Figure 4). The finite element mesh consists of 1,049 nodes and 1,985 triangular elements. The mesh was refined near the tunnel and boreholes, as well as in the surroundings of the Baltic estuary where the strongest gradients of both heads and concentrations were expected. The mesh was also refined near the landfill area (see Figure 3). Five different material zones were defined in the numerical model in order to account for spatial heterogeneity (Figure 4). There is field evidence for a decrease of the fracture zone width towards depth, from a nominal width of tens of metres on the surface to around a width of 1 m at a depth of 70 m (Banwart et al., 1999). Results of hydraulic testing indicate a greater transmissivity at a depth of 45 m than at a depth of 70 m which is consistent with the previous considerations. Three material zones were used to represent the transmissivity of the granite: material zone #1 extends from the surface to a depth of 50 m, material zone #2 extends from 50 m to 150 m depth and, finally, material zone #3 extends from 150 m to a depth of 300 m. Material zones #4 and #5 represent seafloor Baltic sea sediments and the landfill, respectively. Figure 4 shows the geometry of the adopted hydrodynamic zones.

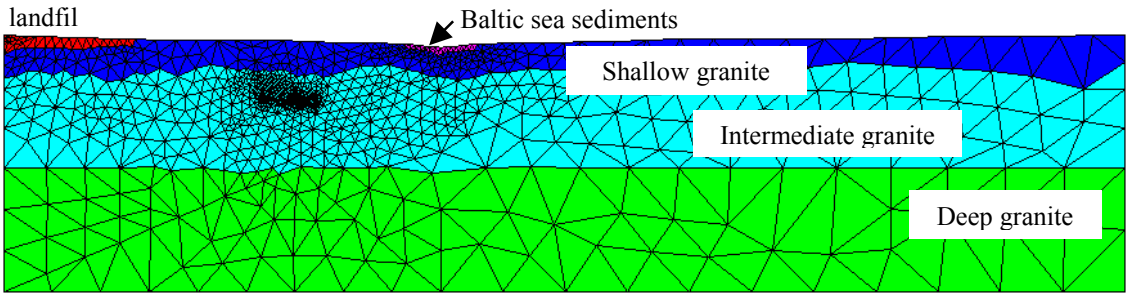

Figure 4. Finite element mesh used for spatial discretisation of the numerical model and spatial assignment of the hydrodynamic zones.

Boundary conditions for groundwater flow include impervious groundwater boundaries at both sides of the model (groundwater divides) and a prescribed recharge of 30 mm/year on the upper boundary. An exception of the upper boundary is the Baltic Sea area where groundwater head was prescribed a value of 0 m. Head at the bottom boundary was prescribed a value large enough to prevent fresh water reaching the bottom boundary. This assumption means that no flow path coming from the surface should cross the bottom boundary at a depth of 300 m. Undisturbed field measurements at the Äspö site indicate a chlorinity around 8,000 mg/L at a depth of 300 m which is consistent with the previous assumption. Parameters for groundwater flow and solute transport processes were collected from the Äspö HRL database (see Molinero, 2000 for details).

Aqueous complexation acid-base reactions, redox, cation exchange and mineral dissolution/precipitation processes has been considered within the coupled groundwater flow and reactive transport model. Chemical components and reactions were selected according to the known hydrochemistry of the system. The hydrochemical system is listed in Table 1.

Table 1. Components and processes considered in the hydrochemical model

Components:	Br^-, Ca^{+2}, Cl^-, Fe^{+2}, H_2O, H^+, HCO_3^-, K^+, Li^+, Mg^{+2}, Mn^{+2}, Na^+, $O_{2(aq)}$, $SiO_{2(aq)}$, SO_4^{-2}, Sr^{+2}
Aqueous complexes:	$Ca(H_3SiO_4)_{2(aq)}$, $CaCl^+$, $CaCl_{2(aq)}$, $CaCO_{3(aq)}$, $CaH_2SiO_{4(aq)}$, $CaH_3SiO_4^+$, $CaHCO_3^+$, $CaOH^+$, $CaSO_{4(aq)}$, $CO_{2(aq)}$, CO_3^{-2}, $Fe(OH)_{2(aq)}$, $Fe(OH)_2^+$, $Fe(OH)_{3(aq)}$, $Fe(OH)_4^-$, Fe^{+3}, $FeCl^+$, $FeCl_{2(aq)}$, $FeCl_4^{-2}$, $FeCO_{3(aq)}$, $FeCO^{3+}$, $FeHCO_3^+$, $FeOH^{+2}$, $FeSO_{4(aq)}$, $H_{2(aq)}$, $H_2SiO_4^{-2}$, $H_4(H_2SiO_4)_4^{-4}$, $H_6(H_2SiO_4)_4^{-2}$, $HCl_{(aq)}$, HS^-, $HSiO_3^-$, HSO_4^-, $KBr_{(aq)}$, $KCl_{(aq)}$, $KHSO_{4(aq)}$, $KOH_{(aq)}$, KSO_4^-, $LiCl_{(aq)}$, $LiOH_{(aq)}$,$LiSO_4^-$, $Mg(H_3SiO_4)_{2(aq)}$, $MgCl^+$, $MgCO_{3(aq)}$, $MgH_2SiO_{4(aq)}$, $MgH_3SiO_4^+$, $MgHCO_3^+$, $MgSO_{4(aq)}$, $Mn(OH)_{2(aq)}$, $Mn_2(OH)_3^+$, Mn_2OH^{+3},$MnCl^+$, $MnCl^{3-}$, $MnCO_{3(aq)}$, $MnHCO^{3+}$, MnO_4^-, $MnOH^+$, $MnSO_{4(aq)}$, $NaBr_{(aq)}$, $NaCl_{(aq)}$, $NaCO_3^-$, $NaHCO_{3(aq)}$, $NaHSiO_{3(aq)}$, $NaOH_{(aq)}$, $NaSO^{4-}$, OH^-, $SrCl^+$, $SrCO_{3(aq)}$, $SrOH^+$, $SrSO_{4(aq)}$
Minerals:	Calcite, Hematite, Pyrite, Quartz
Exchangable Cations:	Ca^{+2}, Na^+

Numerical simulations were carried out using CORE2D (Samper et al., 1998; 2000). CORE2D is a finite element code, developed at the University of A Coruña, which solves groundwater flow, heat transport and multi-component reactive solute transport under variably saturated conditions.

4. RESULTS OF THE BASE NUMERICAL MODEL

Long-term runs of the flow and transport numerical model have been performed to simulate the undisturbed conditions (i.e. prior to tunnel construction). Initially, it is assumed that the domain contains only saline formation groundwater. The numerical model was run for 20,000 days with a fresh water recharge at the upper boundary. Calibration of the flow and transport parameters was performed in order to achieve a numerical solution consistent with available chemical information of undisturbed conditions at a depth of 70 m. Figure 5-A shows a comparison between measured and computed concentrations for undisturbed (natural) conditions at the future tunnel location. In general, a very good agreement between computed and measured concentrations (at a depth of 70 m) was achieved. As expected, the most important discrepancies were found for dissolved sulphates, bicarbonates and iron (Figure 5-A) which can be affected by microbial processes not considered in the numerical model. Figure 5-B shows the comparison between measured and computed chloride concentrations during the Redox Zone Experiment (after the tunnel intersects the fractre zone).

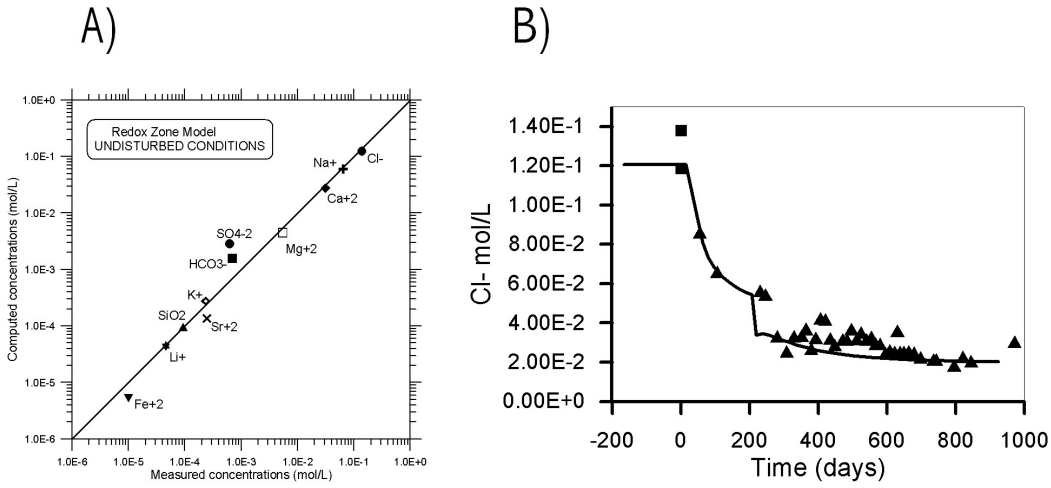

Figure 5. Comparison between measured and computed concentrations for undisturbed conditions at the tunnel location (70 m deep).

5. HYDROBIOGEOCHEMICAL MODEL

Contrary to the rest of species, the base reactive transport model can not reproduce the concentrations of bicarbonate and sulphate recorded during the experiment (Figure 6). This may be caused by microbially-driven DOC oxidation processes. Detailed research activities carried out at Äspö provide firm evidence for microbial processes taking place (Puigdomenech et al., 2001). Fermentation of Particulate Organic Carbon (POC) takes place in the shallow anaerobic zone where POC can be enriched and the intrusion of oxygen coming from the surface can be consumed by aerobic metabolisms near the surface. Fermentation provides the source of Dissolved Organic Carbon (DOC). In the

fermentation processes, organic sulphur contained in POC is released in the form of reduced sulphur such as HS^-. DOC and HS^- are then transported and oxidised in the deeper parts containing the Fe (III)-mineral-enriched-zone. These processes can be represented by:

$$POC + H_2O \Rightarrow DOC + HS^- + H^+ \quad \text{(Equation 1)}$$

$$DOC + Fe^{3+} \Rightarrow HCO_3 + H_2O + Fe^{2+} \quad \text{(Equation 2)}$$

$$HS^- + Fe^{3+} \Rightarrow SO_4^{2-} + Fe^{2+} \quad \text{(Equation 3)}$$

Microbially mediated processes have been included in the numerical model by considering Fe^{3+} as the electron acceptor to account for the oxidation of DOC. By disregarding fermentation processes, the above iron reduction-DOC oxidation process has been combined with other fermentation products, HS^- and H^+, (Equation 2 and Equation 3) into a single equation:

$$\alpha DOC + \beta HS^- + \gamma Fe^{+3} + \delta H^+ \Rightarrow \varepsilon HCO_3^- + \zeta SO_4^{2-} + \gamma Fe^{2+} + \delta H_2O \quad \text{(Equation 4)}$$

The stoichiometric coefficients α, β, γ, δ, ε, ζ, γ and δ are uncertain because the molecular structure of DOC is unknown.

What follows is the calibration of the kinetic rates and the proportional coefficients between the related species. The rate of the reaction is supposed to be controlled by Monod kinetics. The new hydrobiogeochemical model was solved using BIO-CORE (Zhang, 2001), a computer program which extends the capabilities of $CORE^{2D}$ to cope with microbial processes. This code deals with microbial growth-transformation processes considering metabolic competition, decay, metabiosis and endogenous respiration. The codes also consider the availability of substrates for attached microorganisms by coupling a diffusion layer model to account for biofilm resistance.

Figure 6 shows the computed concentration evolution of bicarbonate and sulphate as well as the comparison with measured data (at the tunnel depth). This figure also shows the numerical results computed without including microbially mediated iron reduction-DOC oxidation processes (the hydrogeochemical base model). It is worth noting that including these microbially catalised processes, the numerical model (the hydrobiogeochemical model) is able to reproduce the measured behaviour of bicarbonates and sulphates during the time of the Redox Zone Experiment.

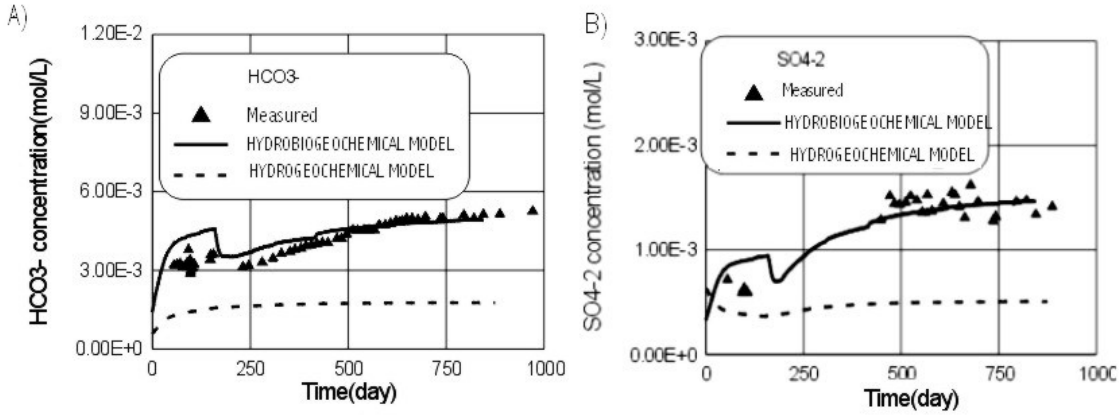

Figure 6. Comparison between measurements (symbols), hydrobiogeochemical model results (solid line) and hydrogeochemical model results (dashed line) for: A) time evolution of dissolved bicarbonates and, B) time evolution of dissolved sulphates.

6. CONCLUSIONS

A coupled groundwater flow and reactive solute transport numerical model has been performed for a kilometre-scale field experiment carried out at the Äspö HRL. This numerical model covers a long time period in order to simulate both natural and disturbed experimental conditions. In this manner, consistent initial conditions for the Redox Zone Experiment (after tunnel intersection) are self-generated for each numerical simulation. The reactive transport numerical model accounts for more than 60 homogeneous reactions, including aqueous complexation, acid-base reactions, gas dissolution and redox processes, as well as 5 heterogeneous reactions including mineral dissolution/precipitation and cation exchange. The model reproduces the measured hydrogeological response, as well as the observed concentrations of most dissolved species both before and after tunnel construction. However, discrepancies were found for some of the species, mainly for dissolved bicarbonates and sulphates. These discrepancies have been attributed to the role of microbially mediated redox processes. Based on field evidence microbially mediated iron reduction and DOC oxidation processes have been included within the base numerical model. The new hydrobiogeochemical model has been solved by using BIO-CORE (Zhang, 2001) a new general-purpose reactive solute transport code which can cope with microbiological processes. The performed hydrobiogeochemical model is able to reproduce accurately the measured time evolution of both dissolved bicarbonates and sulphates, in addition to all the remaining variables considered in the base reactive transport model. This fact provides a quantitative support to the hypothesis of microbially mediated iron reduction-DOC oxidation processes playing a relevant role in the hydrochemical evolution of the Äspö HRL site. These microbially mediated processes can be of great relevance in performance assessment exercises of deep geological repositories hosted in crystalline bedrock.

REFERENCES:

Banwart, S.; Tullborg, E.-L., Pedersen, K., Gustafsson, E., Laaksoharju, M., Nilsson, A.-C., Wallin, B. and Wikberg, P. (1996): Organic carbon oxidation induced by large-scale shallow water intrusion into a vertical fracture zone at the Äspö Hard Rock Laboratory (Sweden). J. Cont. Hydrol., 21, 115-125.

Banwart, S., Gustafsson, E. and Laaksoharju, M. (1999): Hydrological and reactive processes during rapid recharge to fracture zones. The Äspö large scale redox experiment. App. Geochem., 14, 873-892.

Bruton, C.J. and Viani, B.E. (1997): Ion sorption onto hydrous ferric oxides: effect on major element fluid chemistry at Äspö (Sweden). In: Evolution of the Groundwater Chemistry at the Äspö Hard Rock Laboratory. Proceedings of the second Äspö International Geochemistry Workshop. SKB ICR97-04.

Molinero, J. (2000): Testing and Validation of Numerical Models of Groundwater Flow, Solute Transport and Chemical Reactins in Fractured Granites. Ph.D. dissertation. University of A Coruña (Spain).

Pedersen, K., Arlinger, J., Jahromi, N., Ekendahl, S. and Hallbeck, L. (1995): Microbiological investigations. In: The Redox Experiment in Block Scale. Final Reporting of Results from the Three year Project. Chapter 7. Äspö HRL Prog. Rep. (PR 25-95-06), SKB, Stockholm, Sweden.

Puigdomenech, I. (Editor) (2001): O_2 depletion in granitic media The REX project. SKB Tech. Rep. (TR-01-05), SKB, Stockholm, Sweden.

Samper, J., Delgado, J., Juncosa, R. and Montenegro, L. (2000): $CORE^{2D}$: A Code for Nonisothermal Water Flow and Reactive Solute Transport. Users Manual Version 2. ENRESA Publicación Técnica 6/2000.

Tullborg, E.-L. and Gustafsson, E. (1999): 14C in biocarbonate and dissolved organics-a useful tracer?. Appl. Geochem., 14, 927-938.

Wallin, B. (1995): Sulphur cycling in the Redox Zone. In: The Redox Experiment in Block Scale. Final Reporting of Results from the Three year Project. Chapter 6. Steven Banwart (Ed). Äspö HRL Prog. Rep. (PR 25-95-06), SKB, Stockholm, Sweden.

Zhang, G. (2001): Non-isothermal Hydrobiogeochemical Models in Porous Media. Ph.D. dissertation. University of A Coruña (Spain).